Dissertation

submitted to the

Combined Faculties for the Natural Sciences and for Mathematics

of the Ruperto-Carola University of Heidelberg, Germany

for the degree of Doctor of Natural Sciences

presented by

M.Sc, Loredana Iovino

born in Avellino, Italy

Oral-examination: 27th April 2018

Ultrastructural characterization of microtubules at high resolution in the mammalian peripheral nervous system

Referees: Dr. Jonas Ries
Prof. Dr. Stephan Frings

Acknowledgments

First and foremost I would like to thank both my advisors: Dr. Paul Heppenstall and Dr. Yannick Schwab for giving me the opportunity to work on this thesis. I am grateful for the continuous support of my Ph.D study and related research, for their patience, motivation, and immense knowledge. Their guidance helped me in all the time of research and writing of this thesis. I could not have imagined having better advisors and mentors for my Ph.D study.

Besides my advisors, I would like to thank the rest of my thesis committee: Prof. Stephan Frings, Dr. Jonas Ries, Dr. Alba Diz-Munoz, Dr. Daniela Mauceri for their insightful comments and encouragement, but also for the hard question which incented me to widen my research from various perspectives.

It was a great pleasure to work for 4 years in the team of Dr. Yannick Schwab whose help went much beyond the technical and scientific aspects of my Ph.D. He kindly "adopted" me in his research group, giving me access to the laboratories and the EMCF (Electron Microscopy Core Facility) where I found a second family. Therefore, my endless gratitude goes to Rachel Mellwig, Nicole Schieber, Charlotta Funaya, PedroMachado, Paolo Ronchi, Androniki Kolovou, Martin Schorb, Jose Miguel Serra Lleti, Anna Steyer and Matthia Karreman for the stimulating discussions, their constant help, encouragement, and for all the fun we have had in the last four years. Without their precious support it would not be possible to conduct this research.

My sincerest thanks go to my friends and colleagues Pedro Machado and Jose Miguel Serra Lleti who have always been by my side during this frustrating path called Ph.D. They supported me not only from a technical and scientific point of view, but also spiritually throughout writing this thesis and my life in general.

I would like to acknowledge all the collaborators from EMBL Rome, EMBL Heidelberg (especially Shyamal Mosalaganti) and EMBL facilities, for their contribution to this project.

I thank my dearest friends Raffaele Totaro and Anna Maria Subosco for any kind of help and support within and outside EMBL, for having always a warm smile and nice words for me, for making me feel at home every time I was around them, for all the laughs we shared and the frustrations moments they helped me to pass through. They will always have a special place in my heart.

I would like to thank also my colleagues and friends from the Heppenstall group at EMBL Rome: Kalina Stanceva, Fernanda de Castro Reis, Rahul Dhandapani Shane Morley, Linda Nocchi, Laura Castaldi, Mariano Maffei, Chiara Morelli, Laura Batti, Mayya Sundukova. It has always been a joy working with them and sharing many nice moments, even though for a limiting period of time.

A special thank goes to all the friends I met while working at EMBL (Heidelberg and Rome):

- My colleagues from the Ph.D program, class of 2014: Natalie Romanov for being a good friend, for listening to my complains and finding always a way to cheer me up; Katarzyna Buczak, Vilma Jimenez Sabinina, Jørgen Benjaminsen, Sourabh Bhide and Mariana Ruiz Velasco Leyva for being always very friendly;
- Shiying Lu, the first friend I met when I moved to Heidelberg. We have been through the PhD path together, sharing joys and sorrows and being always there for each other in our time of need.
- "The amazing Italian trio" Maria Giubettini, Giulia Di Bartolomei and Floriana Lanza with whom I spent most of my best moments in Heidelberg. Together we had a lot of fun diving into Heidelberg nightlife, but they also got me through

hard times, sad times and confused times, knowing how to cheer me up and laughing until we couldn´t stop.

- Suruchi Sethi, my lovely Suruchina, for the "deep conversations" during coffee breaks, for becoming such a great friend in so little time and for the amazing trip we had together - "honeymoon" – in Kerala. She brought me into her lovely family where I felt loved and happy like at my own place. She taught me how to be strong- "it´s ok Lory" she used to say- and that no matter what, everything would be ok at some point. From selfies to parties and from heartbreak to loneliness, thanks for being there for me through it all and for always making time for me, no matter how far away you are!
- Irma Querques and Matteo Bordi for supporting each others during the hard PhD life, for giving me a shoulder to lean on when I was down but also for all the happy moments celebrated with succulent dinners at Carosello´s.

Then I would like to thank Maria Placentino and Simona Sorrentino for the retail therapy and thermal bath therapy that we gave ourselves sometimes to "survive" the past four years. They have always supported me and been by my side in any kind of situation. Thanks to Matteo Savoia for being a good friend even in my worst moments, for his "pearls of wisdom" and spontaneity.

Thanks to the Pfitzenmaier Fitnessstudio where I used to do my workout 4 times per week. Especially the indoor cycling course helped me to reduce stress and the frustration of "never-a joy" days at work.

My sincerest thanks go to Praveen Kumar Kallappa Ingale who showed me the light in one of my darkest moment. He came into my life like an unexpected hurricane and turned everything upside down. He got me with his joy of life, his pure heart and beautiful smile, which make him an incredible young man. He supported me throughout

writing this thesis and his only presence makes my life happier. His love and help are an unbelievable blessing. I only wish that I had met him earlier.

Last but not the least, I would like to thank my family: my parents Umberto and Maria, my sister Edda, “my brother” Ares, my brother in law Sabatino and my adorable nieces Martina and Ludovica, for being such an amazing family. They supported me in all the stages of my life with their unconditional love and I could not have imagined having a better family. They taught me to be honest and strong, to fight for my dreams, how to handle disappointment and overcome adversities and above all, to have a positive attitude towards life. It would not be enough to thank them a million times over for everything they have done and keep doing for me.

Summary

Mechanotransduction is the ability of living organisms to sense and respond to mechanical forces by converting them into a biological response. In mammals, mechanotransduction is mediated by specialized sensory neurons which are capable of detecting a wide range of mechanical stimuli, relying on the presence of mechanotransducer channels on sensory nerve endings. Surprisingly, little is known about the properties of mechanotransducers in mammals and thus the mechanisms that convert mechanical forces into electrical signals at the peripheral endings of sensory neurons and, especially how the cytoskeleton influences it. In previous work, we have found that mice lacking the α-tubulin acetyltransferase Atat1 display a significant decrease in mechanosensitivity across all major fiber types innervating the skin, strongly affecting light touch and pain, with no impact on other sensory modalities[1]. We also assessed that such a phenotype does not arise from wide-ranging effects on the development, morphology and structure of peripheral sensory neurons but may be caused by the lack of a sub-membrane ring of acetylated α-tubulin that somehow sets the mechanical rigidity of the cells, rendering them more resistant to mechanical deformation[1]. How α-tubulin acetylation is capable of setting cellular rigidity remains poorly understood. Here, an ultrastructural analysis on sensory nerve endings was performed to examine whether the lack of α-tubulin acetylation affect microtubules (MTs) organization and structure along the sensory neuron axis, from the soma of DRG neurons to their peripheral endings. Superresolution microscopy analysis on DRG neurons shows that the lack of α-tubulin acetylation does not affect the overall MTs organization. Moreover, combining high-resolution transmission electron microscopy with image analysis, I investigated MT morphology and distribution in the saphenous

nerve from Atat1^{control} and Atat1^{cKO} mice. Our results demonstrated that no major differences were observed between MTs from the Atat1^{cKO} compared to the Atat1^{control} when minor axis, eccentricity, solidity and perimeter length were compared. These results were also confirmed by Cryo-EM observations, suggesting that lack of acetylation does not affect MTs ultrastructure in mammals in the absence of mechanical stress. Finally, the von Frey assay shows that mice lacking Atat1 not only display a profound loss of light touch and pain sensitivity but, in addition, they develop allodynia only beginning at day 21 post SNI (spared nerve injury), suggesting that microtubule acetylation play an important role in hypersensitivity to mechanical stimuli associated with chronic pain.

Zusammenfassung

Als Mechanotransduktion bezeichnet man die Fähigkeit von lebenden Organismen mechanische Kräfte zu erfassen und diese in eine biologische Antwort zu übersetzten. In Säugetieren existieren spezialisierte sensorische Neurone, welche an ihren sensorischen Nervenenden mechanotransduzierende Kanäle besitzen, mit denen sie eine große Bandbreite an mechanischen Stimuli detektieren können. Wie genau die Mechanotransduktion in Säugetieren funktioniert ist bis heute nicht bekannt, es gibt keine genauen Erkenntnisse darüber wie die mechanischen Kräfte an den Nervenenden in elektrische Signale umgewandelt werden und insbesondere ist es unbekannt wie dieser Vorgang durch das Zytoskelett beeinflusst wird. Vor kurzem konnte gezeigt werden, dass Mäuse mit fehlender α-Tubulin Acetyltransferase (Atat1) Aktivität eine signifikant geringere Mechanosensitivität in allen wichtigen Fasertypen, welche die Haut innervieren, zeigen. Dies führt zu einer geringeren Sensitivität bei der Wahrnehmung von leichter Berührung und Schmerz ohne weitere sensorische Qualitäten zu beeinflussen[1]. Wir nehmen damit an, dass der oben beschriebene Phänotyp nicht auf grundlegende strukturelle Veränderungen in der Entwicklung/ Morphologie von peripheren sensorischen Neuronen zurückzuführen ist, sondern auf das Fehlen eines submembranen Ringes des acetylierten α-Tubulins, was zu einer erhöhten mechanischen Rigidität der Zellen führt und diese resistenter gegenüber mechanischer Deformierung macht[1]. Wie genau dabei α-Tubulin die zelluläre Rigidität beeinflusst ist noch nicht verstanden. Das Ziel dieser Arbeit ist die sensorischen Nervenenden ultrastrukturell vergleichend zu analysieren, um eine mögliche Auswirkung des Fehlens der α-Tubulin Acetyltransferase Aktivität auf die

Organisation und Struktur der Mikrotubuli entlang der sensorischen neuronalen Achse von den Somata der Neurone des Spinalganglions bis hin zu deren peripheren Endungen zu untersuchen. In einem ersten Ansatz konnten wir mittels superauflösender Mikroskopie keinen Unterschied feststellen bezüglich der Organisation der Mikrotubuli in den Neuronen des Spinalganglions mit fehlender α-Tubulin Acetyltransferase und dem Wildtyp. Weiter haben wir die Organisation der Mikrotubuli mittels hochauflösender Transmissions Elektronenmikroskopie untersucht. Die Kombination von hochauflösender Transmissionselektronenmikroskopie und Bildanalyse ermöglichte es uns die Morphologie und Verteilung der Mikrotubuli im Nervus Saphenus in $Atat1^{Control}$ und $Atat1^{cKO}$ Mäusen vergleichend zu untersuchen. Unsere Ergebnisse zeigen hier keinen relevanten Unterschied in der Struktur und Oragnisation der Mikrotubli bezüglich deren Achse, Exentrizität und Solidität. Mit Hilfe von Kryo-Elektronenmikroskopie konnten die oben genannten Resultate bestätigt

werden. Das Fehlen der α-Tubulin Acetyltransferase Aktivität hat laut unseren Ergebnissen keinen Einfluss auf die Ultrastruktur der Mikrotubuli in Säugetierzellen. Des Weiteren konnten wir mittels des von Frey assays, welches nach mechanischen Stress durch SNI durchgeführt wird, zeigen, dass die α-Tubulin Aacetyltransferase depletierten Mäuse nicht nur weniger empfindlich gegenüber leichter Berührung und Schmerz sind, sondern auch eine Verzögerung im Auftretens der Allodynie zeigen, welche hier erst ab Tag 21 auftritt. Daraus können wir schließen, dass die Acetylierung der Mikrotubuli scheinbar auch bei der Entwicklung von Hypersensitivität gegenüber Schmerzreizen eine Rolle spielt, welche mit chronischen Schmerzen assoziiert ist.

Table of Contents

1 Introduction

1.1 The somatosensory System

1.1.1 The somatosensory system: a catch-all term to designate a multimodal sensory system

Through our five sensory systems (hearing, olfaction, somatosensation, taste and vision) we are presented with an immense range of experiences from the world around us, including the sound of our favorite songs, the aroma of roasting coffee, the pleasure of stroking, the taste of good food and the sight of a breathtaking landscape. Each system detects specific types of stimuli and transmits this information to the brain, where they are processed at a different levels of the central nervous system and interpreted finally as sensations of different perceptual characteristics.

Among the five, only the somatosensory system is multimodal, detecting different types of stimuli, including touch (i.e., physical contact with skin) temperature (monitor the temperature of the body, external objects and environment), nociception (detection of noxious mechanical, thermal, or chemical stimuli that give rise to pain sensation), itch, proprioception (information about the position and movement of our body parts through the stimulation of muscle and joints) and interoception (information about internal organs).

The ability to detect and discriminate these wide array of stimuli is called somatosensation and it is achieved in mammalian skin by multiple specialized sensory receptors that relays sensations detected in the periphery and conveys them via sensory afferents to the trigeminal ganglia (the sensory function of the trigeminal nerve, which

is to provide tactile, proprioceptive, and nociceptive afferents to the face and mouth, will not be discussed in this thesis) and dorsal root ganglia, where the cell bodies of the first-order neurons are located. Each pseudo-unipolar neuron possesses a bifurcating sensory afferent that connects the periphery to the spinal cord and then travel through it either in an ipsilateral or a contralateral fashion.

Broadly, the spinal cord contains the second-order neurons for the fibers carrying pain, coarse touch and temperature sensations. The medulla contains the second-order neurons for fibers carrying fine touch, position, and vibratory sensations. The fibers are then either conveyed to the thalamus, where the third-order neurons are located, or conveyed to the cerebellum, carrying information that is not perceived consciously (Figure 1). Finally, from the thalamic nucleus, the sensory afferents are projected to the cortical sensory areas, where information is integrated and analyzed to direct behavior[2].

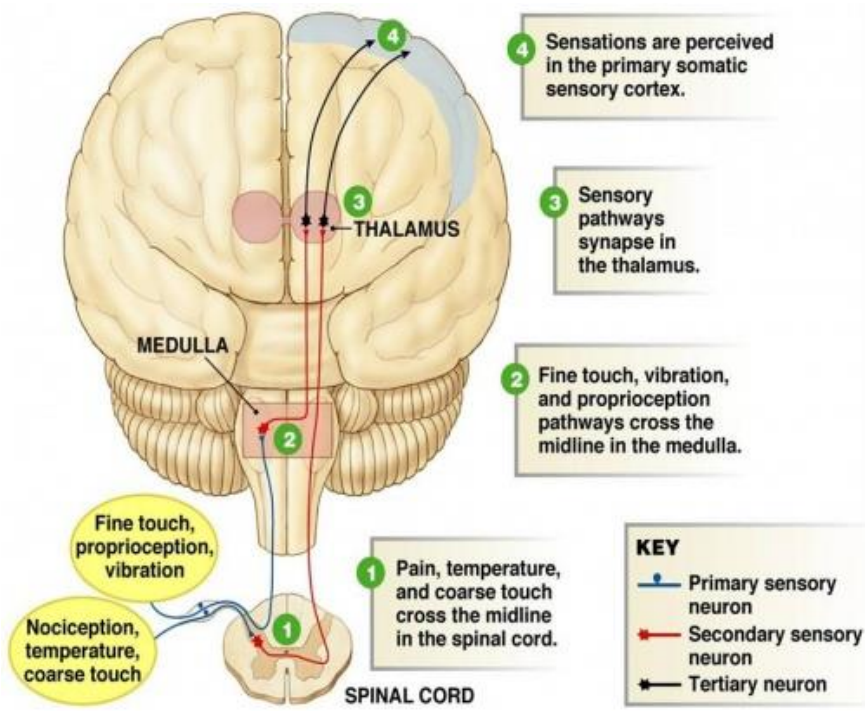

Figure 1. Somatosensory pathways. The somatosensory system is a 3-neuron system that relays sensations detected in the periphery and conveys them via pathways through the spinal cord, brainstem,

and thalamic relay nuclei to the sensory cortex in the parietal lobe. Image from www.physio-pedia.com/Introduction_to_Neuroanatomy.

To initiate a range of sensations, cutaneous sensory neurons display an array of anatomical specializations and physiological properties. They can be classified as Aβ, Aδ or C fibers based on conduction velocity of action potentials along afferent fibers and degree of myelination[3,4]. Aβ afferents are the fastest due to their large diameters and thick myelin sheets. C fibers, which have thin, unmyelinated afferents, are the slowest whereas the thinly myelinated Aδ fibers fall between.

Moreover these receptors can differ in their field size (small or large) and their speeds of adaptation (rapidly adapting or slowly adapting). The receptive field size refers to the amount of skin area that responds to the stimulus, with smaller areas specializing in locating stimuli accurately, while the speed of adaptation refers to how quickly the receptor will react to a stimulus and how long that reaction will be sustained after the stimulus is removed.

Sensory neurons can be further designated as mechanoreceptors, thermoreceptors, nociceptors, depending on their modality or the sensory stimuli to which they respond. They employ a variety of receptor types embedded in the skin, mucous membranes, muscles, joints, internal organs, and cardiovascular system to respond to many different kinds of stimuli

In addition, mechanoreceptors are considered *rapidly adapting* if they adapt to a change in stimulus very quickly or *slowly adapting* if they do not adapt to a change in stimulus very quickly[4,5]. This means that the former can sense right away when the skin is touching an object and when it stops touching that object. However, rapidly adapting

receptors can't sense the continuation and duration of a stimulus (how long the skin is touching an object). These receptors best sense vibrations occurring on or within the skin. The latter instead are very good at sensing the continuous pressure of an object touching or indenting the skin but are not very good at sensing when the stimulus started or ended.

1.1.2 Cutaneous sensory receptors

There are several types of specialized sensory receptors in the skin that can be free receptors or encapsulated (Figure 2). Free nerve endings found throughout the body, in the epidermis of both glabrous and hairy skin, are characterized by both Aδ- and C-responses and detect nociception, heat and cold, and light touch.

Aβ-fibers, such as those innervating slowly adapting, encapsulated Merkel's disks are found in the basal layer of the epidermis of fingertips and lips, respond to light touch and represent about 25% of the mechanoreceptors of the hand[4].

The Merkel's disk is part of the Merkel complex together with a specialized Merkel cell, which contains synaptic vesicles that appear to release peptides that modulate the nerve terminal[6].

Meissner's corpuscles represent about 40% of the sensory innervation of the human hand and consist of an elongated capsule made of connective tissue that comprises several lamellae of Schwann cells. The center of the capsule contains one or more afferent nerve fibers interdigitated between flattened epithelial (laminal) cells. These receptors, found in glabrous skin within the dermal papillae just beneath the epidermis of the fingers, palms, and soles, are Aβ rapidly adapting, encapsulated receptors

transducing information about low-frequency vibrations (30–50 Hz) that occur when textured objects are moved across the skin[4]. Consequently, Meissner corpuscles are considered to be the discriminative touch system's flutter and movement detecting receptors in non-hairy skin.

Ruffini endings represent about 20% of the receptors in the human hand, are localized deep in the dermis as well as in joint ligaments and joint capsules and consist of Aβ slowly adapting, encapsulated receptors that detect skin stretch, joint activity, and warmth[4]. The Ruffini corpuscle is cigar-shaped and contains longitudinal strands of collagenous fibers that are continuous with the connective tissue of the skin or joint so that it can function as cutaneous or proprioceptive receptor depending on its location. These elongated, spindle-shaped capsular specializations are oriented with the long axis parallel to the stretch lines in skin so that they are particularly sensitive to the cutaneous stretching produced by digit or limb movements.

Hair receptors or lanceolate endings are unencapsulated rapidly adapting nerve endings wrapped around the base of hair follicles that detect hair movement and skin deflection. The hair follicle afferents enter the follicle to encircle or to form a lattice pattern around the hair shaft and most of them are rapidly adapting type (Aβ, Aδ or C- fiber type)[5].

Finally, Pacinian corpuscles are encapsulated, Aβ rapidly adapting receptors located in the dermis of glabrous skin, and in the connective tissues of bone, the body wall and body cavity. They make up 10–15% of the cutaneous receptors in the hand and detect transient pressure, tickle and high-frequency vibration[4].

Indeed the Pacinian corpuscle consists of a single afferent terminal that is surrounded by concentrically layered epithelial (laminar) cells that are all encapsulated within a sheath. The resulting capsule acts as a filter, allowing only transient disturbances at high frequencies (250–350 Hz) to activate the nerve endings[7].

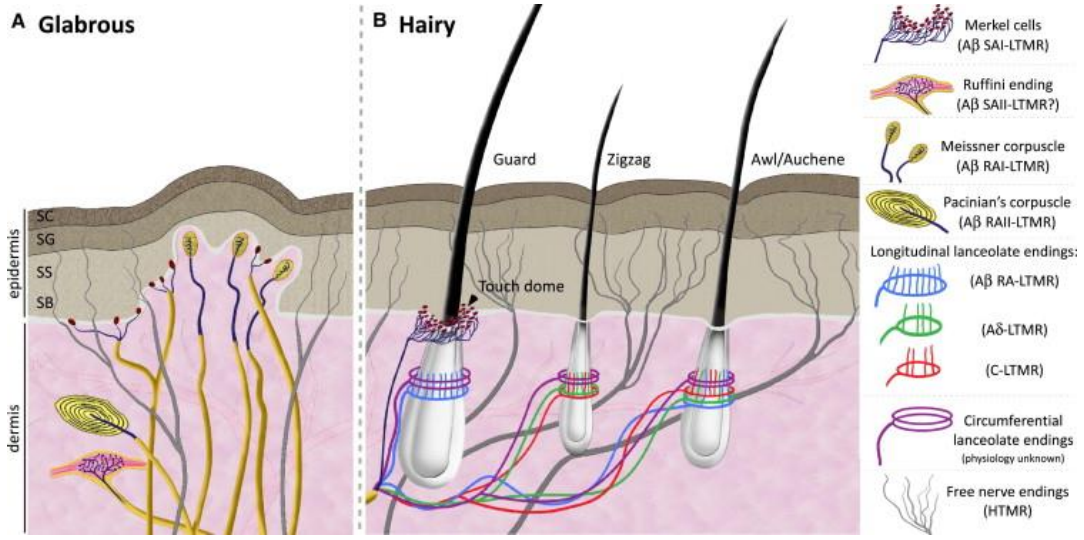

Figure 2. Representation of cutaneous sensory receptor in the skin. Mammalian skin comprises both hairy and non-hairy, or glabrous, skin. Glabrous skin is predominantly found on the hands and feet of most mammals while hairy skin covers more than 90% of the body surface. Examples for free receptors are the lanceolate endings, the hair receptors at the roots of hairs. Encapsulated receptors are the Pacinian corpuscles and the receptors in the glabrous skin: Meissner corpuscles, Ruffini corpuscles and Merkel's disks. Image from Victoria E. Abraira and David D. Ginty, Cell (2013)

Surprisingly, little is known about how these nerves function, the mechanisms that transduce these forces into electrical signals at the peripheral endings of sensory neurons and, especially how the cytoskeleton influences it. Several models have been suggested regarding how the mechanical force triggers channel opening, among these the membrane force model and the tether model seem to be the most accepted. The former is supported by evidence in bacterial mechanotrasduction channels MscS and MscL[8] and eukaryotic potassium channels[9,10], which are gated by the force exerted via lipids in the membrane; while the latter is represented by *Drosophila* NompC ion channels, shown to be tethered to MTs by means of intracellular structures that have been suggested to pull open the channels during mechanotrasduction[11] (Figure 3).

Nevertheless, those models are not mutually exclusive as, in vivo, the cell membrane and other cellular components, such as tethers and/or the underlying cytoskeleton, may act in concert to redistribute membrane tension, thus transmitting forces to the channel gate.

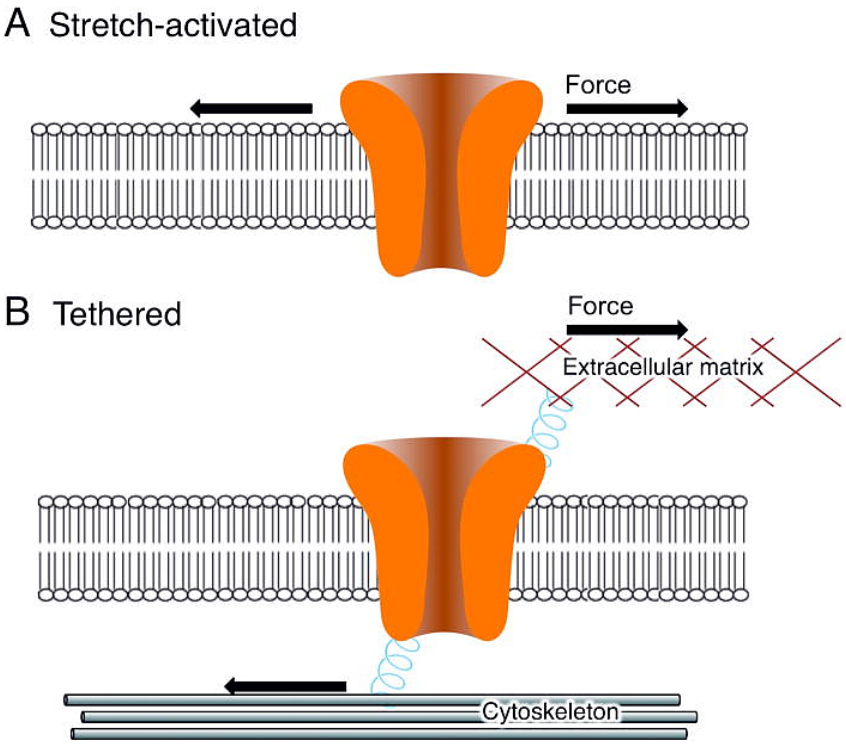

Figure 3. Two proposed models for gating mechanosensitive ion channels in prokaryotes and eukaryotes: A) the bilayer model describes that prokaryotes ion channels are directly gated by forces applied to the lipid bilayer. According to this model the lipid bilayer tension is all that is required for activation. B) the tether model has been proposed for Eukaryotes and it requires the channel to be in contact with the cytoskeleton and/or extracellular matrix before the stimulus occur. Force applied on this tether generates a tension which is thought to pull open the channel. Image from Kara L. Marshall and Ellen A. Lumpkin, Cell (2014).

1.2 Touch sensation

Most of our behaviors depend upon our senses which allow to sample the surrounding world and extract information critical to our survival.

Among these, mechanosensation is thought to be the most ancient and the most commonly represented in the mammalian repertoire of senses[12]. Indeed all living organisms, from single cells to humans, require some form of mechanosensation to survive as early hypothesized by Aristoteles, who linked skills to discriminate different tactile stimulations to human intelligence: "In the other senses man is inferior to many animals, but in the sense of touch he far surpasses them all in acuity; that is why he also the most intelligent of animals[13]".

Multiple senses including touch sensation, proprioception, senses of hearing and balance, regulation of blood pressure and systemic fluid homeostasis as well as many more vital processes depend upon the ability to respond to mechanical stimulation[14].

Genetic, behavioral and physiological studies in simple organisms, such as Bacteria, *C. elegans*[15,16] followed much later by *Drosophila*[17,18] and Zebrafish[19], have improved our understanding of the fundamental mechanisms of mechanosensory transduction.

Moreover the development of selective genetic markers in transgenic mouse models and the advent of rapid gene silencing technologies have allowed on the one hand to manipulate and characterize the functional and anatomical properties of sensory neurons and, on the other hand, to shed light on a new family of mechanotransduction channels, the Piezo family[19-21]. The Piezo proteins are a highly evolutionary conserved group of mechanically activated ion channels and higher levels of Piezo2 transcripts in DRGs placed this gene as a prime candidate to mediate mechanotransduction in touch receptor neurons or nociceptor.

Direct evidences that Piezo2 can account for mechanotransduction in most vertebrate touch receptors come from several studies performed in Zebrafish, mouse and most recently in Humans. In particular it has been reported that Piezo2 is a principal component of mechanosensory signaling in mouse Aβ LTMRs and human LTMRs[20,21]. Indeed gentle touch is mainly mediated by thickly myelinated Aβ afferents with low mechanical thresholds[12] while in humans and several other mammals, C-fibers sensitive to gentle touch have also been found and it is believed that they are involved in social interactions[22] or hypersensitivity after injury[23].

Several studies in *C. elegans* have also suggested that touch sensitivity is dependent on both the actin binding protein β spectrin[24] and the MT cytoskeleton[25]. In particular, in *C. elegans*, six touch receptor neurons (TRNs) sense gentle touch and uniquely contain crosslinked bundles of heavily acetylated 15-protofilament MTs[26]. Targeted disruption of the molecular components of these MTs, MEC7 β-tubulin and MEC12 α-tubulin, and mutation of MEC-17, the major tubulin acetyltransferase[27,28] cause touch insensitivity[25–29], suggesting a specific role of MTs and their acetylation status in nematodes mechanosensation.

In support of this, it has been reported that acetylated MTs may also have an important function in mouse sensory neurons, as these neurons have amongst the highest level of αtubulin acetylation in mouse[30].

In our previous work, we have assessed that mice lacking the α-tubulin acetyltransferase Atat1, the mammalian orthologue of MEC-17, display a significant decrease in mechanosensitivity across all major fiber types innervating the skin with no impact on other sensory modalities[1].

Furthermore electrophysiological and morphological analysis indicate that the loss of mechanosensitivity is not due to generalized effects on neuronal function, such as

axonal transport, axonal outgrowth in vitro, or in the ultrastructure of peripheral nerves and their innervation in the skin and spinal cord in vivo, but it is caused by the ability of sensory neurons to covert mechanical forces into electrical signals[1].

1.3 Neuropathic pain: when a physiological and protective mechanism becomes the cause of a severe health problem

Nociception and acute pain represents a warning signal for the body, whose role is to induce behavioral responses aimed to protect individuals from tissue damage.

Nociception is mediated by well characterized, multi-synaptic relay systems that are triggered in the periphery and then processed at multiple sites in the central nervous system, both in the spinal cord and at higher brain centers (Figure 4). Neuronal fibers that transmit nociceptive stimuli are classified according to their degree of myelination and their diameter in: Aδ, larger and myelinated, and C, smaller and unmyelinated. The former ones convey faster neuronal information and are responsible for discriminative pain sensitivity (well-localized pain); the latter transmit slowly and are responsible for the protopathic pain sensitivity (widespread, poorly-localized pain). Under physiological conditions, pain transmission consists of a chain of events that originate at the terminal endings of the peripheral sensory fibers (primary sensory neurons): at this level a specific stimulus, indicative of a potential tissue damage, may activate nociceptors, thus generating an action potential that is transmitted through the axons of primary sensory neurons to the dorsal horn of the spinal cord[31].

Spinal circuits further process sensory inputs and relay them to brain centers via diverse pathways, where the perception of pain together with its emotional and aversive components is generated[32].

Given its remarkable and complex structure, the nociceptive process is not to be considered a simply neural transmission from the peripheral nociceptors to the central nervous system, but a very dynamic system, consisting of multiple transmission pathways and redundant processes, that can be modulated at each level of the synaptic communication and in which all the cellular components interact in a coordinated manner to produce the adaptive and protective response desired.

Maladaptive processes, triggered by pathophysiological factors (such as neural injury, trauma, amputation, viral infection, inflammation, tumor growth, exposure to neurotoxins, autoimmune disease, vascular diseases, metabolic disorders or stress-related alterations), may induce states of pathological pain, called neuropathic pain and characterized by widespread-pain, sensory deficit, hyper excitability of nociceptive transmission, burning sensation, pain following exposure to light.

Neuropathic pain currently represents one of the most important health problems, as it is generally a type of debilitating and chronic disorder that has a negative impact on the quality of life, in particular on the ability to work and sleep. Indeed, painful stimuli applied to the body regions innervated by the damaged nerves results in abnormal sensitivity to a variety of noxious (hyperalgesia) or innocuous (allodynia) stimuli[33]. Neuropathic pain symptoms are generally refractory to pharmacological treatments and respond only partially to the available therapies, which on the other hand may often induce severe side effects[34].

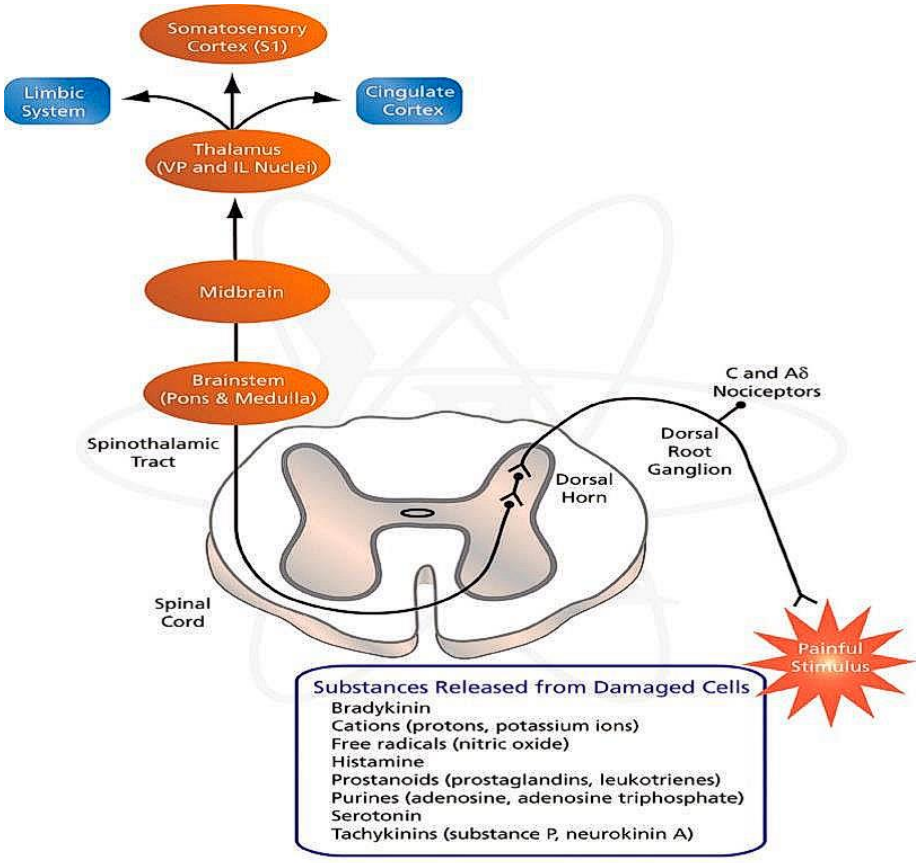

Figure 4. **Ascending pain transmission way. VP, ventroposterior thalamic nucleus; IL, intralaminar nucleus of thalamus.**

From this first point of integration of nociceptive information, axon branch and cross in a ventrolateral direction heading to higher brain centers; the different afferent nerve fibers gather in the spinothalamic beam, directed to the thalamus. From here the information is relayed to the primary and secondary somatosensory cortex through thalamocortical fibers; at the cortical level painful information is processed so that the appropriate responses are generated. **(**Sigma-Aldrich, 2011).

More recent evidences suggest that the transition from acute pain into chronic pain states involves several mechanisms. Indeed, it seems to be caused not only by activity-dependent changes (functional plasticity) occurring at several levels along the nociceptive pathway[35], but also by structural remodeling and reorganization of cells, synapses and circuits. However, the specific nature of circuit alterations along diverse

segments of the nociceptive pathway is yet not well understood and it is not clear whether the structural remodeling represents a cause or a consequence of chronic pain. Several lines of evidence suggest that both mechanisms may be involved in the clinically intractable symptom of allodynia. In particular, two different models, currently accepted, seem to explain the cellular basis of allodynia. Both models are not mutually exclusive and imply both functional plasticity and structural plasticity. In one model, under physiological conditions, sensory information from nociceptors and touch receptors, such as C and Aδ nociceptive fibres, C-type low-threshold mechanoreceptors (C-LTMRs) and non-nociceptive amyloid-β (Aβ) afferents)[36], are processed and modulated by separate neural circuits in the spinal cord. This underlies the diversity and specificity of their functions which are lost under neuropathic conditions, leading to convergence of inputs onto common subset of neurons which typically receives noxious inputs[35]. The other model is based upon the presence of polysynaptic connections between spinal neurons receiving touch and those receiving pain inputs that normally are subjected to strong inhibitions. In neuropathic pain states, physical loss of spinal inhibitory neurons can activate a crosstalk between touch and pain circuits and results in an increased activity in spinal pain pathways.

Interestingly, Dina and colleagues explored a novel role for the cytoskeleton in the regulation of pain plasticity[37,38]. They found that disruption of each of the three major components of the cytoskeleton, actin microfilaments, neurofilaments and MTs, causes a significant reduction of hypersensitivity within sensory neuron terminals from rats, following intradermal epinephrine injection, with no effects on the prostaglandin E2-induced hypersensitivity.

Prostaglandin E2 (PGE2) and epinephrine are inflammatory mediators that act directly through G-protein-coupled receptors (CGRPs) on peripheral nociceptive terminals to

produce mechanical hyperalgesia, via protein kinase A (PKA) alone or a combination of PKA, protein kinase C epsilon (PKCε), and extracellular signal-regulated kinases (ERK1/2), respectively. Using a model of hyperalgesic priming, where rat hindpaws are initially injured with intradermal carrageenan, Dina et al., observed a switch in second messenger signaling in response to a subsequent exposure to PGE2. When PGE2-mediated hypersensitivity becomes long lived after such priming, it shifts its signaling dependence upon PKCε and ERK1/2 as well as PKA and it too became dependent on an intact cytoskeleton.

The most intriguing aspect of this work is that such plasticity in cell signaling, where the cytoskeleton seems to be one of the major player, may represent a key mechanism in the transition from acute pain to chronic pain states and may contribute also in the development of allodynia.

1.4 Microtubules acetylation in cells and disease

1.4.1 Microtubule basics

To function properly, all cells interact physically with each other and their surroundings and respond to external mechanical forces. Therefore they have to be physically robust and maintain their shape and internal organization, but also to rearrange their internal components to carry out essential functions like division and movement.

The variable shape and rigidity of the cell and its ability to move are largely dependent on three groups of cytoskeletal protein filaments: actin filaments, MTs and intermediate

filaments, each of them responsible for different aspects of the cell's spatial organization and mechanical properties.

MTs are the largest type of filament, with an outer diameter of about 25 nanometers (nm), and they are found in eukaryotic cells as well as some bacteria. MTs are involved in many crucial cell processes such as cell shape, motility and division as well as intracellular transport and organelle positioning. They also constitute the internal scaffold (axoneme) of specialized structure, cilia and flagella, present only in some eukaryotic cells.

MTs represent one of the major cytoskeletal components of neurons, essential for cellular migration, intracellular transport, morphological changes during the different stages of neuronal development and synapses formation[39], and are key components for the establishment and maintenance of neuronal polarity, a fundamental feature that enable these cells to perform a variety of unique functions[40].

MTs are composed of a protein called tubulin, a heterodimer formed by two evolutionary conserved globular proteins called α-tubulin and β-tubulin, tightly bound together in a head-to-tail fashion by noncovalent bonds to form long strands called protofilaments that in turn associate laterally to form the hollow, straw-shaped filaments of MTs.

MTs are nucleated from the microtubule-organizating center (MTOC), where γ-tubulin, another type of tubulin, is mostly enriched. Nucleation depends on the γ-tubulin ring complex (γ–TuRC) which serves as template for the formation of MTs[39].

MTs are flexible but also very unstable so that they can disassemble very quickly.

Indeed MTs switch between phases of growth and disassembly in a process named dynamic instability. The change from growth to shrinkage is called a *catastrophe*, while the change to growth is called a *rescue* (Figure 5).

As longitudinal and lateral contacts within the lattice hold most of the subunits (tubulin heterodimer α-β) in a MT in place, the addition and loss of subunits occurs almost exclusively at MTs ends. Each subunit has a distinct structural polarity as it contains a different molecular configuration at each end called "plus" end and "minus" end. The "plus" end of one molecule can only link to the "minus" end of another in a way that they are stacked up to form a linear polar polymer, hence conferring MT lattice itself structural and dynamic polarity. The plus end, terminated by β-tubulin, grows faster, undergoes catastrophe more frequently and is a crucial site for regulating MT dynamics[41].

MTs dynamic instability is mainly directed and controlled by the binding and hydrolysis of the chemical guanosine 5' triphosphate (GTP), within the β-tubulin subunit, and regulated in the cytoplasm by the coordinate action of various MAPs, motor proteins and the so called "tubulin code"[42], which is generated by the expression of different α- and β-tubulin subtypes and by post-translational modification (PTMs) of tubulin.

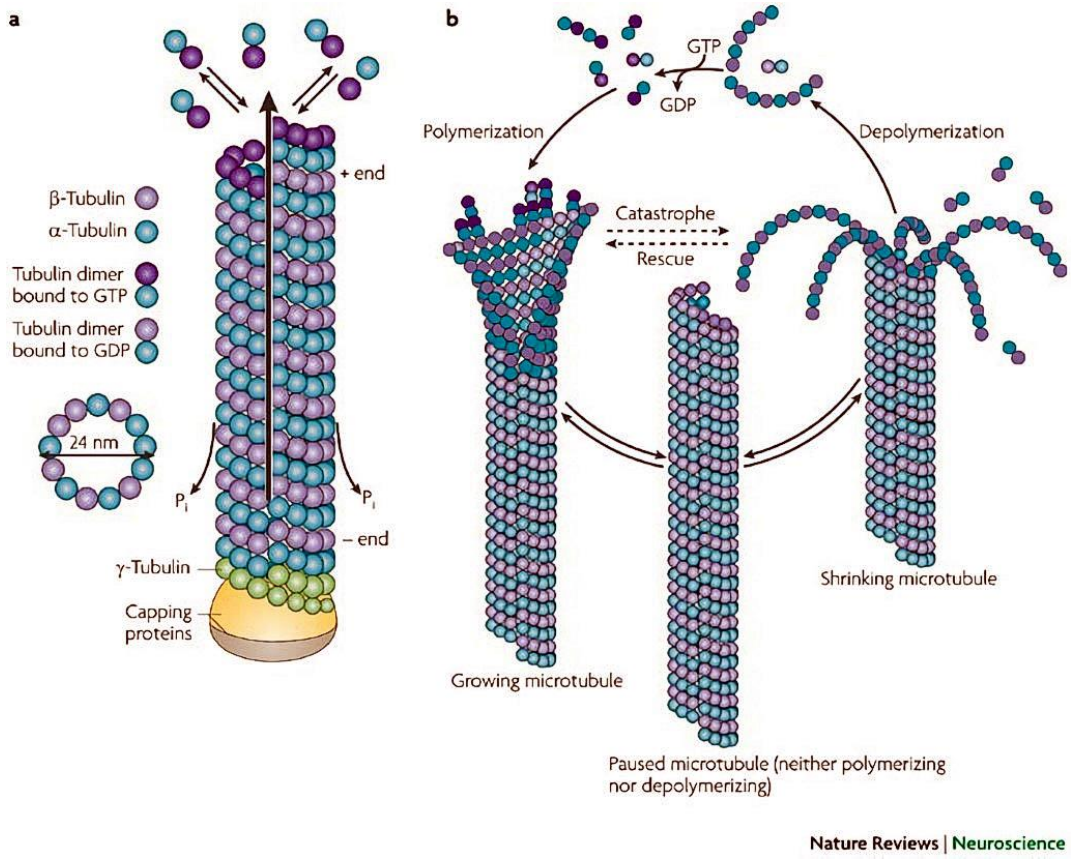

Figure 5. MT assembly, organization and dynamics: the basics. From Cecilia Conte and Alfredo Cáceres, Nature Neuroscience (2009).

1.4.2 Microtubule post-translational modification: "The tubulin code" hypothesis

The ‘‘tubulin code’’ hypothesis is analogous to the "histone code" concept and describes how PTMs of specific tubulin subunits within the polymer direct MT-based functions at that location[42].

Indeed, tubulin and MTs undergo a remarkable number of posttranslational modifications, including detyrosination and tyrosination, Δ2-tubulin generation, acetylation, polyglutamylation, polyglycylation, palmitoylation, sumoylation, phosphorylation and ubiquitylation[27,43]. These PTMs are found in all cells with MTs and they are particularly diverse in neurons, enriching specialized MT structures such as centrioles and basal bodies, neuronal axons, and primary cilia.

Tubulin can be modified as a soluble dimer or in a MT and both conditions can occur at the same time in the cells.

The majority of PTMs is associated with the C-terminal domains of α-tubulin, while few of them localize at the C-termini of β-tubulin as well as at other regions of the tubulin dimers (Figure 6). Many of these modifications occur concurrently and the level of each modification is distinctively regulated by the cell, depending on cell compartment, cell cycle, development and differentiation. In addition, MTs can be modified in a heterogeneous fashion, with different PMTs overlapping or localizing to distinct MT domains[44].

Therefore, the heterogeneity of these modification and the fact that multiple PTMs can occur on individual tubulin dimers has made very challenging our understanding of the rules that these modifications play in determining specific functions.

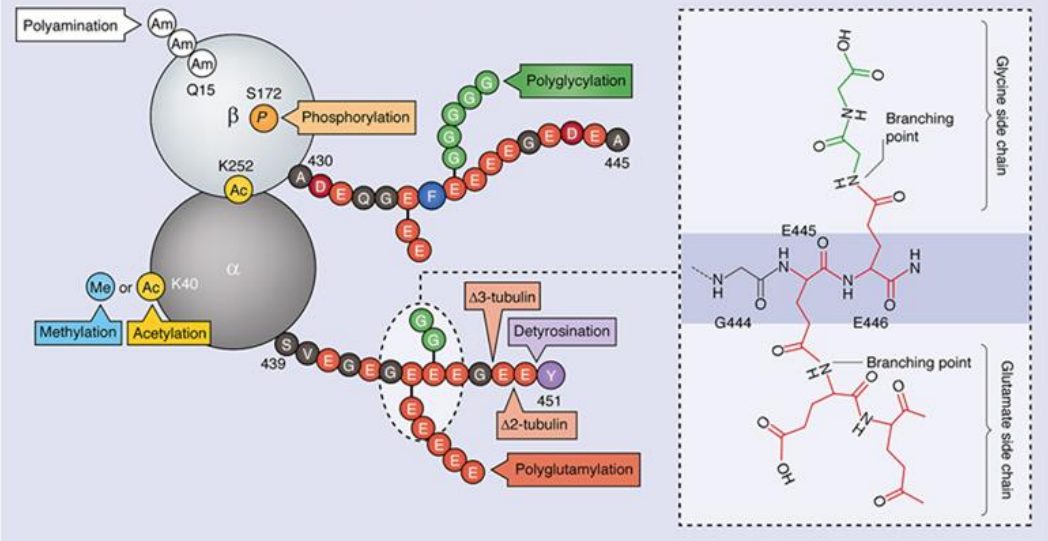

Figure 6. Representation of major tubulin PTMs. From Sudarshan Gadadhar et al., J Cell Sci (2017).

Most α-tubulins contain a C-terminal tyrosine residue which is cyclically removed and re-added during a special cycle of detyrosination-tyrosination.

This detyrosination-tyrosination cycle is conserved in evolution, yet its physiological importance is unknown. It initiates with detyrosination, which is mediated by an unidentified cytosolic carboxypeptidase (CCP) to expose a glutamate. Detyrosinated MTs are enriched in proximal segments of axonal shafts and appear to be associated to MTs longevity. Tyrosination is catalyzed by tubulin Tyr ligase (TTL), the first tubulin-modifying enzyme to be purified[45,46] and identified[47], and it is an ATP-dependent and RNA-independent modification localized prominently on axonal MTs at grown cones. TLL expression is critical for development as it has been observed that TLL-null mice die within 24 h after birth due to alterations in neuronal networks and organization[48].

Further removal of the next C-terminal Glu residue leads to the irreversible generation of Δ2- tubulin[49] and and Δ3-tubulin[50,51]. Even though the functional role of Δ2-MTs

remains poorly understood, it seems to be linked to MT stability as Δ2- tubulin is enriched in differentiated neurons as well as in centrioles and cilia[52].

Polyglutamylation and polyglycylation are extensions of glutamate or glycine side chains on C-terminus of both α- and β-tubulin, mediated by several TTL-like enzymes. Polyglutamilation is enriched in neuronal axons[53], centrioles and cilia[54,55] and it is believed to control MTs stability via interaction with severing enzimes[56]. In contrast to Polyglutamylation, polyglycylation is restricted to ciliary tubulin[55,57] and it seems to be important in the assembly and maintenance of primary cilia and cell proliferation.

Another important tubulin PTM that has been shown to contribute to MTs stability both *in vitro* and *in vivo* is called polyamination, a modification that adds positive charge through covalent addition of polyamines by a transglutaminase (TG2). TG2 has been reported as the primary intracellular tissue-type isoform in brain[58], with activity both in mammalian CNS and PNS[59].

Inhibiting polyamine synthesis or transglutaminase activity significantly decreases MT stability in nervous tissues both *in vitro* and *in vivo* in TG2 KO mice, particularly during development and maturation[60].

Several other PTMs have been identified on tubulin, which are less abundant or less common and, even though little functional insight has been gained, they appear to play an important role in the functional diversity of MTs. For example, phosphorylation of both α- and β-tubulin may be associated with the regulation of MT polymerization[61,62] or MT interaction with membranes[63]; glycosylation or non-enzymatic glycation occur on phosphorylated sites and may regulate protein-protein interaction and activity; palmitoylation could affect protein interactions with membranes and subcellular trafficking; ubiquitination and sumoylation (SUMO) of tubulin have been implicated in the proteolytic degradation of misfolded tubulin in cells, but adding a single ubiquitin

or SUMO may affect protein interactions, enzyme activity, protein transport or localization[64,65].

Tubulin arginylation and methylation[66] have also been reported, but no relevant functions have been provided so far. The recent discovery that MTs are methylated at K40 of α-tubulin, the same residue that is acetylated, is very intriguing as it suggests that methylation and acetylation may have opposing functionality for MTs as for many histone proteins[67].

MT acetylation was first discovered in the flagella of the single-cell green alga *Chlamydomonas reinhardtii* when, following the labelling with tritiated acetate, α-tubulin was found to contain tritium, indicating that the protein contains an acetyl moiety[68,69]. Few years later, thanks to amino acid sequencing and sequence comparison, Lys-40 was identified as the acetylation site, conserved from protists to mammals[70,71] but yeast[72]. Recent advances in proteomics has also identified other multiple acetylated sites on α- and β-tubulin[73], such as lysine 252 (K252) of β-tubulin catalyzed by the San acetyl transferase and expected to regulate MT polymerization[74]. However distributions and functions of other new acetylated sites remain unknown.

The enzymes involved in tubulin acetylation were identified long after the discovery of the modification itself. *In vitro* studies identified several candidates with acetyl-transferase activity including ARD1-NAT1 (arrest-defective 1-amino terminal, α-amino, acetyltransferase 1), suggested to mildly affect tubulin acetylation[75]; the transcriptional elongation regulator ELP3 (elongator protein 3), part of the acetyltransferase complex (ELP, elongator protein complex), shown to affect the acetylation of α-tubulin[76]; and the histone acetyltransferase GCN5[77] (homolog of yeast general control nonderepressible 5). However only recently, MEC-17 and the mammalian orthologue ATAT1 (alpha-tubulin acetyltransferase 1) were identified as

α-tubulin acetyltransferases[27,28]. They both belong to the GCN5 superfamily of lysine acetyltransferases, displaying sequence similarity which are conserved from protists to human[78]. Moreover ATAT1 is now considered as a major tubulin acetyltransferase in mammals, indeed deletion of the mouse gene leads to nearly complete loss of tubulin acetylation in embryos and various tissues[79–81].

On the contrary, enzymes that deacetylate MTs were much easier to identify. Indeed, around 15 years ago, HDAC6[82,83] and SIRT2[84] were shown to be responsible for MT deacetylation. Interestingly, both of the enzymes have additional substrates other than α-tubulin, with HDAC6 having more than 10 identified targets in the cytoplasm.

1.4.3 The role of tubulin acetylation in cell and disease

Acetylation of α-tubulin is the most-studied tubulin modification and it occurs after MT assembly at the ε-amine of α-tubulin Lys40, which is preserved in all α-tubulin isoforms.

The peculiarity of this modification site is its position in the lumen of MTs, therefore, the modifying enzymes need to access the luminal surface to execute their function. How the acetylase gain access to Lys40 has been unclear for many years and the mechanism of luminal entry has recently been described for αTAT1[85,86].

Since its initial discovery, tubulin acetylation has been considered a hallmark for long-lived MTs[49,87–89] as it was found mainly on stable MTs resistant to depolymerization condition induced by cold shock or nocodazole, but not on dynamic MTs such as those in neuronal growth cones[90,91]. However while some early reports supported this,

subsequent studies suggested that tubulin acetylation might be a consequence rather than a cause of enhanced MT stability[92–95].

Indeed, it has been observed that Atat1 overespression destabilizes MTs, but it is its interaction with them rather than its enzymatic activity that contributes to regulate MTs stability[92]. Moreover, in *C. elegans*, MEC-17 loss leads to MT instability and axon degeneration, independent of its acetyltransferase activity[96].

However these observations are not consistent with more recent discoveries where it has been shown that α-tubulin acetylation is required for the mechanical stabilization of long- lived MTs in cells by directly weakening inter-protofilaments interactions. Indeed, microfluidic manipulations demonstrates that inter-protofilaments sliding within the lattice enhances MTs flexibility as it facilitates MTs bending due to repeated mechanical stress generated by MT-based motors and actomyosin contractility. On the contrary, the flexural rigidity of deacetylated MTs has been observed to decrease following each consecutive bending cycle, implying that α-tubulin acetylation directly protects MTs from mechanical fatigue and ageing resulting from compressive forces. Moreover, further *in vitro* reconstitution experiments demonstrate that lack of α-tubulin acetylation makes MTs more sensitive to mechanical breakage, demonstrating that acetylation is directly involved in the modulation of MTs compliance under repeated mechanical stress and increases the mechanical resilience[97,98]. Another example of MT resilience through α-tubulin acetylation comes from the observation that removing MEC-17 from *C. elegans* touch receptor neurons causes severe lattice defects[99,28] that can be rescued by paralyzing the animals[96].

It is known that MEC-17/Atat1 is responsible for nearly all acetylation on α-tubulin in every organism studied[44]. In *C. elegans* touch reception neurons, tubulin acetylation regulates the protofilament number of MTs and it is necessary for maintaining MTs

structure[99,100]. Indeed MEC-17 loss was found to cause several morphological defects in touch receptor neurons as a result of MT defects and reduction of touch sensitivity. However, disappearance of touch sensitivity is not shown to be related to the acetyltransferase activity of MEC-17. Related to this, mice lacking Atat1 display similar morphological defects on sperm flagella[92]. It has also been observed a significant decrease in mechanosensitivity across all major fiber types innervating the skin with no impact on other sensory modalities, that is not due to generalized effects on neuronal function, such as axonal transport, axonal outgrowth *in vitro*, or in the ultrastructure of peripheral nerves and their innervation in the skin and spinal cord *in vivo*, but is caused by the ability of sensory neurons to covert mechanical forces into electrical signals[1].Therefore, in contrast to what has been observed in C. *elegans*, tubulin acetylation *per se* sets the optimal cell stiffness for touch sensation in mammalian mechanosensory neurons.

In addition to regulating MT architecture and cell mechanical elasticity, tubulin acetylation appears to be important in various cellular processes, including intracellular transport, ciliary assembly *in vitro*, cell migration and polarity. It has also been reported that one of the most frequent ER movement, the sliding along MTs, happens preferentially along acetylated MTs[101], suggesting a potential role in the trafficking of ER material to destinations that can also be present on modified MTs[102]. Moreover, tubulin acetylation regulates immune, stress, inflammation and viral responses under challenging conditions *in vivo*[103–107], suggesting potentially important roles under adverse conditions.

Tubulin acetylation is also involved in several neurological disorders.

Charcot-Marie-Tooth is a disorder of the peripheral nervous system due to a mutation in the 27-kDa small heat-shock protein (HSPB1) that causes axonal loss and decreased tubulin acetylation in mice, which can be rescued by HDAC6 inhibitors[108].

Parkinson´s disease (PD) is a common neurodegenerative disorder of the central nervous system that mainly affects the motor system and is caused by a combination of genetic and environmental factors. One of the most common gene implicated in the development of PD is the LRRK2 (leucine-rich repeat kinase 2) that interacts directly with β-tubulin and inhibits α-tubulin acetylation[109]. Parkinson's disease-associated mutations of these gene form filamentous subcellular structures in *Drosophila* that can be prevented by either the expression of Atat1 or the inhibition of HDAC6[110].

Amyotrophic lateral sclerosis, also known as Lou Gehrig's disease, selectively affects motor neurons in the motor cortex of the cerebrum. The cause is not known in 90% to 95% of cases. A possible implication of HDAC6 has been observed in known mice models for this disease. Indeed, loss of Hdac6 associated with increased tubulin acetylation, significantly extends survival of these mice and maintains motor axon integrity[111]. Moreover, HDAC6 may also be involved in dementia associated to Alzheimer´s disease. Inhibition of HDAC6 activity in mice, promotes tubulin acetylation and improves memory by reducing the level of the MT-associated protein Tau, a key marker for Alzheimer's disease[112] and significantly improves learning-based performance in mice with βamyloid-induced hippocampal lesions[113,114].

Tubulin deacetylation, on the other hand, is required for axonal growth and regeneration in a mouse model following injuries[115].

Tubulin acetylation has also been linked to cancer *in vitro*. In particular, elevated tubulin acetylation seems to play a role in breast and pancreatic cancers initiation and

progression[116,117], while loss of tubulin acetylation seems to be involved in multiple myeloma.

More recently, it has been observed that mice lacking α-tubulin acetylation display a profound loss of mechanical sensitivity to both light touch and painful stimuli with no impact on other sensory modalities[1].

2 Aim of the project

Our previous results indicate also that acetylated α- tubulin acetylation influences cellular stiffness and its loss lead to a decrease of cellular elasticity[1]. This is consistent and could be considered as a consequence of what has been observed in more recent discoveries, where acetylation directly increases MTs lattice plasticity, flexibility and resistance to breakage *in vitro*[97,98].

Intriguingly we observed that acetylated tubulin is highly enriched underneath the plasma membrane in peripheral sensory neurons, under the membrane of axons in the saphenous nerve and at sensory neuron terminal endings in the cornea[1].

For all these reasons, the goals of this project is to explore the ultrastructure of the sensory nerve endings and to examine MTs organization and structure along the sensory neuron axis, from DRG neurons to peripheral nerve endings, combining the advantage of different genetically labeled lines of mice with high resolution microscopy techniques, such as high-resolution confocal microscopy, super resolution microscopy and electron microscopy.

In brief, by learning about the ultrastructural organization of MTs and how they can be influenced by their acetylated status, in mammalian peripheral nervous system, this work may contribute to shed light for the first time on the role of MTs in mammalian mechanosensation.

3 Results

In this study I investigated, from an ultrastructural point of view, the contribution of MT acetylation to mammalian mechanosensation, taking advantage of transgenic mouse lines, *Avil-Cre::Atat1$^{fl/fl}$* (referred as Atat1^{cKO}) and *Deleter-Cre::Atat1$^{fl/fl}$* (referred as Atat1^{fullKO}), generated in our laboratory[1]. We assessed in our previous work that mice are viable and develop normally, except for a profound loss of mechanical sensitivity to both light touch and painful stimuli with no impact on other sensory modalities[1].

Here, I combined the advantage of the mice line mentioned above with high resolution microscopy techniques, such as high-resolution confocal microscopy, super resolution microscopy and electron microscopy to explore the ultrastructure of the sensory nerve endings and to examine MTs organization and structure along the sensory neuron axis, from the soma of DRG neurons to their peripheral endings, in the absence of mechanical stress.

In parallel with the ultrastructural characterization of mice tissues, I also performed a behavioral assay, the von Frey assay, following mechanical stress induced by spared nerve injury (SNI)[118], in order to investigate whether the deletion of the α-tubulin acetyltransferase Atat1 from peripheral sensory neurons and from the whole animal could also have some effect on the development of allodynia, which is a severe side effect of neuropathic pain.

3.1 Microtubules organization in sensory neurons

3.1.1 Super-resolution microscopy on sensory neurons from the Atat1^{control} and Atat1^{cKO} mice.

In our previous work, we showed by means of confocal microscopy that acetylated MTs form a predominant ring underneath the membrane of sensory neuron cell bodies and axons, while α-tubulin is broadly distributed across the cytoplasm. Intriguingly, this ring was not observed in non mechano-sensory cells, such as fibroblasts where acetylated α-tubulin is evenly distributed throughout the cell body[1]. Furthermore, it has been observed in osmosensory neurons that mechanotransduction is mediated by a unique interweaved MT organization throughout their soma[119]. We therefore asked whether a similar organization is also evident in peripheral sensory neurons, whether this structure is dependent upon the presence of acetylated tubulin and whether it could be involved in mechanosensation.

In order to investigate this aspect in more detail, super-resolution dSTORM (direct stochastic optical reconstruction microscopy) was performed on DRG neurons stained with the anti-α-tubulin antibody.

The super-resolution images showed that MTs are indeed characterized by an interweaved distributions (Figure 7a-d) in peripheral sensory neurons, similar to osmosensory neurons. No difference in the overall organization of MTs between DRG neurons from the Atat1^{control} and Atat1^{cKO} mice was observed, suggesting that acetylated tubulin is not responsible for that.

The images were also subjected to a quantitative, unbiased automated analysis, performed with the open source software CellProfiler, to measure MTs density, the number of MTs cross points and the angular variance of the MT cytoskeleton. The

results confirmed that no difference in the general MT network morphology was observed between the two genotypes (Figure 8a-i).

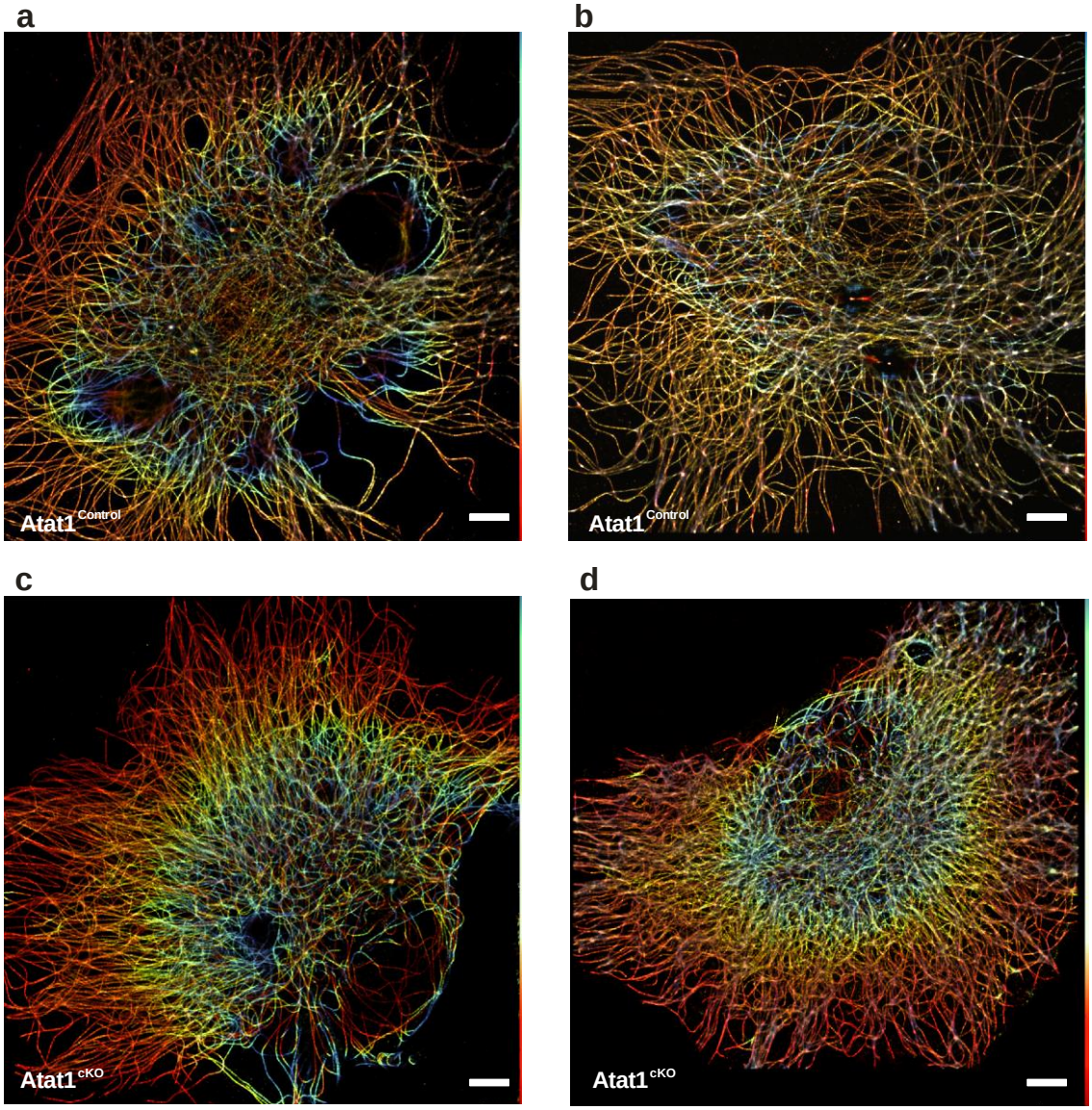

Figure 7. Super-resolution images of MTs in DRG neurons from Atat1^{control} and Atat1^{cKO}. (a-d) Immunostaining for a-tubulin on cultured sensory neurons analyzed by superresolution direct stochastic optical reconstruction microscopy (dSTORM) reveals MT network organization in Atat1^{control} (a and b) and Atat1^{cKO} (c and d). The color code indicates the distance from the objective (red close to objective, blue far away). (Scale bar 5 μm).

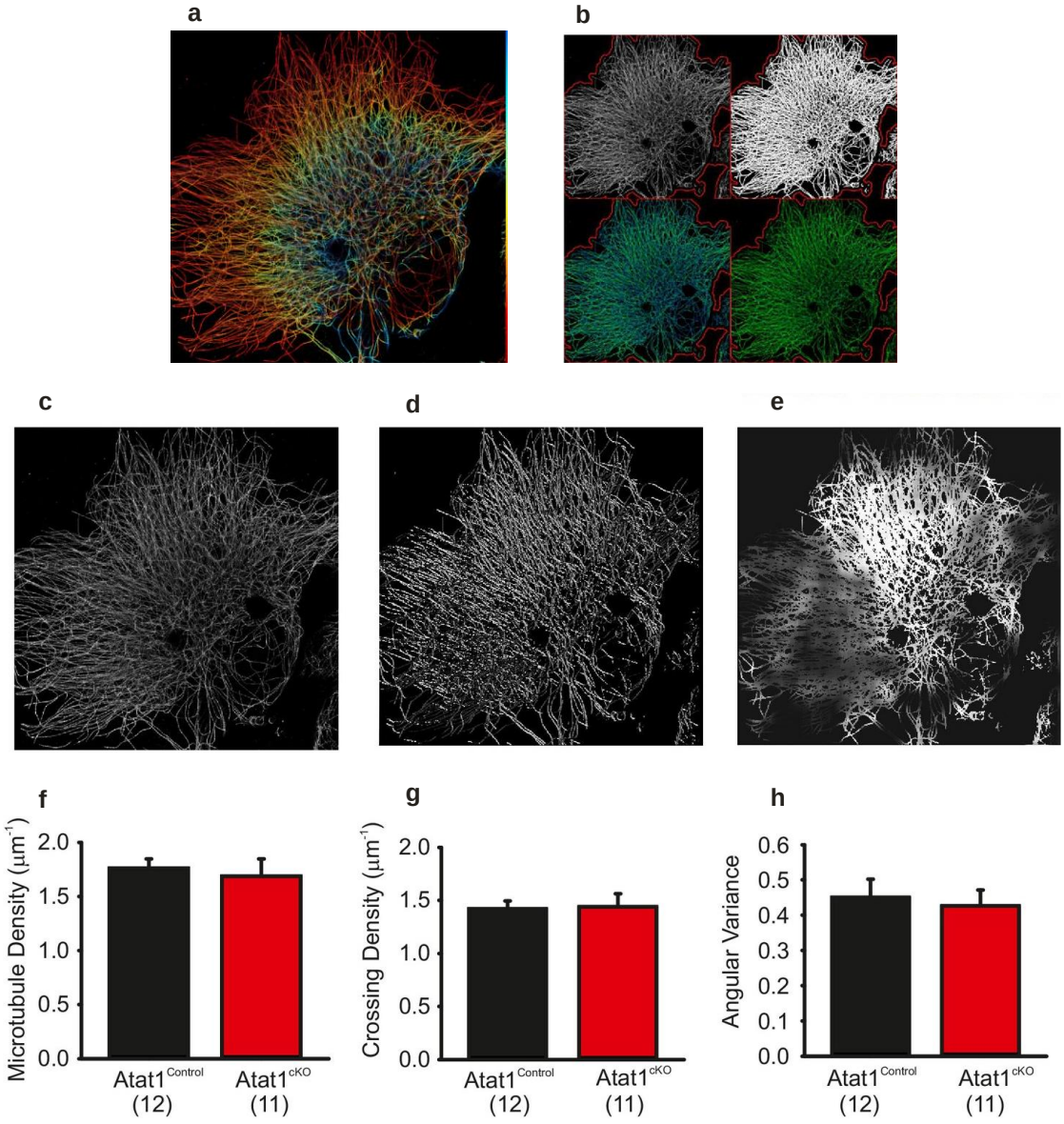

Figure 8. Graphical representation of automated analyses performed on superresolution images of anti - α tubulin stained cultured DRG. a) Superresolution image of anti α-tubulin staining of Atat1^{cKO} cultured DRG. b) The top left image shows the automated selection of the labelled neuron area marked in red. The top right image shows the MT image after binarization. The bottom left image shows a skeletonized MT network (in blue), which was used to evaluate the total area occupied by MTs, overlaid on the MT superresolution image (in green). Finally, the bottom right image shows the number of branch points present in the MT network, with MTs marked in green and the branch points in blue. c) Represents the MT original superresolution image in grey, d) the automatically determined orientation of the MTs, f) the local angular variance of the MT orientation. The bright pixels indicate a high variance and vice

versa. f) Graph showing the MT density in both Atat1^{Control} and Atat1^{cKO} cultured DRG. g) Graph summarizing the density of branch points present in the MT networks between the two genotypes. h) Graph representing the angular variance of the MT cytoskeleton between the two genotypes. No significant difference is observed between the genotypes in any of the parameter investigated. (t-test, $p>0.05$).Error bars indicate s.e.m.

3.2 Ultrastructural analysis of microtubules along the sensory neuron axis, from DRG whole mount and dissociated neurons to peripheral nerve endings, by Electron Microscopy (EM)

Different studies performed in *C. elegans* have shown that touch sensitivity is dependent on six touch receptor neurons (TRNs) that uniquely contain cross-linked bundles of heavily acetylated 15-protofilament MTs[26]. Targeted disruption of the molecular components of these MTs, MEC7 β-tubulin and MEC12 α-tubulin, and mutation of MEC-17, the major tubulin acetyltransferase[27,28] causes touch insensitivity[25,29], suggesting a specific role of the MTs and their acetylation status in the nematode mechanosensation. Moreover, it has been reported that loss of the acetyltransferase MEC-17 alters MT morphology in TRN (touch receptor neurons), which display variability in the number of protofilaments and reduction of MTs number[99]. However, it is yet not clear whether, in *C. elegans*, the loss of touch sensitivity observed is caused by the absence of tubulin acetylation in MEC-17 mutants[27,28] or by other unknown actions of MEC-17[27,29,99,120]. For instance, MEC-17

may play a structural role by binding to the luminal side of MTs and changing some of their key property, such as rigidity/flexibility, or else it could influence the transduction of signals originating from MTs.

In support of what has been reported by Akella et al. and Cueva et al. in *C. elegans*[27,100], we assessed in our previous work that mice lacking the α-tubulin acetyltransferase Atat1, the mammalian orthologue of MEC-17, display a significant decrease in mechanosensitivity across all major fiber types innervating the skin with no impact on other sensory modalities[1]. We also established that this is dependent upon the acetyltransferase activity of Atat1, and that mechanosensitivity can be rescued by mimicking α-tubulin acetylation genetically, in Atat1 deficient sensory neurons.

Our previous results also indicate that acetylated tubulin is highly enriched underneath the plasma membrane in peripheral sensory neurons, under the membrane of axons in the saphenous nerve and at sensory neuron terminal endings in the skin and the cornea, influencing cellular stiffness, elasticity and hence mechanotrasduction[1].

3.2.1 Microtubules organization in whole mount DRG and dissociated neurons from the Atat1^{control} and Atat1^{cKO} mice

For all the reasons listed above, here I sought to investigate whether the lack of Atat1 impact upon mammalian mechanosensation by affecting MTs morphology in DRG neurons and whole amount DRGs. Indeed, Irini Topalidou and colleagues observed that loss of the acetyltransferase MEC-17 alters MTs morphology in *C. elegans* TRN, which display variability in the number of protofilaments and reduction in the number of MTs[99]. In the light of these observation and our previous results, where we found that acetylated tubulin is highly enriched underneath the plasma membrane in peripheral sensory neurons, here I have been trying to determine whether and how the number of protofilaments in MTs changes under the cortex of the sensory neurons and compare it to the one in MTs distributed in the center of the cells, and whether there is variability in the MTs density between the Atat1^{Control} and the Atat1^{cKO} mice.

Freshly dissociated sensory neurons and whole mount DRG from Atat1^{control} and Atat1^{cKO} were prepared for transmission electron microscopy. Multiple protocols were tested in order to improve sample preservation and staining. For both samples, the first fixation was conducted by high pressure freezing (HPF) followed by freeze substitution over 1 day for sensory neurons, 5 days for DRGs, prior to plastic embedment. Seventy-nanometer transverse and cross sections were cut and post stained before imaging. A significant number of cells and MTs per cell is required to obtain statistically significant results.

Although I was able to obtain a good sample preservation, this was not sufficient to resolve at high resolution the protofilament number of MTs or to assess their density within the samples, neither in cultured cells nor in DRG. Indeed the cytoplasm appears too dense and full of features to properly identify MTs (Figures 9a-d and 10a-f).

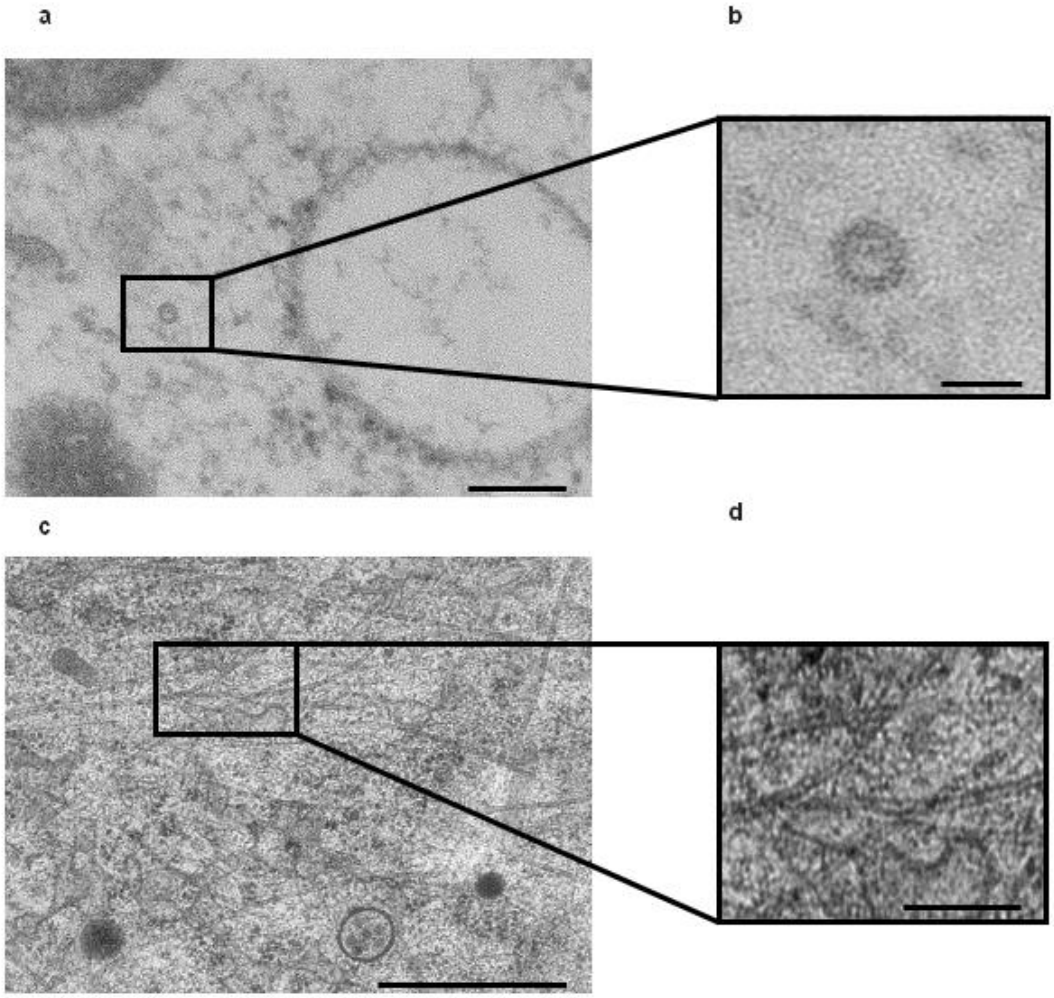

Figure 9. Transmission electron micrographs showing cross sections of whole mount DRGs from Atat1^{control} mice. Images b)-d) show a higher magnification of the images represented in a) and c). the images rapresent DRGs containing a cross section, a) and b), and tangential sections, c) and d), of MTs. (MTs are marked by black boxes. Scale bars: 100 nm image a), 50 nm image b), 500 nm image c) and 150 nm image d)).

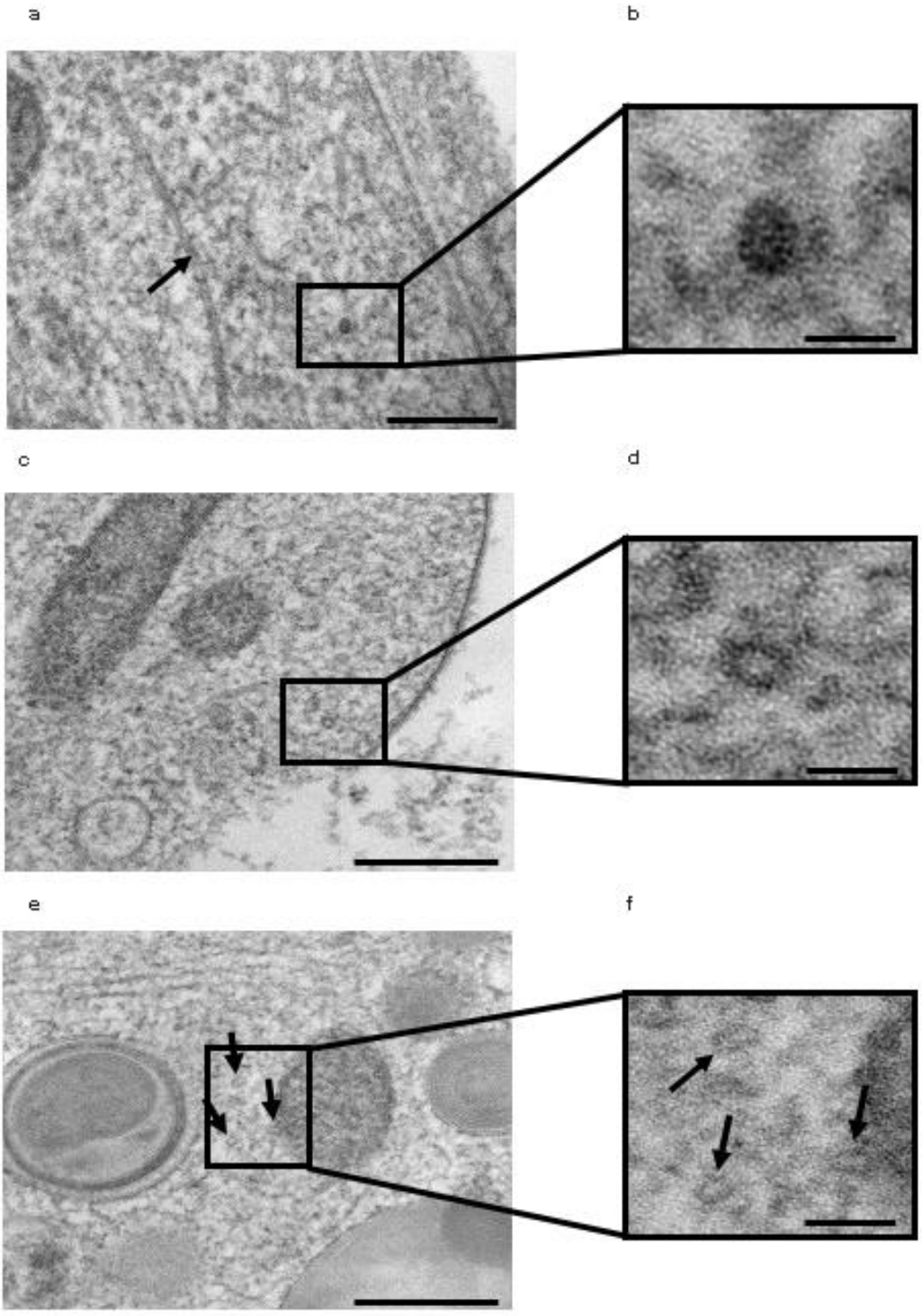

Figure 10. Transmission electron micrographs showing longitudinal sections of cultured DRG neurons from Atat1^{control} mice. b),d) and f) show a higher magnification of the images represented in a), c) and e), marked by black boxes. Cross sections in images a)-f), and a longitudinal section of MTs in image a) are highlighted by black arrows. (Scale bars: 100 nm image a), 200 nm images c), e) and 50 nm images b), d) and f)).

3.2.2 Microtubules organization in the saphenous nerve from the Atat1^{control} and Atat1^{cKO} mice

Here I continued to investigate the effects of Atat1 disruption on the organization of the MTs along the sensory neurons axis, with a focus on the saphenous nerve. The saphenous nerve fits very well with the purpose of this investigation as it is a cutaneous branch of the femoral nerve that contains only sensory afferents.

I optimized a fixation protocol, performing in parallel both chemical fixation and HPF, followed by FS on the Saphenous nerve of the Atat1^{cKO} and Atat1^{control} mice.

Samples were collected and immediately prepared for transmission electron microscopy and electron tomography. Multiple protocols were tested in order to improve sample preservation and staining. Seventy-nanometer transverse and cross sections were cut and post stained before imaging. Semi-thin serial sections (250 nm thick) were collected for electron tomography where each section was viewed at high resolution under multiple tilts to produce two single axis tomograms using marker alignment procedures and internal features to create weighted back-projection models of the tissue in 3D space.

I found that both the chemical fixation and the combination of HPF and FS give good results because not only it allows to count the number the protofilaments in MTs, but also to appreciate whether there is a difference, in the shape of MTs between the Atat1^{control} and the Atat1^{cKO} (Figure 11a-d and 12).

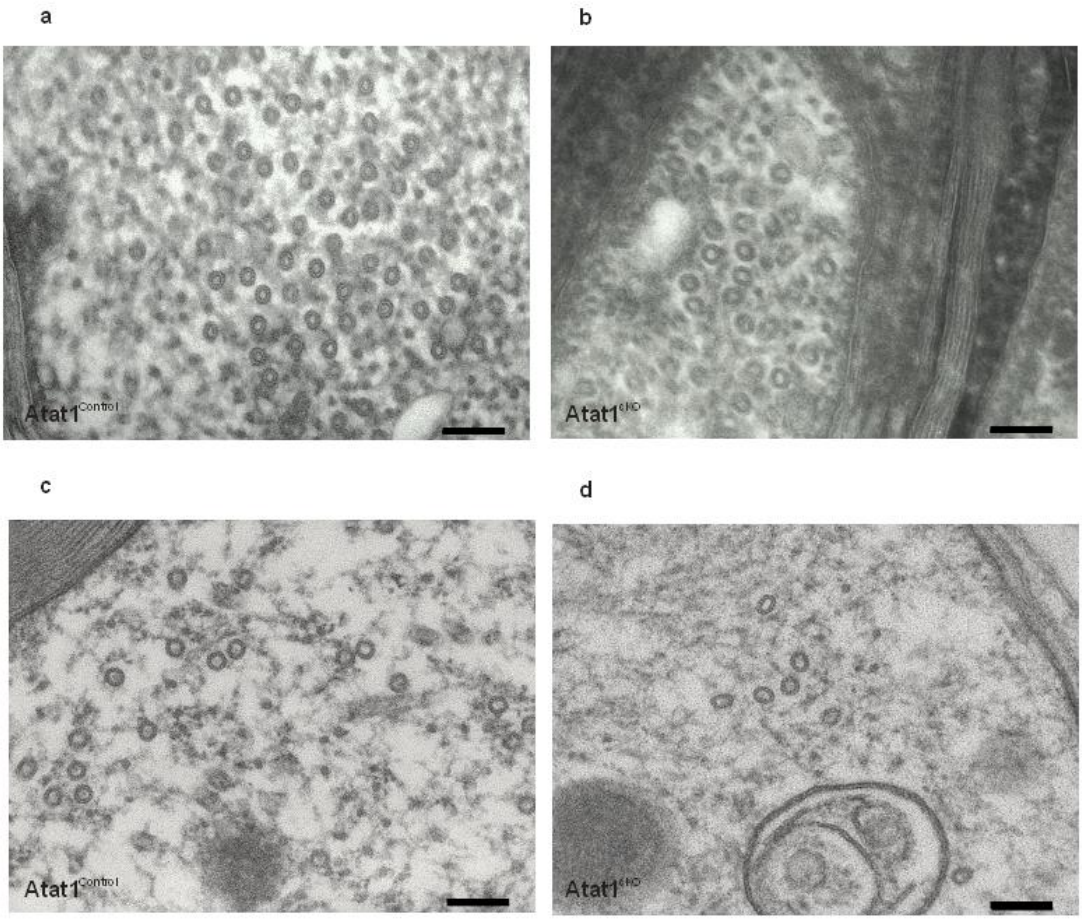

Figure 11. Transmission electron micrographs showing cross sections of chemically fixed saphenous nerve from Atat1^{control} and Atat1^{cKO} mice. a-d) show cross sections of MTs in chemically fixed (a and b) and HPF and FS (c and d) large myelinated primary afferent fibers from Atat1^{control} and Atat1^{cKO} mice (Scale bars 100 nm).

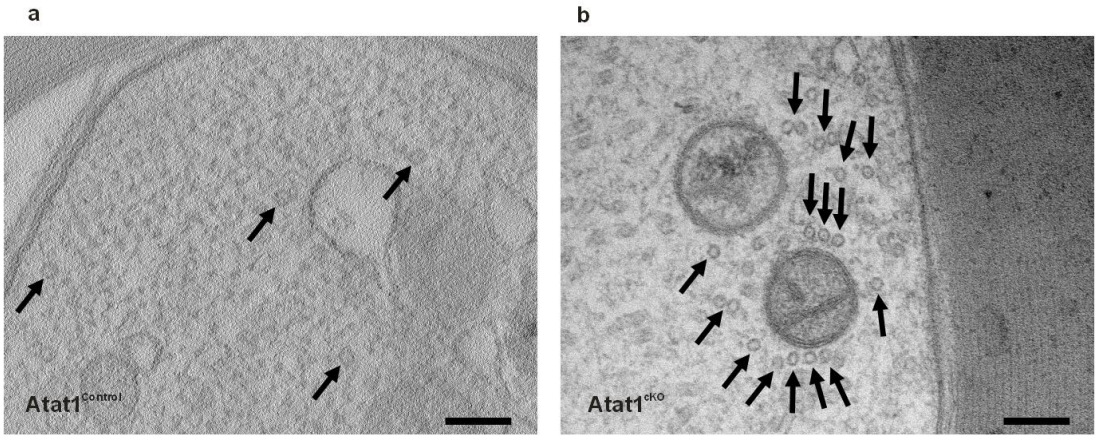

Figure 12. Tomographic slices showing showing cross sections of saphenous nerve from Atat1^{Control} and Atat1^{cKO} mice. a) and b)show cross sections of MTs in HPF and FS large myelinated primary afferent fibers from Atat1^{control} and Atat1^{cKO} mice (Scale bars 600 nm left and 300 nm right image).

Moreover, we reasoned that this aspect should have been assessed more quantitatively. Therefore, we further subjected the images to an unbiased automated analysis, using the open source software RELION (REgularized LIkelihood OptimizatioN).

This analysis is extensively used in Cryo-electron microscopy and consists on the computational averaging of thousands of images containing identical particles in order to achieve higher signal to noise ratio, taking advantage of software algorithms which allow to obtain structures at near-atomic resolution. Several steps are involved in structure determination by Single-Particle Cryo-EM which starts with the analysis of the 2D image dataset, including 2D clustering and generation of class averages, and leads to the 3D model of the specimen. The 2D class averages can be considered a "low resolution" sample refinement where heterogeneous particles (MTs in our case), with variable conformation or composition, are aligned and grouped into more homogeneous subsets using classification procedures.

We reason that including in our investigation only the "low resolution" refinement of the 2D image dataset would be sufficient to fulfill our demands. Indeed, particles are clustered according to their common features (orientation, number of protofilaments, broken or complete MTs) and MTs with the same protofilaments number, for instance, are grouped in the same class. On the contrary, in case of variability in the number of protofilaments or broken MTs, they would fall in different classes.

Initial data from the single particle averaging analysis, performed in collaboration with Shyamal Mosalaganti at EMBL in Heidelberg, show different representative classes of MTs: 5 for the Atat1^{Control} and 5 for the Atat1^{cKO} (Figure 13a, b). According to our results, no difference in the number of representative classes was observed between the Atat1^{cKO} compared to the Atat1^{Control}, suggesting that whether there are differences in MTs features, these seem to be the same in both genotype, as indicated by the same number of classes averages.

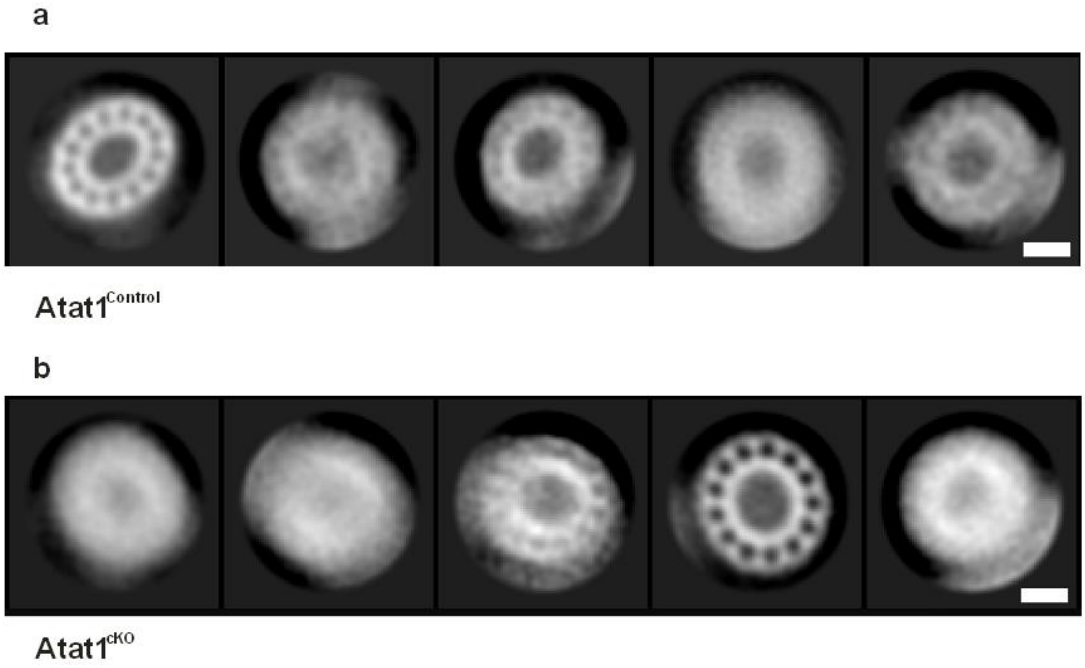

Figure 13. 2D clustering and formation of class averages. a) and b) show representative class averages obtained from 95 images Atat1^{Control} (N=953) and 105 Atat1^{cKO} (N=1358), respectively. Images of similar views are aligned and averaged to achieve higher signal to noise ratio. This process involves both rotational and translational shifting of individual particle images in order to group the data into more

homogenous subsets. Particles were aligned and classified using reference-free alignment and k-means classification programs implemented in RELION (Scale bar 10 nm).

Although this approach is extensively used for structure determination of vitrified specimen, we came across several limitations when adjusted it for our purpose.

One of the limitations we encountered is the size of the dataset. A successful analysis requires a dataset of over 10.000 particles and for the present study I was not able to obtain more than 1000 particles per genotype from 10 mice in total (5 $Atat1^{control}$ and 5 $Atat1^{cKO}$). The reasons for that are the variability of the number of MTs per fibers and the poor quality of the MTs due to sample preparation and orientation within the samples. The last problem is directly related to the second limitation of this method, which is the poor quality of the selected particles. Indeed, including too many poor particle may preclude an accurate classification.

Finally, it is not possible to determine whether the different classes obtained correspond to an average of particles differentiated exclusively on the basis of orientation, variability in the number of protofilaments, broken MTs or a combination of them.

For all the reasons listed above, the method turned out to be not eligible for our demands.

3.2.3 Assessing microtubules distribution and morphology using an image analysis pipeline

I reasoned that a different kind of analysis needed to be implemented in order to assess whether and how the loss of Atat1 activity affects MT architecture. Therefore, in collaboration with Jose Miguel Serra Lleti, a PhD student in Yannick Schwab team at EMBL in Heidelberg, we subjected the EM images to an image analysis workflow followed by different statistical tests.

A comparative study between two genotypes, $Atat1^{control}$ and $Atat1^{cKO}$, was carried out in a total of 13 saphenous nerve sections, belonging to a total of 8 mice (4 $Atat1^{control}$ and 4 $Atat1^{cKO}$), including left and right legs, when possible.

First of all, we sought to determine the average diameter of MTs that is based on the minimum diameter of the fitting ellipse surrounding the MT area or minor axis when the MT is complete. The minor axis is an indication of possible deformations in the MT structure and doesn´t change with the section angle if the full MT shape is present. On the contrary, a distribution of deformed shapes or massive changes in the number of protofilaments would have yield differences in the radius.

After random shuffling of the set of images, we cropped all MTs present on each image and considered for this analysis every MT taking into consideration the MT inner and outer diameter. Objects too blurry to identify a clear density or mixed with other densities in a way that was difficult to determine its shape were discarded.

Our analysis does not show any significant difference in the MTs small radius between the two datasets, suggesting that no change in MTs shape or size, arising from morphological defects can be observed in the $Atat1^{cKO}$ compared to the $Atat1^{control}$ (Figure 14).

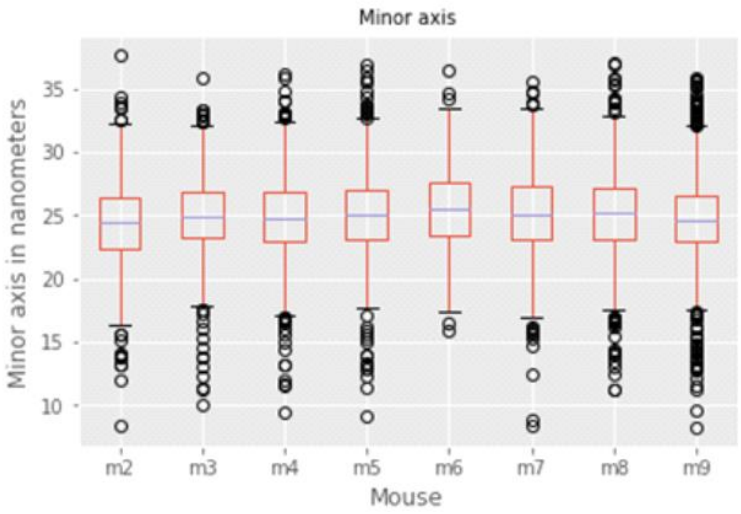

Figure 14. Graph showing the average value of the MTs minor axis per mouse.

Each box plot corresponds to an average value of the minor axis originates from the analysis performed on both legs of each mouse when possible (m2, m6, m7, m8, m9).

The average value is around 25 nm for all the samples investigated and the standard deviation between mice is enough to cover any variability between samples. In order to assess any possible differences between means, an ANOVA statistical test was also performed among all the mice samples, considering both legs when possible. The ANOVA test shows that some of the samples have indeed different populations (ANOVA Test, $p < 0.001$).

Hereafter we asked whether the loss of Atat1 may cause morphological defects in the MTs from the Atat1^{cKO} compared to the Atat1^{control} by measuring MTs eccentricity, as previously reported from Cueva et al., 2012[100]. Eccentricity is a measure of how much a conic section (a circle, ellipse, parabola or hyperbola) varies from being circular. A circle has an eccentricity of zero, so the eccentricity shows how un-circular the curve is. In our case, if there is a big number of MTs with deformations (elliptical), the eccentricity will hint a potential difference between Atat1^{control} and the Atat1^{cKO}.

Our results show a difference in the eccentricity distribution means between the two genotypes (Figure 15a). In particular, we observed slightly higher values of eccentricity in the Atat1^{cKO} compared to the Atat1^{control}. However the cumulative distributions plot

does not confirm this difference (Figure 15b), therefore, the discordant results for eccentricity measurements can´t be considered conclusive. Moreover, eccentricity is not likely a reliable feature to characterize MTs deformation as, besides MTs deformation, it can simply indicate a preferential angle of sectioning more prominent in some samples than in others, a sample handling or preparation effect, or it could be dependent on the regions of the sample where the sections are collected. For instance, there could be the case of a different arrangement and distribution of MTs located at the beginning of the sample compared to the ones in the center or towards the end. To prove that the difference we observed in figure 16 is really caused by deformation, we would need to use additional evidences.

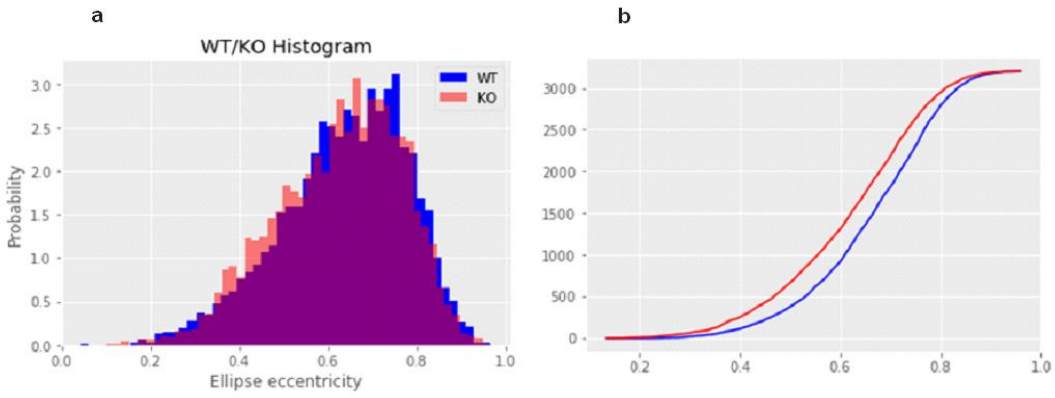

Figure 15. a) Histogram showing the distributions of the eccentricity means and b) representing the cumulative distribution of the eccentricity means from the Atat1^{control} and the Atat1^{cKO} mice. a) shows a slight difference in the distribution of eccentricity means between Atat1^{control} (blue) and the Atat1^{cKO} (red) mice (t-test; $p< 0.05$). b) Shows no significant difference between Atat1^{control} (blue) and the Atat1^{cKO} (red) for MT eccentricity (Kolmogorov test, $p>0.05$).

In the light of what we found so far, we reasoned that further parameters needed to be investigated, such as solidity.

Solidity describes the extent to which a shape is convex or concave. It is defined by the following equation: Area/Convex area, where the area of the shape region is divided by the convex hull area of the shape. The solidity of a convex shape is always 1.

We observed that the MTs from Atat1^{cKO} samples are less solid than the ones from the Atat1^{control}, indicating that they contain a larger number of broken MTs (Figure 16 a, b).

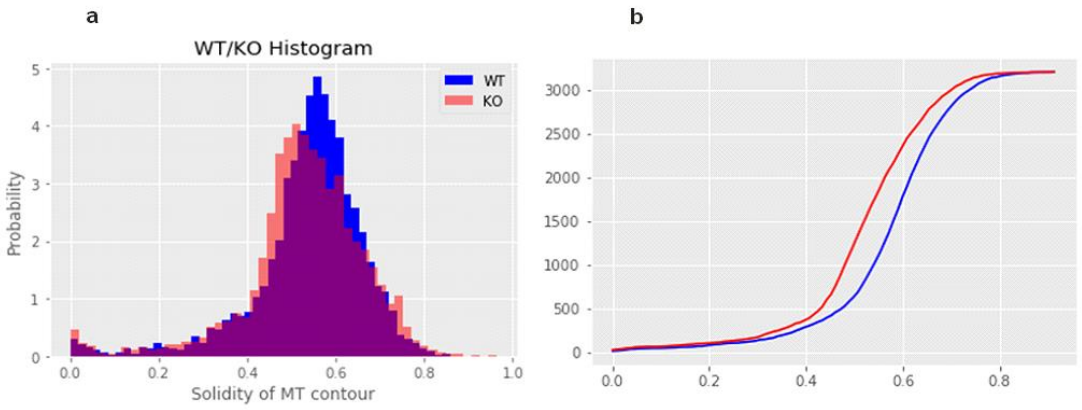

Figure 16. a) Histogram showing the distributions of the solidity means and b) representing the cumulative distribution of the solidity means from the Atat1^{control} and the Atat1^{cKO} mice. a) shows a slight shift between the two distributions, where the Atat1^{cKO} (red) is less solid than the Atat1^{control} (blu) (Maximum solidity is 1, minimum solidity is 0) (t-test; $p < 0.05$). b) shows no significant difference between Atat1^{control} (blue) and the Atat1^{cKO} (red) (Kolmogorov test, $p > 0.05$).

Moreover, we observed once more a high variability within samples from the same genotypes by plotting individual samples. (Figure 17a-h). In order to solve this conundrum and evaluate whether M2 M4r (right leg) and M5l (left leg) behavior is dependent upon sample preparation or handling, we decided to count and classify MTs

between broken or not broken (Figure 18a, b). The user didn't know *a priori* any information about the phenotype and images where randomized.

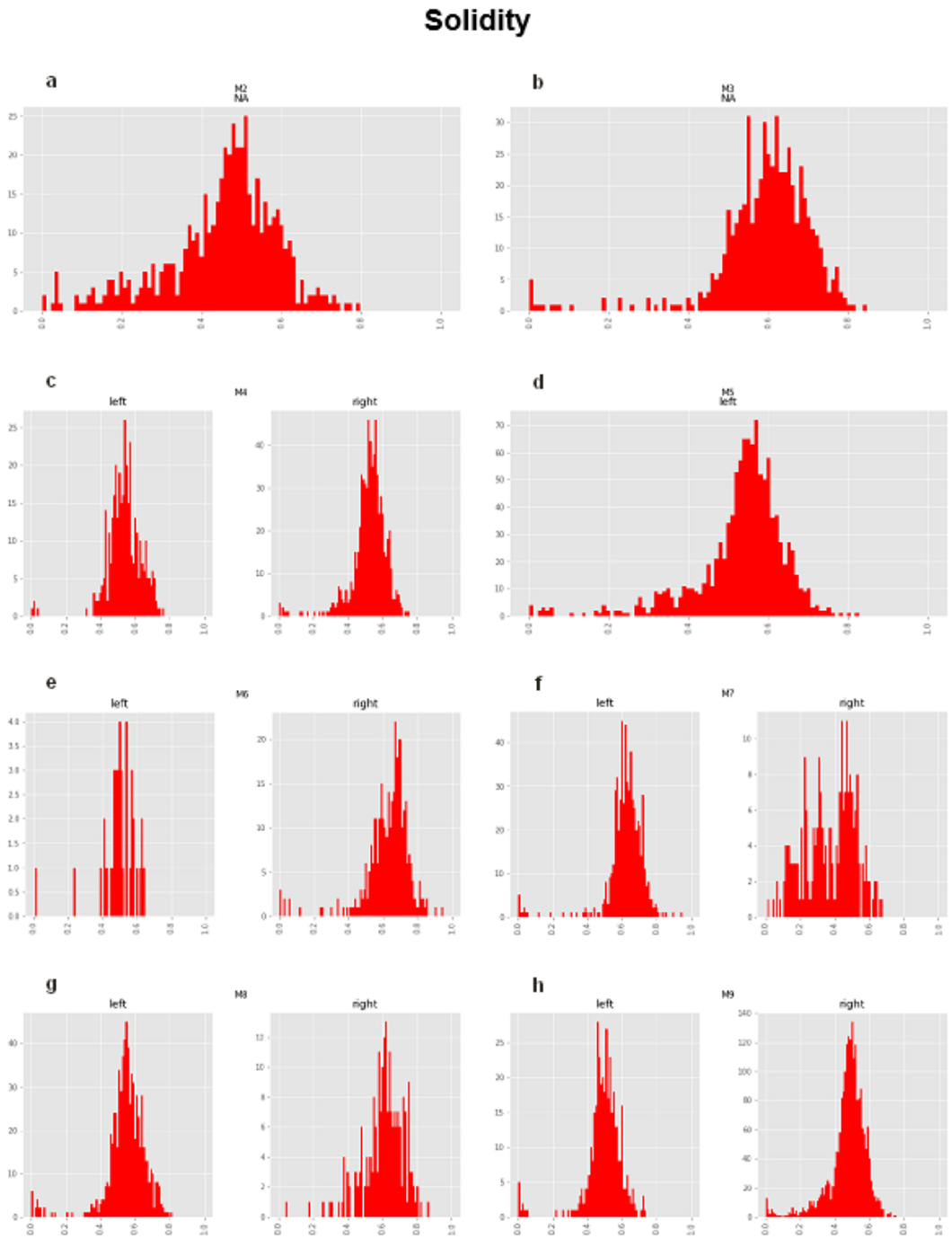

Figure 17. Histograms showing the distributions of the solidity means in Atat1^{Control} and Atat1^{cKO} mice (M2-M9). Both legs are considered separately when possible (M2, M6-M9).

a)-h) Individual histograms show that there is a variability in the distribution of the solidity means within samples belonging to the same genotypes (M2-M5 correspond to Atat1^{Control}, M6-M9 correspond to Atat1^{cKO}). The Atat1^{Control} M2, M4r, M5l and the Atat1^{cKO} M6l-r, M7r and M9l-r for instance, even though belong to different genotypes, show a similar distribution with a relative increase of number of MTs characterized by values below 0.5 in the histograms.

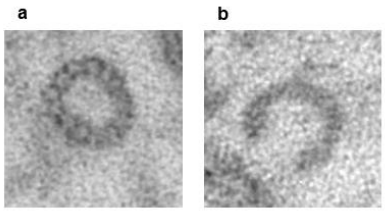

c

	Atat1^{Control}					Atat1^{cKO}							
	M2	M3	M4R	M4L	M5L	M6L	M6R	M7L	M7R	M8L	M8R	M9L	M9R
BROKEN	12	20	51	15	56	18	36	30	18	24	13	13	91
NORMAL	209	538	933	499	1106	181	818	810	403	860	353	299	2215
	0.057416	0.037175	0.054662	0.03006	0.050633	0.099448	0.04401	0.037037	0.044665	0.027907	0.036827	0.043478	0.041084

Figure 18. Transmission electron micrographs showing cropped cross sections of MTs in the saphenous nerve from Atat1^{control} and Atat1^{cKO} mice. Image a) shows an example of not broken MT while image b) shows a broken MT (Scale bar 40 nm). c) The table shows the counting of normal vs broken MTs and the ratio between the two values per each mouse´s leg, when possible.

The results shows that M2, M4r, M5l (Atat1^{control}), M6l-r, M7r and M9l-r (Atat1^{cKO}) have the highest number of broken MTs. According to these observations, we were not able to assess any significant difference between the two genotypes as we observed the presence of broken MTs in both.

Additionally, by observing individual samples we found that within the 4 Atat1^{cKO} samples analyzed, only M7r and M9l have indeed an abundance of broken MTs, as it is shown from minor axis, eccentricity and solidity distributions of individual histograms (Figure 19).

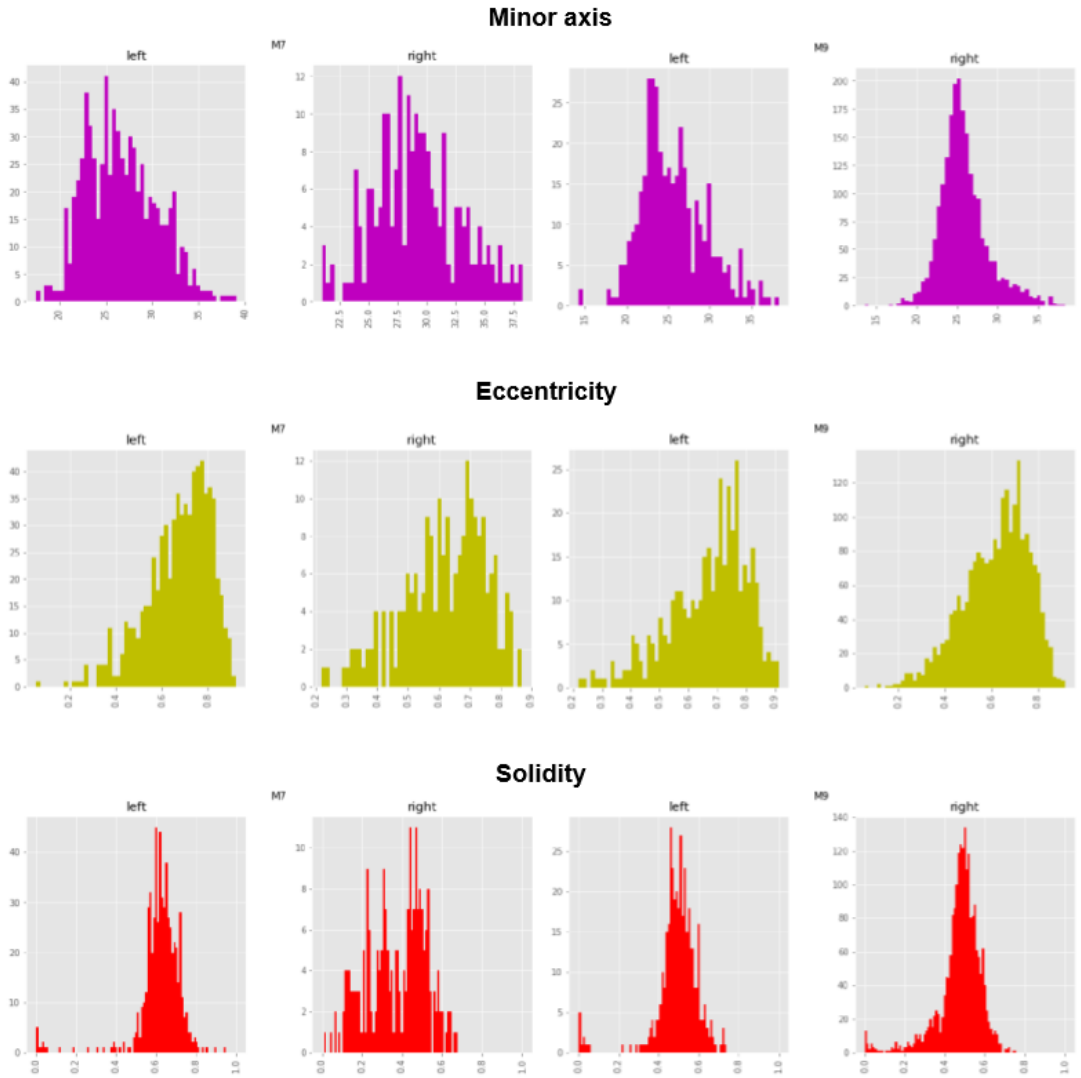

Figure 19. Comparison of Individual histograms showing the minor axis, eccentricity and solidity distributions from both legs of the Atat1^{cKO} M7 and M9. The histograms show variability in the individual distributions for minor axis, eccentricity and solidity in M7r and M9l as indicated by an increase of number of MTs characterized by values below 0.5. The slight variability observed, in only one of the two legs analyzed, is not statistically significant when compared to the Atat1^{control} samples.

However, the results are not consistent as broken MTs were observed only in one leg (Figure 20). We reasoned that this effect can´t be explained by the simple presence of Atat1^{cKO} and hypothesize that other factors in the experimental settings may have affected the sample status, such as mouse history and sample handlings.

The main conclusions of the image analysis pipeline, described above, are summarized as follows:

- No major differences were observed between Atat1^{Control} and Atat1^{cKO} when minor axis, eccentricity and solidity were compared.
- Although M7r and M9l Atat1^{cKO} show a massive disarrangement in MTs distributions for all the parameters investigated, these data are not consistent as were observed in only one of the two legs analyzed and in 2 mice out of 4.
- By comparing the two datasets (from Atat1^{Control} and Atat1^{cKO}) for all the parameters investigated, we are not able to claim dramatic changes in MTs morphology between the two genotypes in the absence of mechanical stress as reported in *C. elegans* and more recently by in vitro observations.

3.2.4 Microtubules organization in whole mount DRG and dissociated neurons from the Atat1^{control} and Atat1^{cKO} mice by CEMOVIS.

Since CEMOVIS is a specialized technique requiring advanced EM skills, I benefited from a collaboration with the Electron Microscopy Core facility (EMCF) at EMBL in Heidelberg.

Here, to overcome the difficulties encountered with samples processed through HPF followed by FS, that may be due to the treatment with chemicals and heavy metals that could have masked the clear visualization of MTs in the sample, I reasoned to subject

the samples in question to CEMOVIS (Cryo-EM of vitreous sections) where they are preserved by rapid freezing, cryo-sectioned and observed by cryo-TEM without further contrasting and embedding.

However, also in this case we encountered some technical problems with the sample preparation as neither cultured cells nor DRGs firmly attached on the EM substrates. For this reason, many samples were lost during HPF that was used as fixation step. Moreover, the few samples we managed to collect were not well preserved most likely because not attached properly.

Since more time was required to optimize a sample preparation protocol in order to obtain a statistically significant number of samples for our observations, I reasoned to invest more time on the saphenous nerve of which I managed to have good sample preparation.

3.2.5 Microtubules organization in the saphenous nerve from the Atat1^{control} and Atat1^{cKO} mice by CEMOVIS

As mentioned above, this technique allows to preserve the sample close to native state since it does not require the use of heavy metals for sample preservation. Indeed, heavy metals are one of the sources of image artifacts as they give rise to complex chemical reactions where ion and water shifts cause changes in volume of cellular and subcellular compartments. On the other hand, cell organelles might be deformed or new cell structures are generated leading to membrane fusion or alteration of cytoskeletal components.

Therefore, I reasoned that a comparison of this technique with plastic embedding would be required to confirm our previous observations.

The Cryo-EM images represented in figure 20 show that there is no difference between the $Atat1^{control}$ and $Atat1^{cKO}$ mice, confirming what I already observed with conventional TEM and image analysis. MTs imaged in their native-like state do not show any morphological defect in the $Atat1^{cKO}$ samples compared to the control groups.

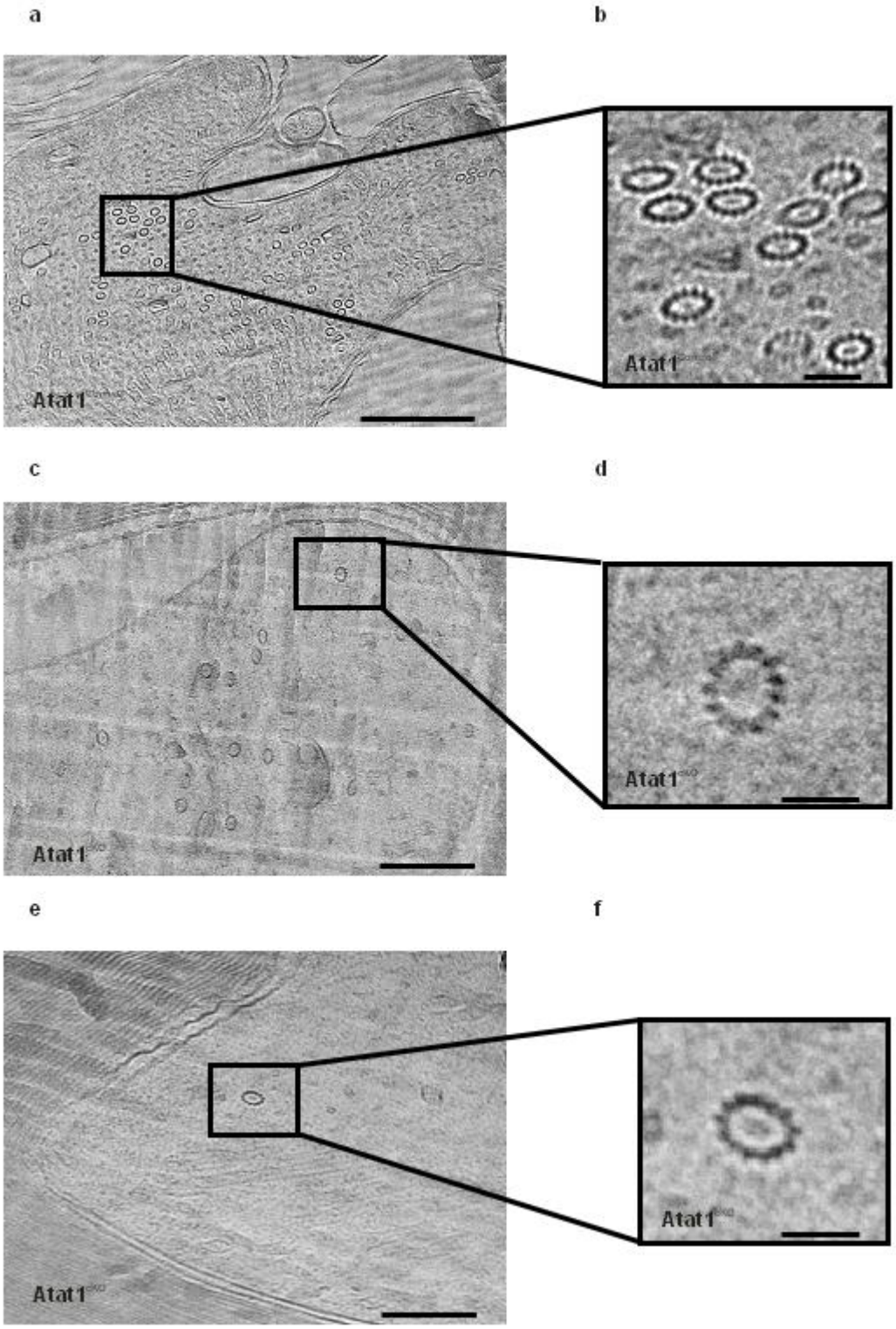

Figure 20. Imaging of vitreous sections by cryo-electron microscopy showing cross sections of saphenous nerve from Atat1^{control} and Atat1^{cKO} mice. b), d), and f) show a higher magnification of cross sections of MTs in large myelinated primary afferent fibers from Atat1^{control} (a) and Atat1^{cKO} mice (c and e) (Scale bar 150nm a), 20nm b), 100nm c) and e), 40nm d) and f)). In the images represented above it is possible to clearly appreciate protofilaments in almost all MTs (highlighted by black arrows)

3.3 Analysis of mechanical allodynia-like behavior induced by Spared Nerve Injury in the mouse

The spared nerve injury (SNI) model is described as a mouse model of peripheral neuropathic pain and involves the ligation of two of the three branches of the sciatic nerve (the tibial nerve and the common peroneal nerve), while the sural nerve is left intact[118,121].

The SNI model induces symptoms of neuropathic pain such as mechanical allodynia i.e. pain due to tactile stimuli that do not normally provoke a painful response[122]. Behavioral modification resulting from mechanical allodynia is quantified by von Frey filaments of increasing bending force, which are repetitively pressed against the lateral area of the paw[123] that is innervated by the spared sural nerve.

SNI is a well-established model of induced mechanical allodynia in mice and I used it here also as method to induce mechanical stress *in vivo.*

We demonstrated in a previous work that the deletion of the α-tubulin acetyltransferase Atat1 from mouse peripheral sensory neurons causes a strong reduction of cutaneous mechanical sensation, with a strong impact on both light touch and pain and no effect on other sensory modalities[1]. It is yet not known whether the lack of α-tubulin acetylation impact on mechanosensation by affecting MTs morphology. I demonstrated, in this work, that deacetylated MTs morphology does not change when compared to acetylated MTs under physiological condition in mice. On the other hand, recent *in vitro* observation demonstrated that deacetylated MTs are more susceptible to breakage when subjected to mechanical stress. Therefore it is interesting to investigate whether MTs morphology and mouse behavior change under mechanical stress conditions in both $Atat1^{cKO}$ and $Atat1^{fullKO}$ mice.

The von Frey test was performed at different time point after surgery (Figure 22a, b). Here I found that both Atat1^{cKO} and Atat1^{fullKO} mice seem not to develop allodynia compared to the Atat1^{Control} mice until day 14 post SNI. Interestingly they do develop allodynia at day 21 post SNI where no significant differences have been observed anymore compared to the control group (Figure 21).

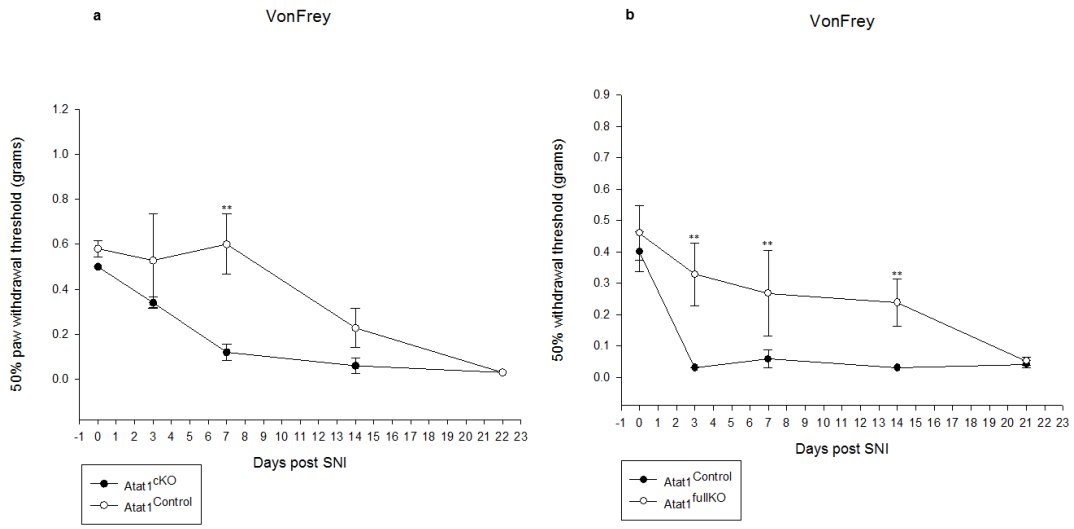

Figure 21. Graphs showing 50% withdrawal thresholds to von Frey hairs after SNI to test mechanical allodynia in the hind paw of Atat1^{control} , Atat1^{cKO} and Atat1^{fullKO} mice. Baseline withdrawal thresholds were assesses in both cases 24 hr prior to SNI. Withdrawal thresholds were assessed at 2, 7, 14, 21 days following SNI. a) Graph of von Frey thresholds showing the significantly lower response frequency in Atat1^{cKO} animals (Two-way RM ANOVA, Holm-Sidak method, $p<0.001$). At day 21 there is no significant difference anymore in the response frequency between the Atat1^{cKO} and Atat1^{Control} groups. b) Graph of von Frey thresholds showing the significantly lower response frequency in Atat1^{fullKO} animals (Two-way RM ANOVA, Holm-Sidak method, $p<0.001$). As per Atat1^{cKO} mice, at day 21 there is no significant difference anymore in the response frequency between the two genotypes. (n = 5-6 mice per treatment group).

4 Discussion

In a previous work we found that lack of α–tubulin acetylation from mammalian peripheral sensory neurons causes a profound loss of mechanical sensitivity in mouse, exclusively affecting light touch and pain sensations[1]. We reasoned that such phenotype arises from structural changes in MTs. Therefore, in this thesis I explored whether and how lack of α–tubulin acetylation affects MTs ultrastructural organization in mammalian cells and tissues by means of high resolution light microscopy and electron microscopy as well as image analysis.

In parallel with the ultrastructure investigation, a behavioral assay called von Frey assay was also performed on mice lacking α-tubulin acetylation compared to the control, following mechanical stress induced by SNI, in order to investigate whether the deletion of the α-tubulin acetyltransferatse Atat1 from peripheral sensory neurons and from the whole animal could also have some effect on the development of allodynia, which is a severe indication of neuropathic pain. Indeed recent *in vitro* studies showed that lack of α–tubulin acetylation renders MTs more susceptible to breakage under mechanical stress[97,98]. Therefore, here, I sought to investigate whether this is also the case in mammals and how this could impact upon the development of allodynia induced by mechanical stress, such as SNI.

4.1 Lack of α-acetylated tubulin does not affect the overall organization of microtubules in mammalian peripheral sensory neurons

Mechanotransduction is the ability of living organisms to sense and respond to mechanical forces by converting them into a biological response. This mechanism is present in eubacteria, archaea and eukarya and is essential for many physiological processes, such as the sense of touch, proprioception, hearing as well as homeostasis.

In mammals, mechanosensation is mediated by specialized sensory neurons which are capable of detecting a wide range of mechanical stimuli, relying on the presence of mechanotransducer channels on sensory nerve endings. Surprisingly, little is known about the properties of sensory mechanotransducers in mammals and thus the mechanisms that convert mechanical forces into electrical signals at the peripheral endings of sensory neurons and, especially how the cytoskeleton influences it. *In vivo* studies in *C. elegans* reported that touch sensitivity is dependent on both the actin binding protein β spectrin[24] and the MT cytoskeleton[25]. In particular, in *C. elegans*, specialized touch receptor neurons (TRNs) sense gentle touch and uniquely contain cross-linked bundles of heavily acetylated 15-protofilament MTs[26]. Targeted disruption of the molecular components of these MTs, MEC7 β-tubulin and MEC12 α-tubulin, and mutation of MEC-17, the major tubulin acetyltransferase[27,28] causes touch insensitivity[25,29], suggesting a specific role of the MTs and their acetylation status in the nematode mechanosensation.

In support of this, it has been reported that acetylated MTs may also have an important function in mouse sensory neurons, as these neurons have amongst the highest level of α-tubulin acetylation in the mouse[30]. Moreover, we have assessed in our previous work

that mice lacking the α-tubulin acetyltransferase Atat1, the mammalian orthologue of MEC-17, display a significant decrease in mechanosensitivity across all major fiber types innervating the skin and a reduction of the amplitude of mechanically activated currents in sensory neurons, strongly affecting light touch and pain, with no impact on other sensory modalities[1]. Since this effect was not due to generalized effects on neuronal function, such as axonal transport, axonal outgrowth *in vitro*, or in the ultrastructure of peripheral nerves and their innervation in the skin and spinal cord *in vivo*, we reasoned that such phenotype may arise from the lack of a sub-membrane ring of acetylated α-tubulin that somehow sets the mechanical rigidity of the cells, rendering them more resistant to mechanical deformation[1].

Indeed, we observed that acetylated tubulin is highly enriched underneath the plasma membrane in peripheral sensory neurons, under the membrane of axons in the saphenous nerve and at sensory neuron terminal endings in the skin and the cornea.

How α-tubulin acetylation is capable to set cellular rigidity remains poorly understood. It has been observed in mammalian osmosensory neurons from the hypothalamus that mechanotransduction is mediated by a unique interweaved MT organization throughout their soma[119]. We therefore asked whether a similar organization is also evident in peripheral sensory neurons, whether this structure is dependent upon the presence of acetylated tubulin and whether it could be involved in mechanosensation.

According to the results obtained with superresolution dSTORM microscopy, where I explored the overall organization of the cytoskeleton in peripheral sensory neurons from the $Atat1^{cKO}$ and $Atat1^{control}$ mice, we observed that, similar to osmosensory neurons, MTs distribute in an interweaved fashion towards the center of the cells. However, no differences or alterations in MTs distribution and arrangement were observed in the absence of Atat1. This results suggest that lack of acetylation do not

affect the gross organization of MTs in sensory neurons, hence it would be interesting to investigate whether the increase of cell stiffness observed is a direct consequence of the increase of MTs rigidity or it arises from secondary effects, such as interaction with other membrane and cytoskeleton components.In light of this results, I reasoned that imaging MTs at higher resolution, using electron microscopy, may give insights into this process.

Moreover, further observations are required to confirm that acetylated tubulin is indeed localized under the membrane of axons and especially neuronal endings in the cornea or in the skin, where mechanotransduction is known to take place *in vivo*. I think that electron microscopy is more suitable than superresolution microscopy to address this particular question considering the high density of MTs in the axons which makes them difficult to differentiate using superresolution microscopy. Therefore, I reasoned that the higher resolution provided by electron microscopy is required in this context.

4.2 Ultrastructural analysis performed on afferent fibers from mouse saphenous nerve, combining EM and Cryo-EM, show that lack of Atat1 does not affect microtubules morphology in the absence of mechanical stress

In contrast to what has been observed in *C. elegans* where α-tubulin acetylation is required for MTs organization but not for touch sensitivity[29,99,120], we demonstrated in our previous study that acetylated MTs are likely responsible for the loss of mechanosensation in Atat1^{cKO} mice[1] suggesting that the two organisms may use Atat1 differently in regulating mechanosensation.

Our data are supported from other models where MTs have been shown to be involved in mechanotransduction, such as *Drosophila* larval dendritic arborization neurons[11] and mammalian osmosensory neurons[119].

How the acetyltransferase activity of Atat1 is able to control touch sensation in mice is not yet known. Our previous results suggest that tubulin acetylation sets the cellular mechanical elasticity, modulating the force distribution in neural membranes, which would be altered in its absence due to a disorganization of MTs network. Therefore, its lack renders cells stiffer and more force is required to indent the plasma membrane and activate mechanosensory channels[1].

In light of the results obtained by superresolution microscopy where the overall organization of MTs seems not to be altered by lack of acetylation, I sought to investigate, taking advantage of more powerful techniques such as EM and Cryo-EM, whether the increase of cellular stiffness associated to a profound loss of

mechanosensation in mouse sensory neurons and sensory fibers innervating the skin is due to local alterations of the MTs structure.

Albeit it is known that, *in vivo*, mechanotransduction occurs at sensory neuron endings, our previous work *in vitro* shows that also the soma of sensory neurons is mechanosensitive as we observed a reduction in mechanically activated currents in sensory neurons upon Atat1 deletion[1]. Moreover, we detected a sub-membrane localization of acetylated tubulin not only in the soma of sensory neurons and at neuronal endings in the cornea, but also in the afferent nerve fibers within the saphenous nerve, which are not in themselves mechanosensitive. Therefore, in this work I sought to investigate whether and how MTs organization and structure change along the sensory neuron axis, from the soma of DRG neurons to their peripheral endings, upon Atat1 deletion. However, I was not able to explore MTs morphology by EM neither in sensory neurons nor in neuronal endings in the cornea. Indeed, in both cases the cytoplasm appeared to be too dense and rich of features to clearly distinguish MTs and its protofilaments. Moreover, sensory neurons in culture were too fragile and sensitive to grow and properly attach on Cryo-EM supports. In addition, more time was required to implement EM and Cryo-EM sample preparation protocols.

Here, combining high-resolution transmission electron microscopy with image analysis, I investigated MTs morphology and distribution in the saphenous nerve from $Atat1^{control}$ and $Atat1^{cKO}$ mice.

Our results demonstrated that no major differences were observed between MTs from the $Atat1^{cKO}$ compared to the $Atat1^{control}$ when minor axis, eccentricity and solidity were compared. These results were also confirmed by Cryo-EM observations, suggesting that lack of acetylation does not affect MTs ultrastructure in mammals in the absence of mechanical stress. Indeed, axons may be subjected to mechanical stress to

a lesser extent compared to peripheral endings *in vivo*, which, on the contrary, present more direct contacts with the environment through the skin.

I speculated that the slight difference in solidity measurements observed between the two genotypes, where the Atat1^{cKO} samples are likely more deformed or broken, may be a consequence of mechanical stress due to several reasons, including sample handling and mouse life history and it is depend upon the topology of the sample. In support of our hypothesis, recent *in vitro* observations demonstrated that acetylation directly protects long-lived MTs from rupture due to mechanical stress and it is particularly enriched in regions of high curvature, suggesting that Atat1 acetylates preferentially regions experiencing mechanical stress[124,125]. Using a system that involves microfluidics manipulations, where MTs are subjected to a cycle of consecutive bending forces to simulate the effect of repetitive intracellular forces inducing mechanical stress, D. Portran and colleagues demonstrated that acetylation exerts its protecting effect by strongly enhancing MTs flexibility and decreasing MTs flexural rigidity after consecutive bending cycles. On the contrary, they observed that deacetylated MTs are more susceptible to breakage following each bending cycle as evidenced by an increase of material fatigue[124,125]. Taken together our results and these observations, I reasoned that further investigations into the mechanical properties of deacetylated MTs are required, for instance, by designing a proper method in which mechanical stress is systematically applied *in vivo* both to Atat1^{control} and Atat1^{cKO} mice. Indeed, I think that under physiological conditions, where MTs are highly bent by intracellular forces, also acetylated MTs are subjected to breakage in small percentages. This is consistent with what has been found *in vitro* and in our results, as we observed a small percentage of broken MTs also in in the control group. This may be a consequence of tissue dissection or sample handling, causing some sort of mechanical

stress. On the other hand, I would expect that the percentage of broken MTs dramatically increases when MTs lack the protection exerted by acetylation, like in the case of the Atat1^{cKO} group, and are subjected to continuous forces inducing mechanical stress.

However, the difference between the two genotypes is not statistically significant as it represents the result of 2 mice out of 4 (4 Atat1^{cKO} mice, considering the samples obtained from each leg). This may reflect the presence of compensation mechanisms arising either from residual responsiveness or simply from the lack of something which is important for the organism. In the latter case, I speculated that this compensation mechanism may act by directly affecting the MTs "tubulin code" through changes in post-translational modifications patterns. Indeed, it is known that MTs post-translational modifications could also modify their mechanical properties and binding interactions[126].

I think that changes in the PTMs patterns accommodate somehow the changing of protofilaments interactions, limiting MTs ultrastructural defects in the absence of mechanical stress but not their mechanical properties changes. This supports our observations that despite no morphological defects in MTs ultrastructure, Atat1^{cKO} mice display a profound loss in touch and pain sensations[1].

Direct observations in real time of MTs behavior under mechanical stress would be the most straightforward way to assess the impact of the lack of a-tubulin acetylation on MTs ultrastructure *in vivo*.

Although there are some difficulties in observing in real time MTs behavior *in vivo*, it would be interesting to investigate whether and how MTs morphology changes, along the sensory neuron axis, from the soma of DRG neurons to their axons, after Atat1^{cKO} mice are subjected to mechanical stress, for instance, after injury (SNI).

4.3 Lack of α-acetylated tubulin causes a delay in the development of allodynia in Atat1^{cKO} mice compared to Atat1^{Control} following SNI

We assessed in our previous work that mice lacking Atat1 display a profound loss of mechanical sensitivity to both light touch and painful stimuli with no impact on other sensory modalities[1].

Therefore, we reasoned that it would have been also interesting to investigate whether Atat1^{cKO} and Atat1^{fullKO} mice would still be able to develop mechanical allodynia which is a severe neuropathic pain condition, following spared nerve injury (SNI)[118]. SNI is a well-established model of induced mechanical allodynia in mice and I thought that it could have also been used as method to induce mechanical stress *in vivo.* Indeed, according to what has been reported in literature, acetylation protects long- lived MTs from flexural breakage *in vitro* when they are subjected to repetitive bending forces. It is yet not known whether that is also the case *in vivo*. In this work, I observed no dramatic changes in MTs morphology in the saphenous nerve of mice lacking α-tubulin acetylation in the absence of mechanical stress[97,98]. Therefore, I reasoned that subjecting the mice to the mechanical stress induced by spared nerve injury could have been a way to investigate both the physiological and the morphological response.

It is well established that mice subjected to SNI experience profound allodynia as early as the day following the surgery. Interestingly, I observed that both Atat1^{cKO} and Atat1^{fullKO} mice develop allodynia only beginning at day 21 post SNI, where no significant differences have been observed anymore compared to the control group. Many mechanisms could be responsible for such phenotype, for instance functional and structural plasticity of the peripheral mechanosensory terminals along the nociceptive

pathway, a delayed activation or miscommunication with the immune system components or a combination of both, just to mention a few. It is known indeed that the immune system is involved in the development and maintenance of neuropathic pain.

In addition, I speculated that the delayed recovery might be caused by the mechanical stress triggered by the injury. Indeed, MTs from the Atat1^{cKO} and Atat1^{fullKO} mice are deprived of the protective action of acetylation and may break when subjected to the mechanical stress caused by the nerve injury, giving rise to the phenotype. However, it is yet not clear whether MTs are the major players here or they act indirectly through interactions with other cellular components. I reasoned that an ultrastructural analysis, combining EM and Cryo-EM, on deacetylated MTs in the sural nerve, following the mechanicals stress induced by SNI, could give more insights into this process. Indeed, the sural nerve is the sensory branch of the sciatic nerve left intact after the injury and it is responsible for the hypersensitivity in the lateral area of the paw.

On the other hand, it would be also interesting to identify the mechanisms behind this rescue-like behavior that I observed at day 21 post SNI and whether and how the "stressed" MTs play a role in this context. It is conceivable that compensatory mechanisms from the complex mechanosensation pathways may reestablish the allodynia-like behavior. Indeed, it is known that sensory information, like touch and pain, are processed by complex circuits involving excitatory and inhibitory interneurons and that changes in the function of these circuits are thought to be implicated in the development and maintenance of inflammatory and neuropathic pain. However, the specific nature of circuit alterations in diverse segments of the nociceptive pathway is not well understood and many studies have reported divergent results. Therefore, the role of the "stressed" deacetylated MTs after injury in the delayed

recovery remains to be investigated *in vivo*. For instance, exploring from an ultrastructural point of view whether and how MTs morphology changes in this context. This results together with our previous work[1] suggest that MT acetylation plays an important role in mechanosensation and that it could be a potential target for novel selective therapeutic drugs to treat mechanical pain and neuropathic pain that unfortunately responds poorly to standard pain treatments.

5 Conclusions and outlooks

Over the past 4 years I have characterized from an ultrastructural point of view MTs organization and structure along the sensory neuron axis, from the soma of DRG neurons to their peripheral endings. In parallel with the ultrastructural characterization of mice tissues, I also performed a behavioral assay, the von Frey assay under neuropathic pain conditions, on mice lacking Atat1 from peripheral sensory neurons and from the whole animal.

The main conclusions of the work are summarized as follows:

- Superresolution microscopy analysis on cultured sensory neurons dissociated from DRGs shows that the lack of α-acetylated tubulin does not affect the gross organization of MTs in mammalian peripheral sensory neurons.
- High-resolution transmission electron microscopy combined with an image analysis workflow and Cryo-EM observations demonstrate that lack of acetylation does not affect MTs ultrastructure in mammals in the absence of mechanical stress.
- The von Frey test shows that both $Atat1^{cKO}$ and $Atat1^{fullKO}$ mice do not develop allodynia compared to the $Atat1^{Control}$ mice until day 14 post SNI, while they do so at day 21 post SNI.

Whether the lack of MT acetylation and Atat1 impact on MTs ultrastructure remain to be elucidated in mammalian organisms. In fact the next step in this work will be to investigate whether and how MTs morphology changes along the sensory neuron axis, from the soma of DRG neurons to their axons, after $Atat1^{cKO}$ mice are subjected to mechanical stress, following SNI for example.

On the other hand, further analysis need to be done also to understand the reasons of the delayed recovery, observed in the Atat1^{cKO} and Atat1^{fullKO} mice. For instance, it would be interesting to explore whether it is dependent upon further morphological changes in "pre-stressed" deacetylated MTs and I believe that EM and Cryo-EM techniques may give more insights into this process.

6 Materials and methods

6.1 Cultures of DRG neurons

Mice were euthanized using CO_2. Dorsal root ganglion neurons (DRG) from adult mice were prepared as previously described[127].

DRGs from all spinal levels were dissected, cleaned from ganglia and collected in a 1.0 ml tube of phosphate-buffered saline (PBS) on ice. DRGs were then centrifuged at 1000 rcf for 3 minutes, supernatant was discarded and they were incubated with 1 mg ml^{-1} collagenase IV (Sigma) for 25 min in a shaker at 37°C and 800 rpm.

After centrifuging at 1000 rcf for 3 minutes, the supernatant was discarded and the DRGs were incubated with 0.05% trypsin (Sigma) for 15 minutes in a shaker at 37°C and 800 rpm.

A trituration step followed by pipetting up and down with the 1ml tip for 10 times. The DRGs were then let sit back to the bottom of the tube, 700 µl of supernatant was transferred in a new tube with 10% horse serum while the rest was put back in the shaker at 37°C and 800 rpm for 10 minutes more. After adding 10% horse serum, the content of both tubes was filtered through a 100 um strainer that was washed afterwards with 500 µl of DRG medium (10% FBS, DMEM + P/S).

After centrifuging at 1000 rcf for 3 minutes, the supernatant was discarded and the pellet was resuspended in a small volume of DRG medium, according to the number of cells and the number of dishes needed. The cells were then spot-plated on poly-l-lysine (1 mg ml^{-1})–laminin (50 µg ml^{-1})-coated coverslips (10 µl of cell suspension per coverslip), and maintained at 37°C in 5% CO_2. Once the cells have attached, 2 hours later, 100 µl of extra medium was added to the dishes.

6.2 Super-resolution microscopy

Super-resolution microscopy was performed in collaboration with Ulf Matti in the lab of Jonas Ries at EMBL Heidelberg. The cells were prepared as described in the paragraph above, washed once with 3 ml of warm PBS and then fixed and permeabilized for 2 min in cytoskeleton buffer containing 0.3% Glutaraldehyde and 0.25% Triton X-100.

Following this, the cells were fixed for 10 min in cytoskeleton buffer containing 2% Glutaraldehyde and treated for 7 min with 2 ml of 0.1% Sodium Borohydride ($NaBH_4$) in PBS. Cells were then washed 3 times for 10 min in PBS. The cells were incubated with primary antibody for 30 min (mouse anti α-tubulin, Neomarker, 1:500) in PBS +2% BSA After washing 3 times for 10 min with PBS, the cells were transferred to the secondary antibody (goat anti mouse Alexa 647, 1:500, Molecular Probes A21236) at room temperature for 30 min. The cells were then washed three times with PBS for 10 min and then mounted for STORM imaging. At the time of imaging cells were overlaid with STORM blinking buffer: 50 mM Tris pH 8.0, 10 mM NaCl, 10% Glucose, 100 U/ml Glucose Oxidase (Sigma-Aldrich), 40 μg/ml Catalase (Sigma-Aldrich).

6.2.1 Superresolution image analysis

The image analysis of MT network morphology on superresolution images of anti - α tubulin stained cultured DRG was performed in collaboration with Christian Tischer in the ALMF facility at EMBL in Heidelberg, using the open source software CellProfiler[128], as described in our previous work[1]. The MT signal was enhanced by a

top-hat filter and then binarised with the same manual threshold for all images. Binary images were skeletonized using CellProfiler's 'skelPE' algorithm and the resulting skeleton was subjected to branchpoint detection. MT density was measured by dividing the skeleton length with imaged cell area and MT crossing density was obtained by dividing the number of branchpoints with skeleton length. Moreover, the local angular distribution of the MTs was measured in order to assess whether they run in parallel, or in a crossing manner (angular variance). To this end, each pixel was subjected to a rotating morphological filter using a linear structural element with a length of 11 pixels, and the angle that gave a maximum response was recorded. The response for angles from 0 to 170 degrees was computed at steps of 10 degrees since there is no information on MT polarity. Next the local circular variance of the MT orientations was measured in a sliding window with a diameter of 51 pixels, using angle doubling as it is commonly done for axial data. The circular variance has a value one if the MTs in a given region are completely parallel and has smaller values (down to 0) if the MTs are oriented in various directions. Finally, the average circular variance of all MT pixels in a given cell was computed. If this value were close to one it would mean that locally, on a length scale of 51 pixels, the MTs are parallel in most of the cell.

6.3 Collection of tissue samples from mice

6.3.1 Surgical procedure for saphenous nerve dissection in mouse

Mice were sacrificed using CO_2 inhalation, each mouse was then pinned to a dissecting board in a supine position and the skin was disinfected with 70% ethanol. As previously described by [129], to expose the saphenous nerve, the skin of the inner side of each leg

was lifted with forceps and an incision was made from the knee toward the inguinal ligament with a pair of sharped scissors, taking great care not to damage the tissue underneath. The skin was then removed to make the saphenous nerve visible on its entire length up to the inguinal ligament. The nerve and the exposed muscle was rinsed with PBS from a syringe frequently.

The saphenous nerve was gently separated from the connective tissue by using a pair of sharpened forceps. First the nerve was detached from the saphenous vessels running side by side with the nerve (as shown in Figure 22a, b) and then the connective tissue was separated from the nerve carefully millimeter by millimeter. Efforts should be made here not to stretch the nerve, as it leads to tearing of the axons.

Finally the nerve was gently lifted using forceps and collected on a small piece of Whatman® Cellulose Filter Paper (diameter 110 mm) by cutting at the proximal and distal ends with the use of spring scissors.

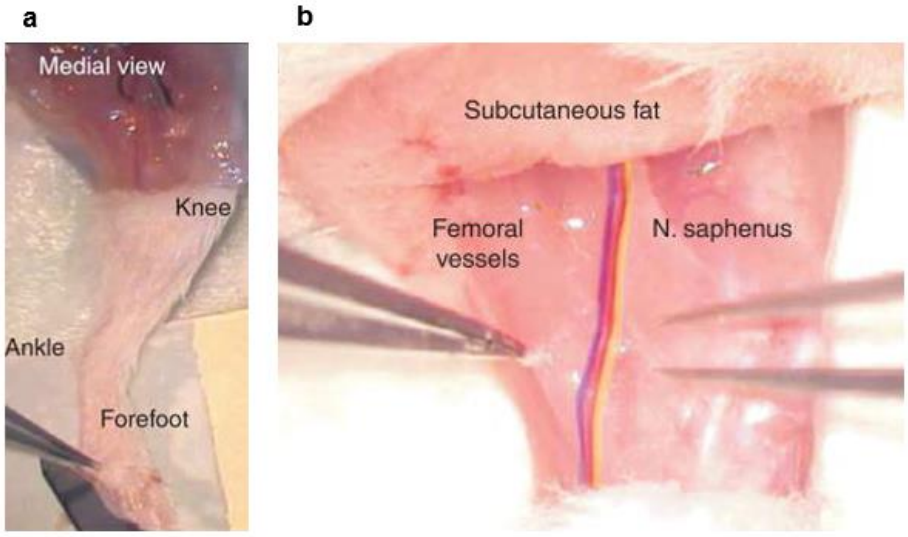

Figure 22. Saphenous nerve dissection. a) shows the medial view of the thigh, lower leg and forefoot: the incision was made from the knee toward the inguinal ligament. b) shows the saphenous nerve and

the femoral vessels (yellow: nerve, red: arterial; blue: venous) run in the middle of the medial aspect of the thigh. Image from Katharina Zimmermann et al., 2009.

6.3.2 Surgical procedure for cornea dissection in mouse

Mice were euthanized using CO_2 and the eyes were immediately removed from the eyeball by gently pulling and cutting as much muscle and connective tissue surrounding it as possible. Effort should be made to squeeze the eyeball as little as possible.

Once all extraneous tissue was removed, the eyes were placed in Ringer´s solution, in order to dissect the cornea out from the eyecup. In fact, the eye will naturally maintain its spherical shape while in suspension, allowing to work with this shape rather than against it.

With the cornea facing up, straight forceps were used to pinch up a small fold on the side of the eyecup along the corneo-scleral divide and a small incision was made using the spring scissors. Holding the eyes still with forceps, the lower scissor blade was inserted into and parallel to the incision in order to make a cut along the corneo-scleral divide until the cornea is completely separated from the sclera and the rest of the eyecup.

6.4 Preparation of mouse samples for Electron Microscopy

Fixation is the first and most important step in any electron microscopy (EM) study. There are two ways to fix the biological specimens for EM: Chemical fixation by using cross-linking agents and physical fixation by high pressure freezing (HPF).

Here both chemical fixation and HPF and freeze substitution (FS) were performed in parallel on mice samples.

6.4.1 Chemical fixation of labeled DRG neurons in culture

Here a transgenic mouse line, *Advil-Cre::Rosa26SNAP^{CaaX}*, generated in our laboratory[130] was used, in order to circumvent the fluorescence quenching of GFP during EM preparation of the sample.

The SNAP-tag is an example of covalent self-labeling and consists of an engineered O6-alkylguanine-DNA alkyltransferase that can be specifically and irreversibly labeled with O6-benzylguanine (BG) derivatives. It satisfies also many of the requirements for an in vivo reporter, such as fast and quantitative one-step labeling, minimal off-target labeling and low cellular toxicity. Although the Snap-tag is not intrinsically fluorescent, the labeling with commercially available fluorophores extending from green to near-infrared emission is efficient in complex tissue, allowing for multicolored imaging in vivo.

I established a protocol for labeling the cornea in vivo, testing among different SNAP substrates (New England *Biolabs Inc.*):

1. BG-430 (excitation maximum at 421 nm and emission maxima at 444 and 484 nm);
2. TMR-Star (excitation maximum at 554 nm and emission maxima at 580 nm);
3. SiR-650 and SiR- 700 (near-infrarerd silicon-rhodamine fluorophores excitable at around 640-650 nm and emit around 660-670).

DRG sensory neuron from adult *Advil-Cre::Rosa26SNAPCaaX* mice were dissected and dissociated as described in the paragraph above (Cultures of DRG neurons).

Sensory neuron cultures were incubated with 5μM of the the near-infrared silicon-rhodamine probes, diluted in DRG medium, for ½ hour at 37 C.

After the labelling, the sensory neurons in culture were washed with PBS buffer (three times for 30 minutes) and imaged in the same buffer. Images were then captured using the Widefield Leica DMR with a High resolution colored CCD camera CD50.

Sensory neuron cultures were finally processed for EM by chemical fixation with 2. 5% Glutaraldehyde in PHEM buffer for 2h.

The neurons were Post-fixed in Osmium diluted in PHEM buffer for 1h, at different concentration: 0%, 0, 25%, 0,75%, 1%. To enhance sample contrast, an *en bloc* stain with 1% Uranyl Acetate (in Water) was performed for 1h.

The sensory neurons were then progressively dehydrated in a series of Acetone washes: 50%, 70%, 90%, 95% and 100% 3 times, each for 10 minutes. A standard Epon 812 resin recipe was used for infiltration beginning with a 1:2 dilution of Epon to 100% Acetone, followed by 1:1 and 2:1, each for 15 minutes. Finally, samples were left for 2 hours in 100% Epon before polymerization for 48 h at 60°*C*.

The fluorescence was checked after each step of preparation of the sample with the Widefield Leica DMR and analyzed with ImageJ software.

6.4.2 Chemical fixation of the saphenous nerve

A total of 20 adult male mice (10 $Atat1^{control}$ and 10 $Atat1^{cKO}$), 8-10 weeks old and weighing between 25–30 g were sacrificed using CO2 inhalation and the saphenous nerves from both legs of each mouse were dissected out and placed immediately in a petri dish with fresh fixative containing a mixture of 2% Glutaraldehyde, 1% tannic acid and 1.8% glucose in a 0.1M Phosphate buffer. Here the nerves were further cut in smaller pieces (3 pieces for each nerve) in order to facilitate the penetration of the fixative into the tissue. The samples were then transferred in 2 ml tubes submerged in fixative, left at RT for 45-60 minutes. Half of the samples were placed at 4°*C* for 4 weeks while the other half was first left at RT for further 30 minutes and then processed through a microwave-assisted post fixation under vacuum at 80W on a cycle of 2 min on-off-on.

Then to enhance sample contrast, an *en bloc* stain (0.5% aqueous uranyl acetate) was used in the microwave at 150 W with vacuum on 1 min on-off-on cycle.

The nerves were then progressively dehydrated in a series of ethanol washes (40%, 50%, 70%, 90%, 95%, 100%), each for 40s in the microwave without vacuum at 250 W.

Resin infiltration was under vacuum beginning with a 1:2 dilution of standard recipe Epon 812 resin to 100% ethanol followed by 1:1 and 2:1, each for 3 min at 250 W. This was repeated twice with 100% Epon before polymerization in specific molds for flat embedding at 60°*C* in the oven.

Finally, ultrathin sections of 50-70 nm were cut with a diamond knife in an ultra-microtome, picked up on the Formvar-coated 100 mesh copper/palladium grids and analyzed by the Transmission electron microscope (Biotwin CM120 Philips) operated at 120kV.

6.4.3 High pressure freezing and freeze substitution of the saphenous nerve

A total of 10 adult male mice (10 $Atat1^{control}$ and 10 $Atat1^{cKO}$), aged postnatal-week 8-10 and weighing between 25–30 g were sacrificed using CO2 inhalation and the saphenous nerves from both legs of each mouse were dissected out and placed in a petri dish containing PBS. Here the nerves were further cut at the extremities under the binocular in order to remove the damaged part of the tissue caused by the dissection.

Then the nerve were transferred in specimen carriers (0.1/0.2 mm) filled with Yeast paste, used as cryoprotectant, mixed with PBS until the paste had a creamy consistence. A second sample carrier (0.3 mm) was placed flat side down as a lid on top of the loaded carrier. The whole sandwich was then inserted into the holder of the high pressure freezing machine

(Leica EM HPM10) and frozen. After freezing, the carriers containing the samples were immersed in liquid nitrogen and the lids of the carrier sandwich were removed. Sample were transferred into cryotubes and stored in liquid nitrogen.

The high-pressure frozen samples were subjected to freeze-substitution for dehydration and chemical stabilization of their fine structure.

Freeze-substitution was carried out in the AFS-2c unit from Leica according the following scheme (Wiebke et al): 100 hours at -90°*C* in 0.1% tannic acid in acetone; washing with acetone 4x30 min; 7 hours at – 90°*C* in 2% OsO_4 in acetone; warming up to 4°*C* by incrementing of 10°*C*/h; 1 hour incubation at 4°*C*; washing with acetone 3x20 min; infiltration in Epon resin:acetone mix 1:1 over 3 hours at 4°*C*; overnight incubation in 90% Epon in acetone at RT; 6 hours incubation in 100% Epon at RT.

The samples were finally removed from the specimen carriers, transferred in embedding molds for flat embedding and let polymerize at 60°*C* in the oven. Ultrathin

sections of 50-70 nm were cut with a diamond knife in an ultra-microtome, picked up on the Formvar-coated 100 mesh copper/palladium grids and analyzed by the Transmission electron microscope (Biotwin CM120 Philips). Semi-thin serial sections (250 nm thick) were also collected for electron tomography and (Tecnai F30, FEI), examined at an accelerating voltage of 300 kV, where each section was viewed at high resolution under multiple tilts (tilt increments of 1° ranging from ~ +60 to −60 degrees along an axis perpendicular to the incoming electron beam) to produce two single axis tomograms using marker alignment procedures and internal features to create weighted backprojection models of the tissue in 3D space.

6.4.4 Chemical fixation of the corneas

Before attempting to chemically fix corneas, 3 fixation cocktails were tested on the corneas from TRPM8BAC-EYFP+/+ mice:

- 2.5% Glutaraldehyde, 4% PFA in 0.1M PHEM buffer pH 6.9 for 2h at RT.
- 2.5% Glutaraldehyde, 4% PFA in 0.1M Cacodylate buffer pH 6.93 for 2h at RT.
- 2.5% Glutaraldehyde, 4% PFA in 0.1M Phosphate buffer pH 7.2 for 2h at RT.

To accelerate the process and produce improved morphological results, the corneas were post-fixed through a microwave-assisted post fixation under vacuum, with 1% Osmium tetroxide buffered in 0.1 M PHEM, 0.1M Cacodylate or 0.1M Phosphate, at 80W on a cycle of 2 min on-off-on.

Then to enhance sample contrast, an *en bloc* stain (0.5% aqueous uranyl acetate) was used in the microwave at 150 W with vacuum on 1 min on-off-on cycle. The corneas

were then progressively dehydrated in a series of ethanol washes (40%, 50%, 70%, 90%, 95%, 100%), each for 40s in the microwave without vacuum at 250 W.

Resin infiltration was under vacuum beginning with a 1:2 dilution of standard recipe Epon 812 resin to 100% ethanol followed by 1:1 and 2:1, each for 3 min at 250 W. This was repeated twice with 100% Epon before polymerization in specific molds at 60°*C* in the oven.

Sections of 70 nm were cut with a diamond knife in an ultra-microtome, picked up on the Formvar-coated 100 mesh copper/palladium grids and analyzed by the Transmission electron microscope (Biotwin CM120 Philips) operated at 120kV.

6.4.5 High pressure freezing and freeze substitution of corneas

Optimal fast freezing requires cryo-immobilization of tissues in a state that is as close to native as possible.

When tissues are rapidly frozen, all contents are immobilized almost immediately. These fast-freezing methods involve time scales of milliseconds and are preferable to chemical fixation methods that have time scales of seconds or minutes depending on the tissue

For HPF, mice were sacrificed using CO2 inhalation and the eyes were immediately placed in Ringer´s solution, in order to dissect the cornea out from the eyecup.

These corneas were then placed in specimen carriers and fast frozen using a Leica EM HPM10 machine. Yeast paste was used as cryoprotectant, obtained by mixing fresh yeast with PBS until the paste had a creamy consistence. This because Yeast paste can be removed from the sample after freeze-substitution and Epon infiltration by gently tapping with forceps.

Corneas were then transferred to liquid nitrogen and processed by a relatively long freeze substitution scheme: 12 hours at -90°*C* in FS medium containing 0, 5% UA in Acetone; warming to -45°*C*; washing with acetone, infiltration with Lowicryl resin over 12 hours at -45°*C*, 4 hours at -35C, 30 hours at -25°*C*; polymerization by UV light for 2 days at -25°*C* followed by 15 hours at 20°*C*. After embedding, blocks were cut with a diamond knife in an ultra-microtome in order to get 70 nm sections, picked up on the Formvar-coated 100 mesh copper/palladium grids and analyzed by the Transmission electron microscope (Biotwin CM120 Philips).

6.4.6 Olympus Biosystems Cell^R, UV cutting for marking sensory terminals into the corneal epithelium

Here a CLEM (Correlative light and Electron Microscopy) approach was designed for this specific purpose. The method takes advantage of a Pulsed 355 nm laser to create a marker into the region of interest. It is a method for isolating specific single cells or entire areas of tissue from a wide variety of tissue samples based on microscopic imaging and utilizing a laser that burns the area of interest. The thickness, texture and preparation technique of the original tissue are relatively unimportant.

First step was to localize the sensory fiber in the cornea from a TRPM8BAC-EYFP$^{+/+}$ mouse with a fluorescent microscope (Olympus CutR widefield nanosurgery) with a 20x objective lens, taking advantage of its fluorescence. Then with the laser (laser power 10%) a region around the fiber of interest was burned in order to create a square that could have survived the EM preparation of the sample, as the fluorescence is quenched.

6.5 Analysis of the 2D image datasets

The 2D class averaging analysis on electron micrographs representing MTs in peripheral sensory afferents from the mouse saphenous nerve was performed in collaboration with Shyamal Mosalaganti at EMBL in Heidelberg.

Once the datasets from 5 $Atat1^{control}$ and 5 $Atat1^{cKO}$ mice were collected, the images were randomly chosen and subjected to particle picking in order to select the best quality particles (referred to MTs). Particles can be selected in a manual, semi-automated, and fully automated manner. Here 953 MTs from 95 $Atat1^{control}$ images and 1358 MTs from $Atat1^{cKO}$ images were windowed out manually using the e2boxer tool embedded in the EMAN2 suite[131] and assembled into a stack. The window size should exceed the approximate particle size by at least 30%.

Particles were then aligned and classified into more homogenous subsets using reference-free alignment and k-means classification programs implemented in RELION[132] (REgularized LIkelihood OptimizatioN).

Images of similar views were aligned and averaged to achieve higher signal to noise ratio. This process involves both rotational and translational shifting of individual particle images, which generally gives information about the 2D views of the sample and its inherent heterogeneity. The goal of clustering is to assign *n* objects to K classes (or groups) such that objects within each class are similar to each other, while the group averages are as dissimilar from each other as possible. The number of classes K has to be decided and then the algorithm is either started in a deterministic or random manner. Here, a random initialization was performed where K randomly selected objects from the entire set are used as initial templates. After initialization the algorithm proceeds in an iterative manner. For each object its similarity to all class averages are computed

and the object is assigned to the most similar average, then based on the new assignments, new class averages are computed.

6.6 Image analysis on microtubules morphology

Here a pipeline workflow was implemented, in collaboration with Jose Miguel Serra Lleti at EMBL in Heidelberg, in order to characterize different microtubule features in TEM images. A comparative study between two conditions: Atat1Control (WT) and Atat1cKO (Mutant) was carried out on a total number of 13 saphenous nerves from 8 mice (4 Atat1Control and 4 Atat1cKO). The following schema illustrates the total amount of samples used, names and classification between left and right which indicates the mouse´s legs:

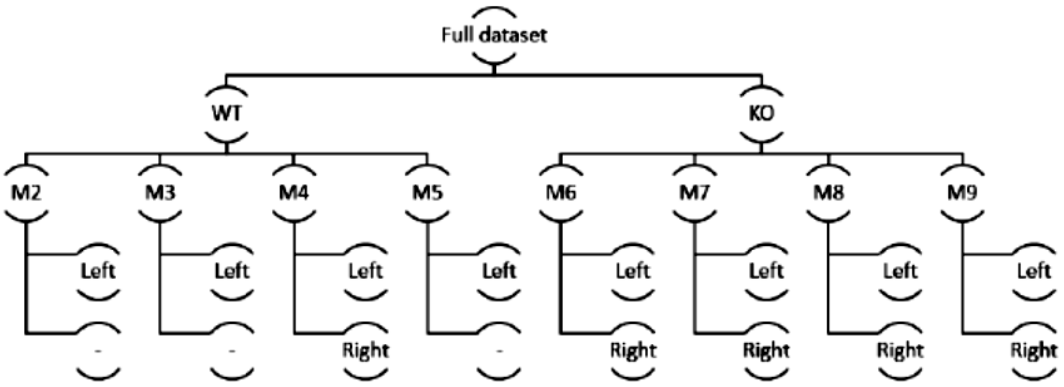

After random shuffling, the set of images was assembled into a stack and all the MTs were windowed out from each image in a 100x100 pixel box for further segmentation, using a Fiji plugin called **Box2Image** that was developed for this purpose. Once all the MTs from the stack were selected and windowed out, the crops were saved with image

coordinates followed by the stack image number. Objects too blurry to identify a clear density or mixed with other densities in a way that was difficult to determine its shape were discarded:

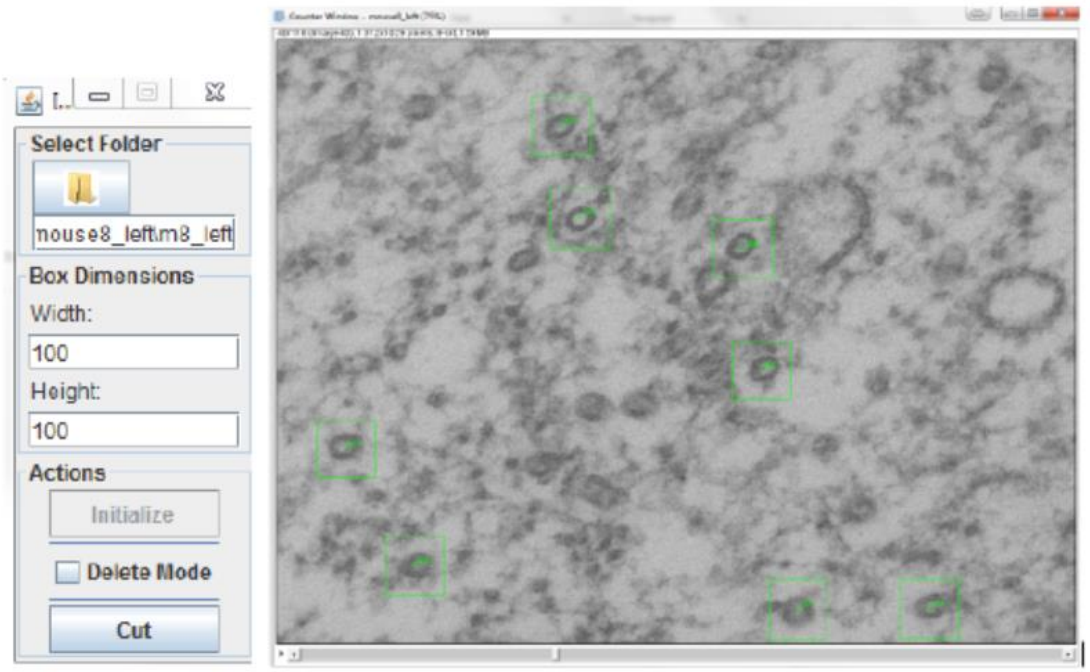

Segmentation proceeded according the following steps: Raw gray value data were thresholded using adaptive mean thresholding and thresholded MTs were binarized as follows: opening morphological operator, removal of borders (10 pixels), tophat to detect small particles followed by a xor to remove them, closing and opening morphological operators to clean small objects and finally selecting the biggest connected component.

After binarization, the pipeline consisted in obtaining the 7th moment fourier descriptor to fit the contour of the biggest binary object. From the result, the contour was obtained and used to calculate the area and the fitting ellipse. Ellipse data was hence stored for statistical analysis. Ellipse data were hence stored for statistical analysis.

First of all, the average diameter of MTs in EM sections was determined. The MT diameter is based on the minimum diameter of the fitting ellipse surrounding the MT area, or minor axis, when the MT is complete. The minor axis is an indication of possible deformations in the MT structure and does not change with the section angle if the full MT shape is present.

The eccentricity of MTs was calculated as described by Cueva et al., 2012[100]. Eccentricity is a measure of how much a conic section (a circle, ellipse, parabola or hyperbola) varies from being circular. A circle has an eccentricity of zero, so the eccentricity shows how un-circular the curve is, in this case how un-circular MTs are.

Finally, solidity was calculated by taking the 7th order fourier descriptor of each MT. The resultant contour was compared to the fitting ellipse of the convex hull. From this solidity was computed by comparing the approximated smoothed area to the elliptic area:

Solidity = (Area) / (Convex Area) 

6.7 Cemovis

Cryo-electron microcopy of vitrified samples (CEMOVIS) allows to observe cells and tissues at high resolution in a close-to-native state. Here chemical fixation and staining are fully avoided. Therefore, all steps must be carried on below devitrification temperature to obtain successful results. Cemovis was performed in collaboration with the EMCF facility at EMBL in Heidelberg.

Sample preparation

Mice were euthanized using CO_2. DRGs from all spinal levels were dissected out, cleaned from ganglia and transferred in a gold-coated copper type A carrier (0,1/0,2 mm) filled with 20% dextran, used as cryoprotectant. A second sample carrier (0.3 mm) was placed flat side down as a lid on top of the loaded carrier. The whole sandwich was then inserted into the holder of the high pressure freezing machine HPM010 (Abra Fluid) and immediately vitrified (2100 bars, -196°C).

Dorsal root ganglion neurons (DRG) from adult mice were prepared as previously described in the paragraph above (Cultures of DRG neurons) with the following modification: neurons were spot-plated on grids specific for CEMOVIS called finder grids, prepared as described in(). After 2 days, cells were vitrified in a HPM 010 high-pressure freezer (2100 bars, -196°C) using the adapted carriers. The cell-bearing grid was sandwiched between a gold-coated copper type A carrier (0,1/0,2 mm) and the flat side of a type B aluminium carrier with the cells facing the 0,1 mm deep side of the type A carrier.

Saphenous nerves from adult mice were prepared as previously described in the paragraph above (Surgical procedure for saphenous nerve dissection in mouse). Once dissected out, samples were transferred in a gold-coated copper type A carrier (0,1/0,2 mm) filled with 20% dextran, used as cryoprotectant. A second sample carrier (0.3 mm) was placed flat side down as a lid on top of the loaded carrier. The whole sandwich was then inserted into the holder of the high pressure freezing machine HPM010 (Abra Fluid) and immediately vitrified (2100 bars, -196°C).

After the freezing and under liquid nitrogen immersion, the B carrier was discarded and the samples, mounted on the A carrier, were stored in LN2 until further use.

Cryo-ultramicrotomy was performed with a Leica UC6/FC6 cryo-ultramicrotome. A 45° cryo trim diamond knife was used for trimming away the surrounding material.

A 35° cryo-immuno diamond knife and micromanipulator from Diatome (Studer et al. 2014) were used for cryo-sectioning. Both trimming and sectioning were performed at -150°C. 50 nm ultra-thin sections (speed to 0,4 mm/s) were collected on C-flat holey carbon grids, transferred to a Cryo-TEM Holder (Gatan, Pleasanton) kept at a temperature below 170°C, and inserted in cryo-electron microscope, Tecnai Spirit (FEI, Eindhoven), operated at 120 kV.

6.8 Von-Frey assay*:* Mechanical sensitivity tests

This assay represent a measurement of Mechanical sensitivity to a stimulus. Mechanosensitivity can be determined as the minimum amount of force required to elicit a behavioural response, such as the withdrawal of a paw.

Mice were placed in a plastic mesh on an elevated wire grid and sets of Von-frey filaments caliberated to different forces (0.008-6g) are applied to the hindpaw one by one. The paw withdrawal threshold is determined for both ipsilateral and contralateral paws using the Dixon's up-down method. The basic premise is that lack of response to a filament corresponds to the next higher filament, while a positive response corresponds to the next lower filament. This variability can result in a bias since repeated testing can change the responsiveness of the animal. I used a modified

approach called SUDO (simplified Up-Down approach). This method uses only five filament presentations per assay unlike 8 to 9 filament presentations used in up-down method[133].

This simplifies the entire protocol and it is less time consuming. Usually the 5th filament is presented first. If the animal responds three out of five times, it is possible to proceed on to the lower filament or else to the next higher filament. In this way, threshold for response is calculated for each force applied.

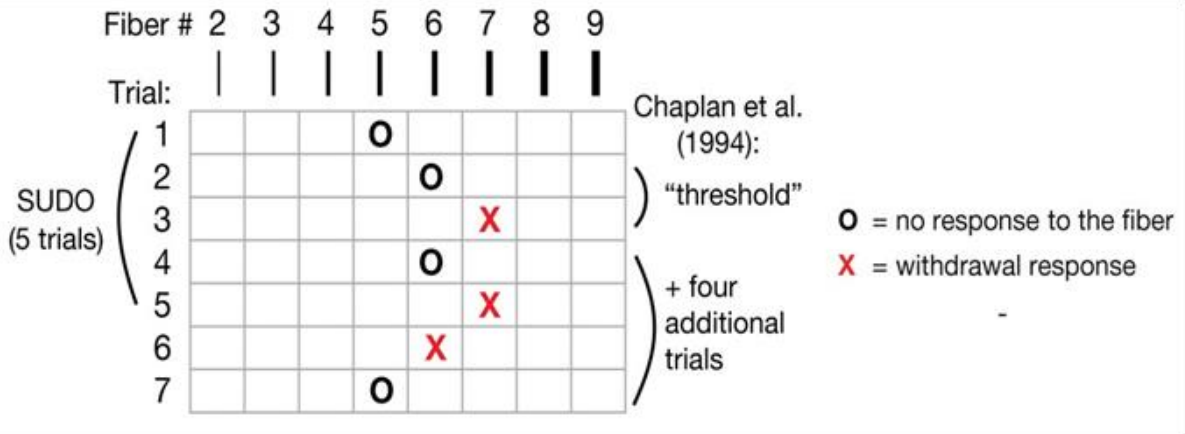

Figure 23: SUDO approach to study mechanical sensitivity. The image shows the Simplified Up-Down method for mechanosensitivity assay, as adapted from RP Bonin.et.al.,Molecular pain,(2014).

7 References

1. Morley, S. J. *et al.* Acetylated tubulin is essential for touch sensation in mice. *Elife* **5,** 25 (2016).
2. Kandel, E. R., Schwartz, J. H., Jessell, T. M., Siegelbaum, S. A. & Hudspeth, A. J. *Principles of Neural Science, Fifth Edition*. *Neurology* **3,** (2014).
3. Brown, a G. & Iggo, a. A quantitative study of cutaneous receptors and afferent fibres in the cat and rabbit. *J. Physiol.* **193,** 707–733 (1967).
4. Birder, L. a & Perl, E. R. Cutaneous sensory receptors. *Journal of clinical neurophysiology : official publication of the American Electroencephalographic Society* **11,** 534–552 (1994).
5. Victoria E. Abraira and David D. Ginty. Neuron The Sensory Neurons of Touch. *Neuron* **79,** 1–44 (2013).
6. Maksimovic, S. *et al.* Epidermal Merkel cells are mechanosensory cells that tune mammalian touch receptors. *Nature* **509,** 617–621 (2014).
7. Purves, D. *et al.* Neuroscience. 2nd edition. *Sunderland (MA): Sinauer Associates; 2001*. 109–12 (2001). doi:978-0878937257
8. Brohawn, S. G., del Marmol, J. & MacKinnon, R. Crystal Structure of the Human K2P TRAAK, a Lipid- and Mechano-Sensitive K+ Ion Channel. *Science (80-.).* **335,** 436–441 (2012).
9. Brohawn, S. G., Su, Z. & MacKinnon, R. Mechanosensitivity is mediated directly by the lipid membrane in TRAAK and TREK1 K^+ channels. *Proc. Natl. Acad. Sci.* **111,** 3614–3619 (2014).
10. Brohawn, S. G., Campbell, E. B. & MacKinnon, R. Physical mechanism for gating and mechanosensitivity of the human TRAAK K+ channel. *Nature* **516,**

126–130 (2014).

11. Zhang, W. *et al.* Ankyrin Repeats Convey Force to Gate the NOMPC Mechanotransduction Channel. *Cell* **162,** 1391–1403 (2015).
12. Lumpkin, E. A., Marshall, K. L. & Nelson, A. M. The cell biology of touch. *Journal of Cell Biology* **191,** 237–248 (2010).
13. Aristotle. De Anima. in *A New Aristotle Reader* 161–205 ST–De Anima (1987).
14. Syntichaki, P. & Tavernarakis, N. Genetic models of mechanotransduction: the nematode Caenorhabditis elegans. *Physiol. Rev.* **84,** 1097–1153 (2004).
15. Chalfie, M. & Sulston, J. Developmental genetics of the mechanosensory neurons of Caenorhabditis elegans. *Dev. Biol.* **82,** 358–370 (1981).
16. Sulston, J., Dew, M. & Brenner, S. Dopaminergic neurons in the nematode Caenorhabditis elegans. *J. Comp. Neurol.* **163,** 215–226 (1975).
17. Eberl, D. F., Duyk, G. M. & Perrimon, N. A genetic screen for mutations that disrupt an auditory response in Drosophila melanogaster. *Proc. Natl. Acad. Sci.* **94,** 14837–14842 (1997).
18. Kernan, M., Cowan, D. & Zuker, C. Genetic dissection of mechanosensory transduction: Mechanoreception-defective mutations of drosophila. *Neuron* **12,** 1195–1206 (1994).
19. Sidi, S. NompC TRP Channel Required for Vertebrate Sensory Hair Cell Mechanotransduction. *Science (80-.).* **301,** 96–99 (2003).
20. Ranade, S. S. *et al.* Piezo2 is the major transducer of mechanical forces for touch sensation in mice. *Nature* **516,** 121–125 (2014).
21. Mahmud, A. A. *et al.* Loss of the proprioception and touch sensation channel PIEZO2 in siblings with a progressive form of contractures. *Clin. Genet.* **91,** 470–475 (2017).

22. Löken, L. S., Wessberg, J., Morrison, I., McGlone, F. & Olausson, H. Coding of pleasant touch by unmyelinated afferents in humans. *Nat. Neurosci.* **12,** 547–548 (2009).

23. Seal, R. P. *et al.* Injury-induced mechanical hypersensitivity requires C-low threshold mechanoreceptors. *Nature* **462,** 651–655 (2009).

24. Krieg, M., Dunn, A. R. & Goodman, M. B. Mechanical control of the sense of touch by β-spectrin. *Nat. Cell Biol.* **16,** 224–233 (2014).

25. Bounoutas, A., O'Hagan, R. & Chalfie, M. The Multipurpose 15-Protofilament Microtubules in C. elegans Have Specific Roles in Mechanosensation. *Curr. Biol.* **19,** 1362–1367 (2009).

26. Chalfie, M. & Thomson, J. N. Structural and functional diversity in the neuronal microtubules of Caenorhabditis elegans. *J. Cell Biol.* **93,** 15–23 (1982).

27. Akella, J. S. *et al.* MEC-17 is an alpha-tubulin acetyltransferase. *Nature* **467,** 218–222 (2010).

28. Shida, T., Cueva, J. G., Xu, Z., Goodman, M. B. & Nachury, M. V. The major -tubulin K40 acetyltransferase TAT1 promotes rapid ciliogenesis and efficient mechanosensation. *Proc. Natl. Acad. Sci.* **107,** 21517–21522 (2010).

29. Fukushige, T. *et al.* MEC-12, an alpha-tubulin required for touch sensitivity in C. elegans. *J. Cell Sci.* **112 (Pt 3,** 395–403 (1999).

30. Kalebic, N. *et al.* Tubulin Acetyltransferase TAT1 Destabilizes Microtubules Independently of Its Acetylation Activity. *Mol. Cell. Biol.* **33,** 1114–1123 (2013).

31. Milligan, E. D. & Watkins, L. R. Pathological and protective roles of glia in chronic pain. *Nature Reviews Neuroscience* **10,** 23–36 (2009).

32. Gangadharan, V. & Kuner, R. Unravelling Spinal Circuits of Pain and

Mechanical Allodynia. *Neuron* **87,** 673–675 (2015).

33. Jensen, T. S. & Finnerup, N. B. Allodynia and hyperalgesia in neuropathic pain: Clinical manifestations and mechanisms. *The Lancet Neurology* **13,** 924–935 (2014).

34. Jongen, J. L. M., Hans, G., Benzon, H. T., Huygen, F. & Hartrick, C. T. Neuropathic pain and pharmacological treatment. *Pain Pract.* **14,** 283–95 (2014).

35. Hirth, M., Gandla, J. & Kuner, R. A checkpoint to pain. *Nature Neuroscience* **20,** 897–899 (2017).

36. Arcourt, A. & Lechner, S. G. Peripheral and spinal circuits involved in mechanical allodynia. *Pain* **156,** 220–221 (2015).

37. Dina, O. A., McCarter, G. C., De Coupade, C. & Levine, J. D. Role of the sensory neuron cytoskeleton in second messenger signaling for inflammatory pain. *Neuron* **39,** 613–624 (2003).

38. Bhave, G. & Gereau IV, R. W. Growing pains: The cytoskeleton as a critical regulator of pain plasticity. *Neuron* **39,** 577–579 (2003).

39. Kapitein, L. C. & Hoogenraad, C. C. Building the Neuronal Microtubule Cytoskeleton. *Neuron* **87,** 492–506 (2015).

40. van Beuningen, S. F. B. & Hoogenraad, C. C. Neuronal polarity: Remodeling microtubule organization. *Current Opinion in Neurobiology* **39,** 1–7 (2016).

41. Akhmanova, A. & Steinmetz, M. O. Tracking the ends: A dynamic protein network controls the fate of microtubule tips. *Nature Reviews Molecular Cell Biology* **9,** 309–322 (2008).

42. Verhey, K. J. & Gaertig, J. The tubulin code. *Cell Cycle* **6,** 2152–2160 (2007).

43. Janke, C. & Chloë Bulinski, J. Post-translational regulation of the microtubule

cytoskeleton: mechanisms and functions. *Nat. Rev. Mol. Cell Biol.* **12,** 773–786 (2011).

44. Song, Y. & Brady, S. T. Post-translational modifications of tubulin: Pathways to functional diversity of microtubules. *Trends in Cell Biology* **25,** 125–136 (2015).

45. Murofushi, H. Purification and characterization of tubulin-tyrosine ligase from porcine brain. *J. Biochem.* **87,** 979–84 (1980).

46. Schroder, H. C., Wehland, J. & Weber, K. Purification of brain tubulin-tyrosine ligase by biochemical and immunological methods. *J. Cell Biol.* **100,** 276–281 (1985).

47. Ersfeld, K. *et al.* Characterization of the tubulin-tyrosine ligase. *J. Cell Biol.* **120,** 725–732 (1993).

48. Erck, C. *et al.* A vital role of tubulin-tyrosine-ligase for neuronal organization. *Proc. Natl. Acad. Sci.* **102,** 7853–7858 (2005).

49. Janke, C. & Bulinski, J. C. Post-translational regulation of the microtubule cytoskeleton: mechanisms and functions RID A-7279-2011. *Nat. Rev. Mol. Cell Biol.* **12,** 773–786 (2011).

50. Chakraborti, S., Natarajan, K., Curiel, J., Janke, C. & Liu, J. The emerging role of the tubulin code: From the tubulin molecule to neuronal function and disease. *Cytoskeleton* **73,** 521–550 (2016).

51. Berezniuk, I. *et al.* Cytosolic carboxypeptidase 1 is involved in processing ??- and ??-tubulin. *J. Biol. Chem.* **287,** 6503–6517 (2012).

52. Paturle-Lafanechère, L. *et al.* Accumulation of delta 2-tubulin, a major tubulin variant that cannot be tyrosinated, in neuronal tissues and in stable microtubule assemblies. *J. Cell Sci.* **107 (Pt 6,** 1529–1543 (1994).

53. Audebert, S. *et al.* Developmental regulation of polyglutamylated alpha- and

beta-tubulin in mouse brain neurons. *J. Cell Sci.* **107 (Pt 8,** 2313–22 (1994).

54. Abal, M., Keryer, G. & Bornens, M. Centrioles resist forces applied on centrosomes during G2/M transition. *Biol. Cell* **97,** 425–434 (2005).

55. Gaertig, J. & Wloga, D. Chapter 4 Ciliary Tubulin and Its Post-Translational Modifications. *Current Topics in Developmental Biology* **85,** 83–113 (2008).

56. Janke, C. & Kneussel, M. Tubulin post-translational modifications: Encoding functions on the neuronal microtubule cytoskeleton. *Trends in Neurosciences* **33,** 362–372 (2010).

57. Sloboda, R. D. Posttranslational Protein Modifications in Cilia and Flagella. *Methods Cell Biol.* **93,** ii (2009).

58. Cooper, A. J. L., Jeitner, T. M., Gentile, V. & Blass, J. P. Cross linking of polyglutamine domains catalyzed by tissue transglutaminase is greatly favored with pathological-length repeats: Does transglutaminase activity play a role in (CAG)n/Qn-expansion diseases? in *Neurochemistry International* **40,** 53–67 (2002).

59. Hand, D., Campoy, F. J., Clark, S., Fisher, A. & Haynes, L. W. Activity and Distribution of Tissue Transglutaminase in Association with Nerve-Muscle Synapses. *J. Neurochem.* **61,** 1064–1072 (1993).

60. Song, Y. *et al.* Transglutaminase and Polyamination of Tubulin: Posttranslational Modification for Stabilizing Axonal Microtubules. *Neuron* **78,** 109–123 (2013).

61. Fourest-Lieuvin, A. *et al.* Microtubule Regulation in Mitosis: Tubulin Phosphorylation by the Cyclin-dependent Kinase Cdk1 □ D. *Mol. Biol. Cell* **17,** 1041–1050 (2006).

62. Laurent, C. E., Delfino, F. J., Cheng, H. Y. & Smithgall, T. E. The human c-Fes

tyrosine kinase binds tubulin and microtubules through separate domains and promotes microtubule assembly. *Mol. Cell. Biol.* **24,** 9351–9358 (2004).

63. Wloga, D., Gaertig, J., Wloga, D. & Gaertig, J. Post-translational modifications of microtubules Post-translational modifications of microtubules. *J. Cell Sci.* **123,** 3447–3455 (2011).

64. Flotho, A. & Melchior, F. Sumoylation: A Regulatory Protein Modification in Health and Disease. *Annu. Rev. Biochem.* **82,** 357–385 (2013).

65. Komander, D. & Rape, M. The Ubiquitin Code. *Annu. Rev. Biochem.* **81,** 203–229 (2012).

66. Kim, Y. *et al.* Methylation-dependent regulation of HIF-1α stability restricts retinal and tumour angiogenesis. *Nat. Commun.* **7,** (2016).

67. Latham, J. A. & Dent, S. Y. R. Cross-regulation of histone modifications. *Nature Structural and Molecular Biology* **14,** 1017–1024 (2007).

68. L'Hernault, S. W. & Rosenbaum, J. L. Chlamydomonas ??-tubulin is posttranslationally modified in the flagella during flagellar assembly. *J. Cell Biol.* **97,** 258–263 (1983).

69. L'Hernault, S. W. & Rosenbaum, J. L. Chlamydomonas alpha-tubulin is posttranslationally modified by acetylation on the epsilon-amino group of a lysine. *Biochemistry* **24,** 473–8 (1985).

70. Piperno, G. & Fuller, M. T. Monoclonal antibodies specific for an acetylated form of α-tubulin recognize the antigen in cilia and flagella from a variety of organisms. *J. Cell Biol.* **101,** 2085–2094 (1985).

71. Piperno, G., LeDizet, M. & Chang, X. J. Microtubules containing acetylated alpha-tubulin in mammalian cells in culture. *J. Cell Biol.* **104,** 289–302 (1987).

72. Yang, X.-J. & Grégoire, S. Class II histone deacetylases: from sequence to

function, regulation, and clinical implication. *Mol. Cell. Biol.* **25,** 2873–2884 (2005).

73. Choudhary, C. *et al.* Lysine acetylation targets protein complexes and co-regulates major cellular functions. *Science (80-.).* **325,** 834–840 (2009).

74. Chu, C.-W. *et al.* A novel acetylation of -tubulin by San modulates microtubule polymerization via down-regulating tubulin incorporation. *Mol. Biol. Cell* **22,** 448–456 (2011).

75. Ohkawa, N. *et al.* N-acetyltransferase ARD1-NAT1 regulates neuronal dendritic development. *Genes to Cells* **13,** 1171–1183 (2008).

76. Creppe, C. *et al.* Elongator Controls the Migration and Differentiation of Cortical Neurons through Acetylation of α-Tubulin. *Cell* **136,** 551–564 (2009).

77. Conacci-Sorrell, M., Ngouenet, C. & Eisenman, R. N. Myc-nick: A cytoplasmic cleavage product of Myc that promotes α-tubulin acetylation and cell differentiation. *Cell* **142,** 480–493 (2010).

78. Steczkiewicz, K., Kinch, L., Grishin, N. V., Rychlewski, L. & Ginalski, K. Eukaryotic domain of unknown function DUF738 belongs to Gcn5-related N-acetyltransferase superfamily. *Cell Cycle* **5,** 2927–2930 (2006).

79. Kim, G. W., Li, L., Gorbani, M., You, L. & Yang, X. J. Mice lacking alpha-tubulin acetyltransferase 1 are viable but display alpha-tubulin acetylation deficiency and dentate gyrus distortion. *J. Biol. Chem.* **288,** 20334–20350 (2013).

80. Kalebic, N. *et al.* αTAT1 is the major α-tubulin acetyltransferase in mice. *Nat. Commun.* **4,** (2013).

81. Aguilar, A. *et al.* A-tubulin K40 acetylation is required for contact inhibition of proliferation and cell-substrate adhesion. *Mol. Biol. Cell* **25,** 1854–66 (2014).

82. Hubbert, C. *et al.* HDAC6 is a microtubule-associated deacetylase. *Nature* **417,** 455–458 (2002).

83. Matsuyama, A. *et al.* In vivo destabilization of dynamic microtubules by HDAC6-mediated deacetylation. *EMBO J.* **21,** 6820–6831 (2002).

84. North, B. J., Marshall, B. L., Borra, M. T., Denu, J. M. & Verdin, E. The human Sir2 ortholog, SIRT2, is an NAD+-dependent tubulin deacetylase. *Mol. Cell* **11,** 437–444 (2003).

85. Coombes, C. *et al.* Mechanism of microtubule lumen entry for the α-tubulin acetyltransferase enzyme αTAT1. *Proc. Natl. Acad. Sci.* **113,** E7176–E7184 (2016).

86. Ly, N. *et al.* αtAT1 controls longitudinal spreading of acetylation marks from open microtubules extremities. *Sci. Rep.* **6,** (2016).

87. Westermann, S. & Weber, K. Post-translational modifications regulate microtubule function. *Nature Reviews Molecular Cell Biology* **4,** 938–947 (2003).

88. Wloga, D. & Gaertig, J. Post-translational modifications of microtubules. *J. Cell Sci.* **124,** 154–154 (2011).

89. Janke, C. The tubulin code: Molecular components, readout mechanisms, functions. *J. Cell Biol.* **206,** 461–472 (2014).

90. Cambray-Deakin, M. A., Morgan, A. & Burgoyne, R. D. Sequential appearance of cytoskeletal components during the early stages of neurite outgrowth from cerebellar granule cells in vitro. *Dev. Brain Res.* **37,** 197–207 (1987).

91. Robson, S. J. & Burgoyne, R. D. Differential localisation of tyrosinated, detyrosinated, and acetylated α-tubulins in neurites and growth cones of dorsal root ganglion neurons. *Cell Motil. Cytoskeleton* **12,** 273–282 (1989).

92. Kalebic, N. *et al.* αTAT1 is the major α-tubulin acetyltransferase in mice. *Nat. Commun.* **4,** (2013).

93. Friedmann, D. R., Aguilar, A., Fan, J., Nachury, M. V. & Marmorstein, R. Structure of the -tubulin acetyltransferase, TAT1, and implications for tubulin-specific acetylation. *Proc. Natl. Acad. Sci.* **109,** 19655–19660 (2012).

94. Palazzo, A., Ackerman, B. & Gundersen, G. G. Cell biology: Tubulin acetylation and cell motility. *Nature* **421,** 230 (2003).

95. Howes, S. C., Alushin, G. M., Shida, T., Nachury, M. V. & Nogales, E. Effects of tubulin acetylation and tubulin acetyltransferase binding on microtubule structure. *Mol. Biol. Cell* **25,** 257–266 (2014).

96. Neumann, B. & Hilliard, M. Loss of MEC-17 leads to microtubule instability and axonal degeneration. *Cell Rep.* **6,** 93–103 (2014).

97. Portran, D., Schaedel, L., Xu, Z., Théry, M. & Nachury, M. V. Tubulin acetylation protects long-lived microtubules against mechanical ageing. *Nat. Cell Biol.* **19,** 391–398 (2017).

98. Xu, Z. *et al.* Microtubules acquire resistance from mechanical breakage through intralumenal acetylation. *Science (80-.).* **356,** 328–332 (2017).

99. Topalidou, I. *et al.* Genetically separable functions of the MEC-17 tubulin acetyltransferase affect microtubule organization. *Curr. Biol.* **22,** 1057–1065 (2012).

100. Cueva, J. G., Hsin, J., Huang, K. C. & Goodman, M. B. Posttranslational acetylation of α-tubulin constrains protofilament number in native microtubules. *Curr. Biol.* **22,** 1066–1074 (2012).

101. Friedman, J. R., Webster, B. M., Mastronarde, D. N., Verhey, K. J. & Voeltz, G. K. ER sliding dynamics and ER-mitochondrial contacts occur on acetylated

microtubules. *J. Cell Biol.* **190,** 363–375 (2010).

102. Westrate, L. M., Lee, J. E., Prinz, W. A. & Voeltz, G. K. Form Follows Function: The Importance of Endoplasmic Reticulum Shape. *Annu. Rev. Biochem.* **84,** 791–811 (2015).

103. Misawa, T. *et al.* Microtubule-driven spatial arrangement of mitochondria promotes activation of the NLRP3 inflammasome. *Nat. Immunol.* **14,** 454–460 (2013).

104. Wang, B. *et al.* Microtubule acetylation amplifies p38 kinase signalling and anti-inflammatory IL-10 production. *Nat. Commun.* **5,** (2014).

105. Ishiguro, K., Ando, T., Maeda, O., Watanabe, O. & Goto, H. Cutting Edge: Tubulin Functions as an Adaptor in NFAT-Importin Interaction. *J. Immunol.* **186,** 2710–2713 (2011).

106. Sabo, Y. *et al.* HIV-1 induces the formation of stable microtubules to enhance early infection. *Cell Host Microbe* **14,** 535–546 (2013).

107. Mackeh, R. *et al.* Reactive oxygen species, amp-Activated protein kinase, and the transcription cofactor p300 regulate α-Tubulin acetyltransferase-1 (αtat-1/mec-17)-Dependent microtubule hyperacetylation during cell stress. *J. Biol. Chem.* **289,** 11816–11828 (2014).

108. D'Ydewalle, C. *et al.* HDAC6 inhibitors reverse axonal loss in a mouse model of mutant HSPB1-induced Charcot-Marie-Tooth disease. *Nat. Med.* **17,** 968–974 (2011).

109. Law, B. M. H. *et al.* A direct interaction between leucine-rich repeat kinase 2 and specific β-Tubulin isoforms regulates tubulin acetylation. *J. Biol. Chem.* **289,** 895–908 (2014).

110. Godena, V. K. *et al.* Increasing microtubule acetylation rescues axonal transport

and locomotor deficits caused by LRRK2 Roc-COR domain mutations. *Nat. Commun.* **5,** (2014).

111. Taes, I. *et al.* Hdac6 deletion delays disease progression in the sod1g93a mouse model of als. *Hum. Mol. Genet.* **22,** 1783–1790 (2013).

112. Selenica, M. L. *et al.* Histone deacetylase 6 inhibition improves memory and reduces total tau levels in a mouse model of tau deposition. *Alzheimer's Res. Ther*. **6,** (2014).

113. Yu, C. W., Chang, P. T., Hsin, L. W. & Chern, J. W. Quinazolin-4-one derivatives as selective histone deacetylase-6 inhibitors for the treatment of Alzheimer's disease. *J. Med. Chem.* **56,** 6775–6791 (2013).

114. Zhang, L. *et al.* Tubastatin A/ACY-1215 improves cognition in Alzheimer's disease transgenic mice. *J. Alzheimers. Dis.* **41,** 1193–205 (2014).

115. Cho, Y. & Cavalli, V. HDAC5 is a novel injury-regulated tubulin deacetylase controlling axon regeneration. *EMBO J.* **31,** 3063–3078 (2012).

116. Boggs, A. E. *et al.* α-Tubulin acetylation elevated in metastatic and basal-like breast cancer cells promotes microtentacle formation, adhesion, and invasive migration. *Cancer Res.* **75,** 203–215 (2015).

117. Bailey, J. M. *et al.* DCLK1 marks a morphologically distinct subpopulation of cells with stem cell properties in preinvasive pancreatic cancer. *Gastroenterology* **146,** 245–256 (2014).

118. Richner, M., Bjerrum, O. J., Nykjaer, A. & Vaegter, C. B. The Spared Nerve Injury (SNI) Model of Induced Mechanical Allodynia in Mice. *J. Vis. Exp.* 3–5 (2011). doi:10.3791/3092

119. Prager-Khoutorsky, M., Khoutorsky, A. & Bourque, C. W. Unique Interweaved Microtubule Scaffold Mediates Osmosensory Transduction via Physical

Interaction with TRPV1. *Neuron* **83,** 866–878 (2014).

120. Davenport, A. M. *et al.* Structural and functional characterization of the α-tubulin acetyltransferase MEC-17. *J. Mol. Biol.* **426,** 2605–2616 (2014).

121. Decosterd, I. & Woolf, C. J. Spared nerve injury: An animal model of persistent peripheral neuropathic pain. *Pain* **87,** 149–158 (2000).

122. Costigan, M., Scholz, J. & Woolf, C. J. Neuropathic Pain: A Maladaptive Response of the Nervous System to Damage. *Annu. Rev. Neurosci.* **32,** 1–32 (2009).

123. Chaplan, S. R., Bach, F. W., Pogrel, J. W., Chung, J. M. & Yaksh, T. L. Quantitative assessment of tactile allodynia in the rat paw. *J. Neurosci. Methods* **53,** 55–63 (1994).

124. Xu, Z. *et al.* Microtubules acquire resistance from mechanical breakage through intralumenal acetylation. *Science (80-.).* **356,** 328–332 (2017).

125. Portran, D., Schaedel, L., Xu, Z., Théry, M. & Nachury, M. V. Tubulin acetylation protects long-lived microtubules against mechanical ageing. *Nat. Cell Biol.* **19,** 391–398 (2017).

126. Robison, P. *et al.* Detyrosinated microtubules buckle and bear load in contracting cardiomyocytes. *Science (80-.).* **352,** (2016).

127. Hu, J. & Lewin, G. R. Mechanosensitive currents in the neurites of cultured mouse sensory neurones. *J. Physiol.* **577,** 815–828 (2006).

128. Carpenter, A. E. *et al.* CellProfiler: Image analysis software for identifying and quantifying cell phenotypes. *Genome Biol.* **7,** (2006).

129. Zimmermann, K. *et al.* Phenotyping sensory nerve endings in vitro in the mouse. *Nat. Protoc.* **4,** 174–196 (2009).

130. Yang, G. *et al.* Genetic targeting of chemical indicators in vivo. *Nat. Methods*

12, 137–139 (2015).

131. Tang, G. *et al.* EMAN2: An extensible image processing suite for electron microscopy. *J. Struct. Biol.* **157,** 38–46 (2007).

132. Scheres, S. H. W. RELION: Implementation of a Bayesian approach to cryo-EM structure determination. *J. Struct. Biol.* **180,** 519–530 (2012).

133. Bonin, R. P., Bories, C. & De Koninck, Y. A simplified up-down method (SUDO) for measuring mechanical nociception in rodents using von Frey filaments. *Mol. Pain* **10,** (2014).

134. Kukulski, W. *et al.* Correlated fluorescence and 3D electron microscopy with high sensitivity and spatial precision. *J. Cell Biol.* **192,** 111–119 (2011).

8 Appendix

8.1 EM chemical fixation of labeled DRG dissociated neurons from the *Avil-Cre::Rosa26SNAP^{CaaX}* mouse

Here I took advantage of a mouse transgenic line, *Advil-Cre::Rosa26SNAP^{CaaX}* , generated in our laboratory[130] in order to circumvent the fluorescence quenching of GFP during EM preparation of the sample.

I applied the Snap-tag system for cell-imaging coupled with the silicon-containing rhodamine derivatives SiR-carboxyl and processed the cells for electron microscopy in order to test if the fluorescence survives the EM preparation of the sample and thus develop novel CLEM strategy.

The fluorescence was checked after each step of preparation of the sample with the Widefield Leica DMR and I found that synthetic fluorophores preserve their post-embedding fluorescence in the presence of uranyl acetate but not in the presence of osmium tetroxide (Figure 24a-f).

However, osmium tetroxide is really necessary for the preservation of DRG neuron membranes and to enhance the contrast of the image (data not shown).

For this reason, I optimized an HPF and Freeze sub protocol that don’t need Osmium.

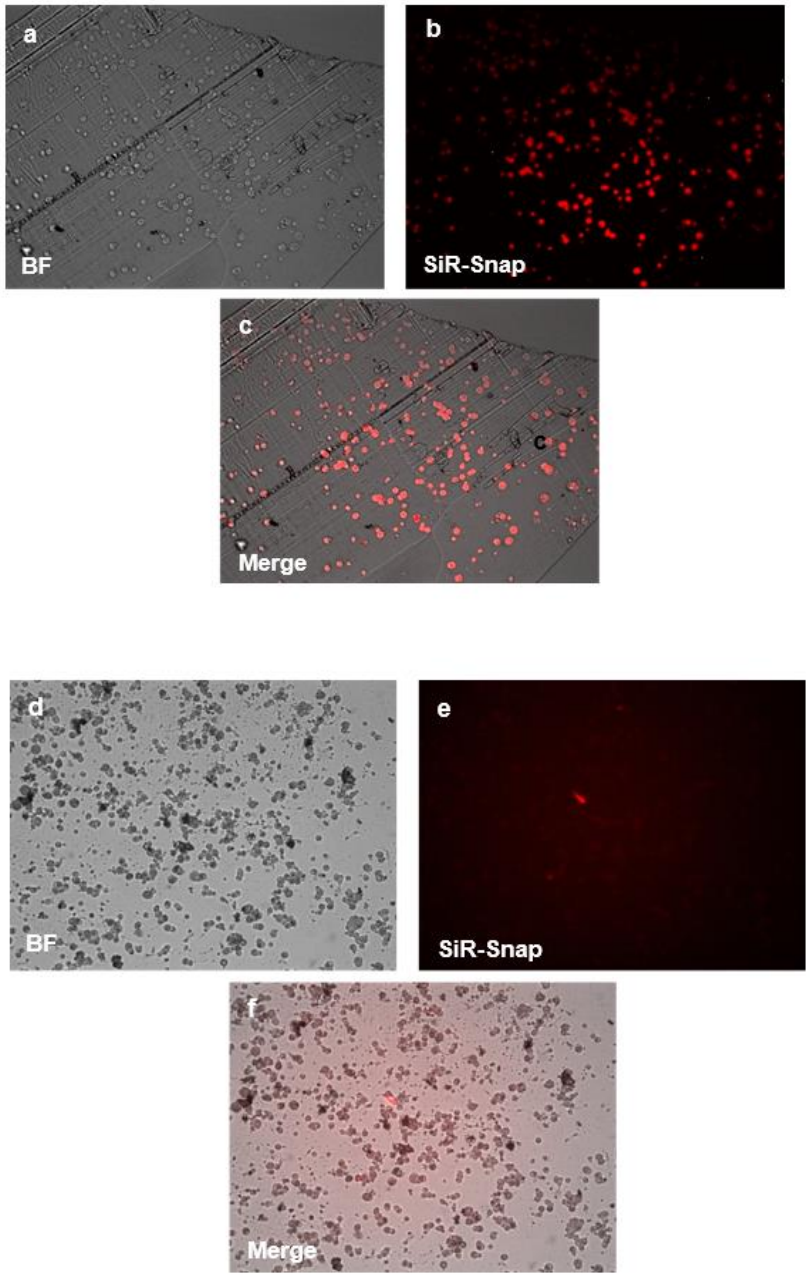

Figure 24. Light microscopy of dissociated sensory neurons embedded into Epon. a)-f) are fluorescence microscope images of 500-nm resin sections of DRG sensory neurons tagged with the SNAP system and incubated with the SiR-700 substrate. The pictures show the preservation of the fluorescent signal after EM preparation of the sample, in absence of osmium tetroxide a)-c). d)-f) show the fluorescence quenching by 0.25% Osmium tetroxide in DRG sensory neurons during the post-fixation step of EM preparation (Scale bar 50 μm).

8.2 Ultrastructural analysis of the microtubules in the mouse cornea by EM

In our previous work we have shown that acetylated α-tubulin is also enriched under the membrane of axons in the saphenous nerve and apparently at sensory neuron terminal endings in the cornea where mechanotrasduction takes place[1]. For this reason it would be interesting to further investigate at the ultrastructural level, with electron microscopy, the morphology of microtubules and their eventual modifications at the peripheral sensory terminals.

Here I performed in parallel both chemical fixation and HPF followed by FS on the corneas both from *TRPM8BAC-EYFP*$^{+/+}$ and *Avil-Cre::Rosa26SNAP*^{CaaX} mice, in order to find the best sample preparation protocol that would allow fine ultrastructure preservation.

8.2.1 Chemical fixation of corneas

The electron micrographs show a very well-resolved structure of the corneal epithelium. However, the sensory terminals lose their myelin sheath early while entering the cornea and this makes their tracking very challenging (Figure 25a, b, 26a, b).

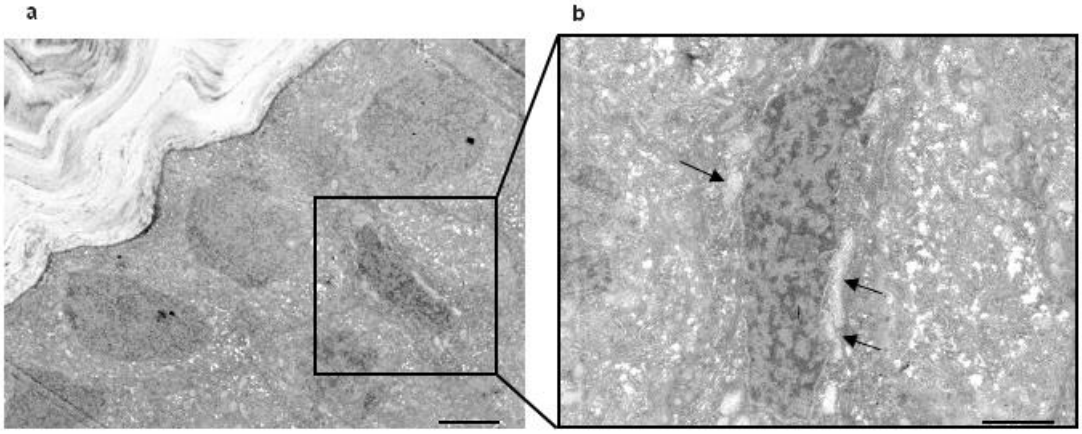

Figure 25. Transmission electron micrographs of cornea cross-sections showing basal cells in the basal layer of corneal epithelium. a) and b) The right panel shows at higher magnification what may represent peripheral sensory fibers (black arrow) running between basal epithelial cells (Scale bars 5 μm left and 2 μm right panel).

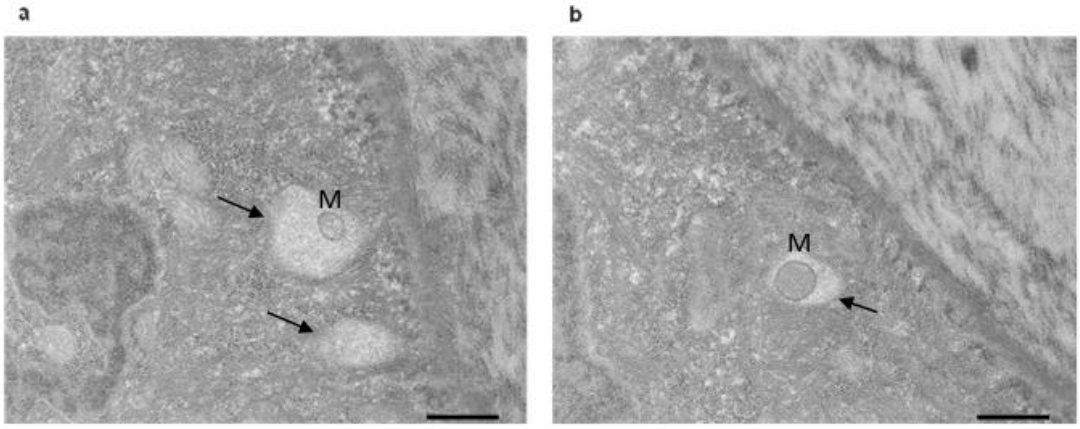

Figure 26. Transmission electron micrographs of Tangential view of potential sensory fibers in the basal layer of the corneal epithelium. a) and b) show cross-sections of peripheral sensory fibers (highlighted by black arrows) containing one of the characteristic hallmarks, a mitochondria (M) that identify such nerve terminals (Scale bars 2 μm).

.

8.2.2 Olympus Biosystems Cell^R, UV cutting for marking sensory terminals into the corneal epithelium (CLEM approach)

To overcome the problem described above, I used the following approach to prove that the regions of interest seen in the chemical fixed tissue are indeed sensory fibers. First I localize the sensory fiber in the cornea from *TRPM8BAC-EYFP*$^{+/+}$ mice with the fluorescent microscope, taking advantage of its fluorescence and then I burned with the laser a region around the fiber of interest in order to create a square that could have survived the EM preparation of the sample, that would help me locate the fiber of interest in the final resin block, as the fluorescence is quenched (Figure 27a,b, 28a, b).

I encountered several disadvantages using this method.

First of all, it doesn't allow to be fully aware of the square size and of the etching depth at which the sample is burned. Indeed one of the problem we observed was to make the marker in a layer of the tissue I was not interested in, burning too deep.

Second it takes a lot of time and effort to find back the marker, once the sample is embedded into the resin for the EM preparation.

Therefore we decided to continue using the on-section CLEM protocol described later (see High pressure freezing and freeze substitution of corneas).

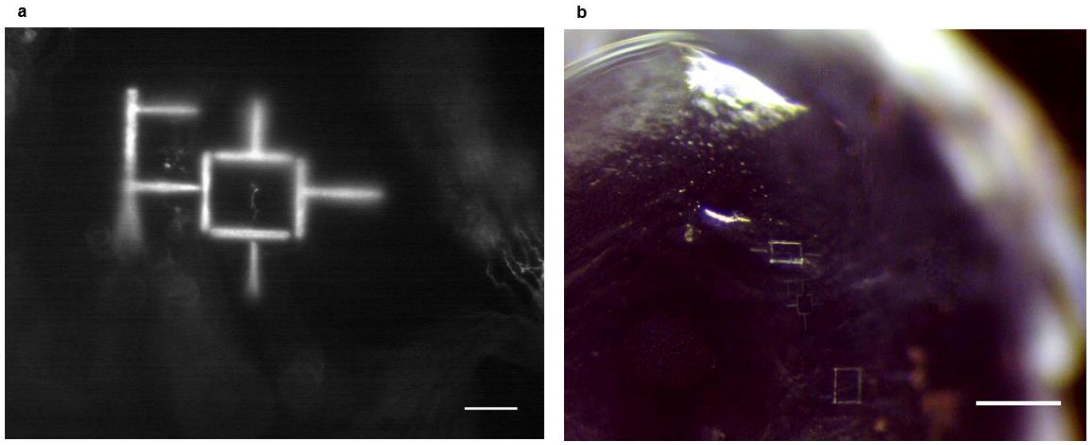

Figure 27. Cornea etching with the Olympus Cut^R. a) The left panel shows a fluorescence microscopy image of the square made by the laser surrounding the sensory terminal in the cornea from the *TRPM8BAC-EYFP*$^{+/+}$ mouse. b) The right panel is a micrograph of the same sample as in panel a) taken by the Leica stereo microscope and showing the preservation of the tissue after etching (Scale bars 5μm left and 6 μm right panel).

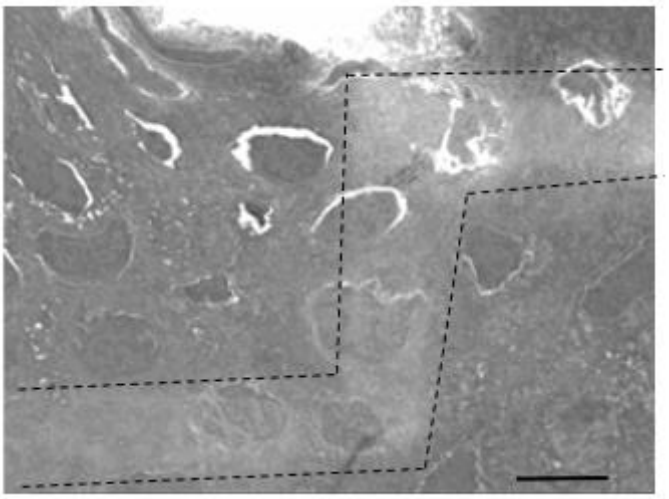

Figure 28. Electron micrograph showing the preservation of the burning square (dotted lines), made by the Olympus Cut^R in the corneal epithelium, after EM preparation of the sample. Cross section of the cornea from the *TRPM8BAC-EYFP*$^{+/+}$ mouse after chemical fixation and resin embedding.(Scale bar 10 μm).

8.2.3 High pressure freezing and freeze substitution of corneas

To overcome the problems described above, I reasoned that HPF would be the best approach. This would allow us to use a protocol that preserves the fluorescence in the block and do *on-section* CLEM[134].

When tissues are rapidly frozen, all contents are immobilized almost immediately. These fast-freezing methods involve time scales of milliseconds and are preferable to chemical fixation methods that have time scales of seconds or minutes depending on the tissue.

For this reason I tried to optimize a CLEM protocol for the cornea from the *Avil-Cre::Rosa26SNAP^{CaaX}* mouse line.

Unfortunately, I encountered some technical problems with the labeling of the tissue for unknown reasons and, since I would have also needed a triple transgenic mouse line that allows to have both the fluorescence and the reduction of mechanosensitivity, *Avil-Cre::Rosa26SNAP^{CaaX}::Atat1^{cKO}*, I reasoned to continue working only on the *Avil-Cre::Atat1^{cKO}* mouse line.